Analysis of Dryer and Vapor Absorption Refrigeration Systems Powered by Geothermal Energy

By

Yonas Tetemke

A Thesis Submitted to

Thermal and Aerospace Engineering Program

School of Mechanical, Chemical and Materials Engineering

Presented in partial fulfillment of the requirement for the degree of Master of Science in Thermal Engineering

Adama Science and Technology University

Adama, Ethiopia

September, 2019

Analysis of Dryer and Vapor Absorption Refrigeration Systems Powered by Geothermal Energy

By: Yonas Tetemke

Advisor: Dr. Gezahegn Habtamu

A Thesis Submitted to

Thermal and Aerospace Engineering Program

School of Mechanical, Chemical and Materials Engineering

Presented in partial fulfillment of the requirement for the degree of Master of Science in Thermal Engineering

Adama Science and Technology University

Adama, Ethiopia

September, 2019

APPROVAL OF BOARD OF EXAMINERS

We, the undersigned, members of the Board of Examiners of the final open defense by **Yonas Tetemke Dereso** have read and evaluated his thesis entitled "**Analysis of Dryer and Vapor Absorption Refrigeration Systems Powered by Geothermal Energy**" and examined the candidate. This is, therefore, to certify that the thesis has been accepted in partial fulfillment of the requirement of the Degree of Master of Science in Thermal Engineering.

______________________	______________	____________
Advisor	Signature	Date
______________________	______________	____________
Chairperson	Signature	Date
______________________	______________	____________
Internal Examiner	Signature	Date
______________________	______________	____________
External Examiner	Signature	Date

CANDIDATE'S DECLARATION

I hereby declare that this MSc Thesis is my original work and has not been presented for a degree in any other university, and all sources of material used for this thesis have been duly acknowledged.

Name: Yonas Tetemke Dereso

Signature: ___________

This MSc Thesis has been submitted for examination with my approval as thesis Advisor.

Name: Dr. Gezahegn Habtamu

Signature: ___________

Date of submission: ________________

ADVISOR’S APPROVAL SHEET

To: SoMCM Engineering Thermal and Aerospace Engineering Department

Subject: Thesis Submission

This is to certify that the thesis entitled “**Analysis of Dryer and Vapor Absorption Refrigeration Systems Powered by Geothermal Energy**” submitted in partial fulfillment of the requirements for the degree of Master’s in Thermal Engineering, the graduate program of the department of Thermal and Aerospace Engineering, and has been carried out by Yonas Tetemke Dereso Id.No. A/PR15327/10 under my supervision. Therefore, I recommend that the student has fulfilled the requirements and hence hereby he can submit the thesis to the department.

Advisor	Signature	Date

ACKNOWLEDGEMENT

First, I would like to express my most profound gratitude toward my Advisor, Dr Gezahegn Habtamu for his great proffesional, short & precise guidance and support throughout this work. I would like to use this chance to express my appreciation towards his qualities both in academics and sociablity. He believes in creating productive and competitive minded generations in the field of thermal systems. He was much more than an academic supervisor to me.

Secondly, it gives me great pleasure to thank Dr. Addisu Bekele (*Assistant Professor, Thermal and Aerospace Engineering Dep.t, ASTU*), for his valuable lectures and advices in the classes. He was the only appointed person I ever seen in all his jobs.

I would like to thank everyone at ASTU, Departement of Thermal and Aerospace Engineering; this work would never have been possible without financial support from Adama Science and Technology University.

Without the great support of Tariku Figa (Expert, Gede'o Zone Water, Mineral, & Energy Sector) and Fikru Tadele (Dean, School of Mechanical & Automotive Enginering, Dilla University), data collection would have not been possible for that I convey my heart felt gratitude towards them.

I am also very much grateful to my families; my father Tetemke Dereso (*Ababa*), my mother Ayelech Toga (*Galchule or Aadixxe*), my brothers; Tadesse Tetemke (*Gaashe was my only teacher at my early age*), Abraham Tetemke (*Abe*), Temesgen Tetemke (*Teme*), and Tariku Tetemke (*Taare*) who supported me in everything in my life.

And thanks are extended to all my colleagues, Hashim Mohammed, Dereje Ayele, Ephrem Milkias, Zemach Yohannes, Hiywot Birhanu, Rediwan Ali, Tiko Rago, Bonsa Mosisa, Eskedar, Degaga Abdi, Usman Teshta, Mebrathom Baza, and others. I always remember good times we had together.

Most of all I would like to worship the almighty God, who I strongly believe gave me the power and the strength to accomplish this task.

ABSTRACT

Geothermal energy, one of the renewable energies in the earth, have extensively been used worldwide. Its applications falls in to two classifications; first, utilizing heat energy in the source directly and second, indirectly converting it in to another energy form (electricity). In Ethiopia, with an estimated geothermal potential of 4200 – 11000 MW, Aluto Langano of Oromia region morethan 7.2 MW of electrical power is existing indirect application. Besides bathing and swimming which are estimated to consume about 2.2 MW, there has been no investigation on direct geothermal energy use in Ethiopia.

In this thesis, with an objective to analyze dryer system and vapor absorption refrigeration system (VARS), the systems powered by geothermal energy for thermal applications such as drying of agricultural products and cooling of water, respectively; thermodynamic and mathematical analyses of the systems are separately done. In the first part, when ambient air is forced to flow across the bundle of tubes, heat and mass transfer model is used to quantify amount of heat energy transferred and moisture removed. In the second part, mass & energy conservations principle have been used to analyze components of VARS to cool drinking water of Dilla University from 37.8^{o}C to 16^{o}C within 16 hrs.

In the first part, it is assumed that 500 kg of different agricultural products are dried in the cabinet of same dryer. The results show that each of the crops requires different operating parameters due to differences in their thermal properties such as moisture contents, heat capacity, and so on.

In the second part, designed VARS operating at evaporation rate of 103.12 kW is capable to cool 66,000 liters of drinking water to the required temperature within 16 hrs each day. It has to be noted that evaporation rate varies with the time needed to cool. If the water to be cooled is within short time, high evaporation rate is then required.

Based on the results obtained, it is clear that geothermal energy at Gedeo and Gujji Zones can be utilized for dryer and VAR systems. Furthermore, cost analysis of VARS shows that application of this system will highly contribute to save money and energy of the country.

Key words: Food drying System, Absorption Refrigeration System, Geothermal Energy

TABLE OF CONTENTS

LISTS OF FIGURES

LISTS OF TABLES

NOMENCLATURES/ABBREVIATIONS/SYMBOLS

Nomenclature	Definitions	Unit
$\dot{Q}$	Heat transfer rate per unit area	kW
Q	Heat transfer rate from tube bank	kW
$T_{w,\ hot\ in}$	Hot inlet water temperature	^oC
$T_{a,\ cold\ in}$	Cold inlet air temperature	^oC
R_{eq}	Equivalent resistances	$^oC/W$
R_{air}	Air-side thermal resistances	$^oC/W$
R_{wall}	Wall conducting resistances	$^oC/W$
$R_{hot,\ w}$	Water-side thermal resistances	$^oC/W$
h_{air}	Air-side heat transfer coefficient	$W/m^2.^oC$
A_{out}	Outer surface area	m^2
d_{out}	Outer tube diameter	m
d_{in}	Inner tube diameter	m
k_{wall}	Thermal conductivity	$W/m.^oC$
L	Tube length	m
h_{water}	Water-side heat transfer coefficient	$W/m^2.^oC$
A_{in}	Inner surface area	m^2
Nu	Nusselt number	-
R_E	Reynolds number	-
P_r	Prandtl number evaluated at mean temperature	-
P_{rs}	Prandtl number evaluated at tube surfaces temperature	-
V	Fluid velocity	m/s
ν	Dynamic viscosity	m^2/s
T_f	Fluid temperature	^oC
T_S	Tube surface temperature	^oC
T_∞	Free stream air temperature	^oC
A_S	Surface area	m^2
S_T	Transverse pitch	cm
S_L	Longitudinal pitch	cm
S_D	Diagonal pitch	cm
N	Total number of tubes	-
N_L	Number of tubes per row	-
N_T	Number of tubes per column	-

Nomenclature	Definitions	Unit
F	Correction factor of N	-
$\dot{V}$	Volumetric flow rate	m^3/s
$\dot{m}$	Mass flow rate	Kg/s
ΔT_{ln}	Logarithmic mean temp. difference	^oC
$T_{w,hot\ out}$	Hot outlet water temperature	^oC
$T_{a,cold\ out}$	Cold outlet air temperature	^oC
Q_{dryer}	Heat required for complete dry	kW
$Q_{heat\ up}$	Heat required for heat-up	kW
$Q_{evaporate}$	Sensible heating	kW
$\dot{m}_a$	Mass flow rate of air	Kg/s
C_{pp}	Specific heat capacity	$kJ/kg.^oC$
ΔP_{maj}	Major pressure losses in the tube	Pa
λ	Darcy-Weisbach friction coefficient of straight pipe/tube	-
ρ_i	Fluid density at inlet temperature	Kg/m^3
D_h	Hydraulic diameter	m
k	Surface roughness	m
k_L	Local loss coefficient used in	-
g	Gravitational acceleration	m/s^2
ΔP_{min}	Minor pressure losses in the tube	Pa
ΔP_D	Total pressure losses	Pa
$P_{m,D}$	Mechanical power required	kW
$P_{el,D}$	Electrical power	kW
M_r	Amount of moisture to be removed	kg
M	Capacity of dryer	kg
H_{r_1}	Initial water content	%
H_{r_2}	Final water content	%
W_2	Weight of died grain	kg
W_1	Weight of wet grain	kg
M_a	Quantity of air required	kg
t	Time taken for drying	s

Nomenclature	Definitions	Unit
V_{total}	Water consumption rate per day	m^3/s
$T_{w,initia}$	Initial drinking water temperature	^oC
$T_{w,fina}$	Final drinking water temperature	^oC
$\dot{Q}_{tot}$	Heat rejected in the evaporator	kW
m	Mass of water	kg
t_{tot}	time taken to freeze water	s
P_K	Condenser pressure	Pa
t_K	Condenser temperature	Pa
h_1	Saturated vapor enthalpy at t_K	kJ/kg
h_2	Saturated liquid enthalpy at t_K	kJ/kg
h_3	Liquid refrigerant's enthalpy equals to h_2	kJ/kg
P_E	evaporator pressure	Pa
t_E	Evaporator temperature	^oC
h_4	Saturated vapor enthalpy at t_E	kJ/kg
h_5	Enthalpy of weak solution	kJ/kg
h_6	Enthalpy equals to h_6	kJ/kg
h_7	Enthalpy of strong solution	kJ/kg
h_8	Enthalpy equals to h_7	kJ/kg
$\dot{m}_w$	mass flow rate of weak solution	kg/s
$\dot{m}_s$	mass flow rate of strong solution	kg/s
$\dot{Q}_{eva}$	Capacity of the VARS	kW
$\dot{m}_r$	mass flow rate in refrigerant circuit	kg/s
x_S	ammonia conc. of strong solution	%
x_r	ammonia conc. of refrigerant circuit	%
x_w	ammonia conc. of weak solution	%
Δt_m	Logarithmic temperature difference	^oC
Q_C	Heat of condensation	kW
$\dot{Q}_v$	Volumetric flow of forced air	m^3/s
ΔL	increment in length	m
Δt	Refrigerant's temperature drop in condenser	^oC
Δh_1	enthalpy changes of 1st section for isenthalpic flow	kJ/kg
f	Friction factor of capillary tube	-
Q_E	Refrigeration capacity	kW

Nomenclature	Definitions	Unit
Δh	enthalpy changes for isenthalpic flow	kJ/kg
C_p	Specific heat of water	kJ/kg^oC
A_C	Condenser tube surface area	m^2
FA	Face area	m^2
D_E	Effective diameter of condenser	m
h_i	Refrigerant-side heat transfer coefficient	$W/m^2.^oC$
μ_f	Kinematic viscosity	kg/m.s
k_f	Refrigerant conductivity at t_{am}	$W/m.^oC$
t_{am}	mean temperature of ammonia in condenser	^oC
t_c	Refrigerant's temperature in condenser	^oC
Δt_r	refrigerant-side temperature drop	^oC
h_o	*air-side* heat transfer a coefficient	$W/m^2.^oC$
t_a	Condenser's mean temperature of air	^oC
k_a	Air conductivity at t_a	$W/m.^oC$
Δt_a	temperature rise of condenser air	^oC
A_t	total fin-side surface area	m^2
η_f	finned surface efficiency	%
U_t	overall heat transfer coefficient	$W/m^2.^oC$
Δp	Total pressure drop in capillary tube	Pa
Δp_F	Pressure drop due to friction	Pa
Δp_A	Momentum pressure drop	Pa
x_1	quality at the end of first section	-
h_c	constant enthalpy	kJ/kg
h_{f_1}	specific enthalpy of saturated liquid	kJ/kg
h_{fg_1}	specific enthalpy of saturated liquid	kJ/kg
v_1	specific volume at end of first section	m^3/kg
v_{f_1}	specific volume of saturated liquid	m^3/kg
v_{g_1}	specific volume of saturated vapor	m^3/kg
$\dot{m}_{in}$	Mass flow rate of refrigerant in	kg/s
$\dot{m}_{out}$	Mass flow rate of refrigerant out	kg/s
u_c	Constant velocity at tube entrance	m/s
v_c	specific volume at tube entrance	m^3/kg
u_1	Velocity of refrigerant at 1st section end	m/s
v_1	Specific volume at end of 1st section	m^3/kg
G	Mass constant	$kg/s.m^2$

Nomenclature	Definitions	Unit
Q_G	Energy added from hot source	kW
T_H	temperature of hot source	°C
L_c	Length of generator's coiled tube	m
r_o	Outer radius of tube	cm
r_i	Inner radius of tube	cm
T_{atm}	Atmospheric air temperature	°C
A_i	Inner area of tube	m^2
A_o	Outer area of tube	m^2
Q_A	heat of absorption rejected	kW
F_P	pressure force	N
A_P	Poppet area subjected to pressure	m^2
P_r	Cracking pressure	N/m^2
k_{rv}	Spring stiffness	N/m
x_o	Spring pre-compression distance	m
d	Circular poppet seat diameter	m
F_d	pressure force on closed poppet	N
F_P	pressure force on opened poppet	N
ΔP_{min}	Pressure drop when poppet closed	Pa
ΔP_{max}	Pressure drop when poppet opened	Pa
$\overline{ab}$	side of the truncated cone area	mm
x	Poppet displacement	mm
d_P	poppet area's diameter	mm
A_t	Throttle area	m^2
d	diameter of inlet to poppet	m
ΔP	pressure rise in the pump	Pa
P_G	generator/condenser pressure	Pa
P_A	absorber/evaporator pressure	Pa
$\dot{V}_s$	volumetric flow rate	m^3/s
$A_{p,cross}$	cross-section	m^2
L_s	stroke length	m
N_S	shaft rotational speed	rpm
$P_{m,s}$	mechanical power	kW
H_s	Head	m
V_g	geometric volume of pump	m^3
A_E	Surface area of evaporator tubes	m^2
P_S	shaft power	kW

Nomenclature	Definitions	Unit
P_h	Input mechanical power	kW
η_p	pump efficiency	%
$P_{el,s}$	Electrical power	kW
η_{el}	motor efficiency	%
ΔH_h	Head losses	m
λ_C	Correction factor for *coiled tube*	-
L_T	total length of tube	m
COP_A	Coefficient of performance	-
	Abbreviations	
DU	Dilla University	
TJ/yr	Terra joule per year	
CSA	Central statistical authority	
CFC	Chlorofluorocarbon	
HCFC	Hydrochlorofluorocarbon	
H_2O	Water	
VARS	Vapor absorption refrigeration system	
VCRS	Vapor compression refrigeration system	
DU	Dilla University	
MW	Mega watt	
TWh	Terra watt hour	
BC	Before Christ	
km	Kilo meter	
NH_3	Ammonia	
GWh/yr	Giga watt hour per year	
ToE/yr.	Ton of energy per year	
LiBr	Lithium bromide	
KWH	Kilo watt hour	
ETB	Ethiopian birr	
m	Meter	
WHO	World health organization	
kg	Kilo gram	
	Symbols	
%	percent	
α	Cone vertex angle	rad
ρ	Density of fluid	kg/m^3
π	Pi	3.14
°C	Degree Celsius	

CHAPTER-ONE
INTRODUCTION

1.1. Background

Geothermal energy which is one of renewable energies and comes from inner side of earth can be used in electricity generation, cooking and other direct uses like heating, carbon dioxide enrichment in greenhouses, bathing, space heating and cooling, or crops drying, and skin healing. This energy is stored as heat in the magma, or molten rock, of the earth's interior, where temperatures are extremely high; in hot water and rocks several kilometers below the earth's surface; and in some parts of the world in shallow ground (Nguyen, 2015).

In addition, according to Sanja et al., (2011), some of direct heat use that have been technically and economically proven during the last decades are space conditioning (heating and cooling of rooms), drying and dehydration of agricultural products, desalinization of sea water, (for example, *Kimolos desalinization plant in Greece*), Snow melting, and Absorption refrigeration system.

The earliest reported use of geothermal energy dates from the pre-pottery period, before 11000 BC, when people in Japan were using hot springs for bathing and washing clothes and the archeological evidence has shown that this energy being used in Northern America more than 10,000 years back. Industrial use started in the late eighteenth century, when steam from under the ground was used to extract boric acid from volcanic mud near what is now the town of Larderello in Tuscany, Italy. Just over a century later, in 1904, the world's first geothermal power generator was tested at Larderello by Italian scientist Piero Ginori Conti, using steam to generate electricity (Nguyen, 2015).

Now aday potential uses of geothermal energy around the world has already been identified as optimal choice other than conventional fuels whose costs and enviromental impacts increases exponentially.

Based on Nguyen, (2015), at present, 24 countries use geothermal power to generate electricity, and another 11 are developing and testing geothermal systems, including Australia, France, Germany, Japan, Switzerland and the United Kingdom of Great Britain and Northern Ireland.

Ethiopia, (2015) presented that Ethiopia in the horn of Africa landed on 1.13 million squares km of area with inhabitants more than 90 million growing at a rate of 2.3% has geothermal potential of 4,200 – 11,000 MW in addition to huge solar potential of 2.199 million TWh per annum. The development begun in the early seventies and continued during the eighties and nineties were surface investigations, temperature gradient of wells and test drilling in selected sites. The first pilot plant was established at Aluto Langano, Oromia region, in 1998 which produces 7.2 MW of electricity. In addition, Corbetti, Tulu Moye and Abaya sites were licensed for exploration by a private firm.

It has been reported by different literatures that Ethiopia has not used endowed renewable energy resources as compared to other African countries which have a potential of renewable energy due to economic problem, lack of interested local private investors to participate in this field, lack of initial investment and knowledge. The only use of vapor compression system in refrigeration technology, in the other hand, demonstrates that the country is not utilizing available huge renewable energies.

Apart from this, spoilage of products during the peak harvesting time in cash crop areas of the country remains problems against farmers working in agricultural field. One of the reasons for this is drying of the products is supported only by natural system.

However, now a day, different researches have been carried out all over the world and their results show that, renewable energies are the best alternative energy sources to replace the conventional fuel.

As to prove how to use these renewable energies, in this thesis, the feasibility of geothermal energy found around Dilla University is investigated for the use in thermal applications such as crop drying and vapor absorption refrigeration systems.

Gedeo and Guji Zones which are about 359 kms and 373 kms from Addis Ababa to the south of Ethiopia and along the main road to Nairobi Kenya, are parts of Ethiopia endowed with this geothermal energy that ever never studied yet and average measured temperatures of these sources are approximately more than 54^{o}C (Appendix B-4) and 88.25^{o}C (Appendix B-5), respectively.

Barsiso/Chombe of Gedeo Zone is located about 3.5 km from Dilla University and that of Wallame of West Gujji zone according to Bureau, (2015), is about 12 km. Based on lindal diagram of Popovski, (2001); Prasetya, (2017); Hristov, (2019) shown in Figure 1, Barsiso/Chombe and Wallame geothermal sources can be used directly for drying fish, absorption refrigeration, green house, balneology, aquaculture, bi-degradation fermentation, agriculture, chicken's egg incubation system, etc.

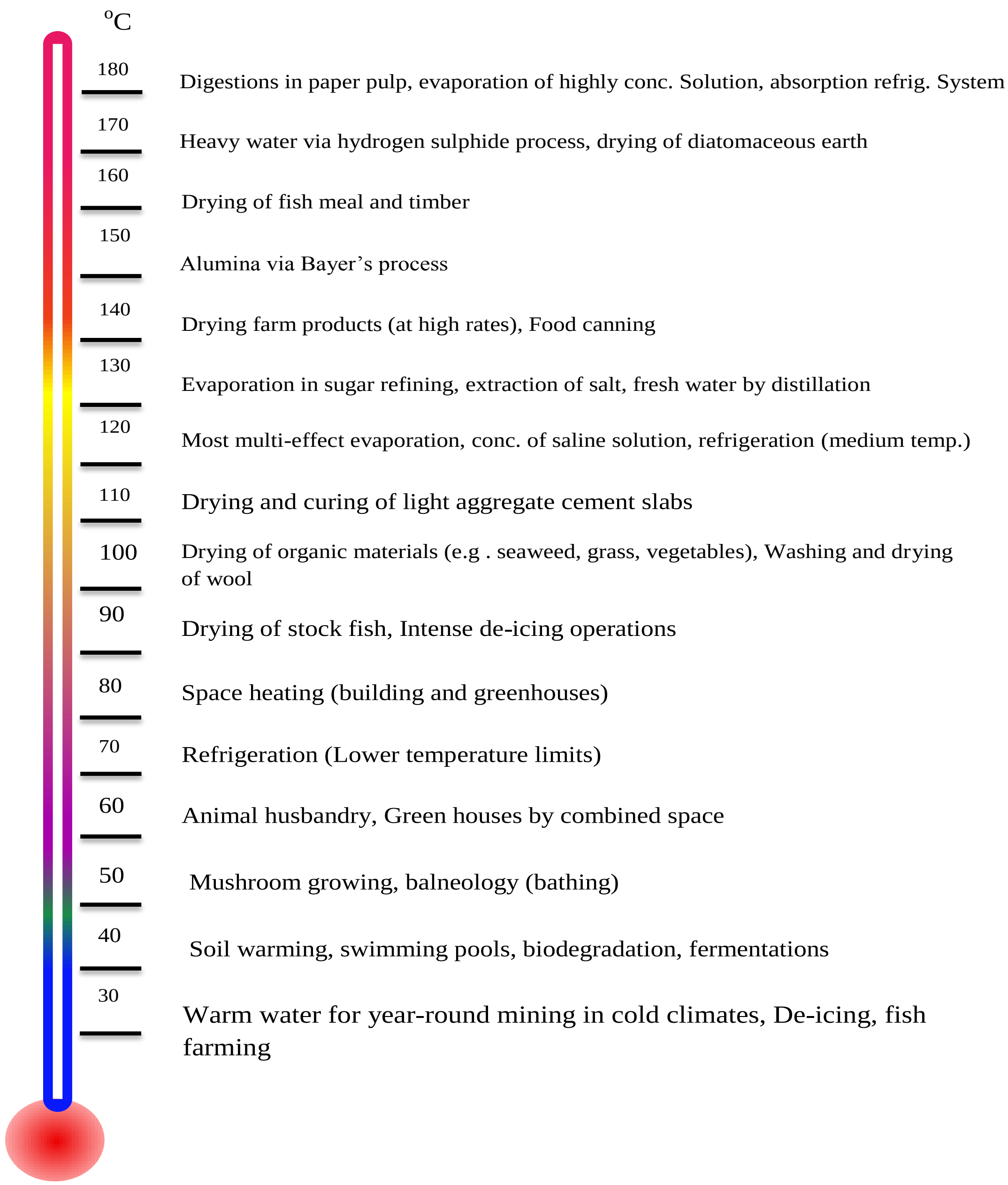

Figure 1: Lindal Diagram

Now a day, balneology and swimming pools are the only direct applications of these geothermal sources as shown in Figure 2 at Barsiso. In addition, peoples from different parts of Ethiopia are visiting the areas for healing purpose. There was an expectation as of Bureau, (2015) that *Wallame* thermal spring, if well-developed, can be site of thermal bathing and multipurpose tourist recreations.


(a)


(b)

Figure 2: Direct use of "*Barsiso*/*Chombe*" geothermal source, Dilla. (a) Swimming pool (b) Bathing rooms

1.2. Statements of problem

The average measured temperature of drinking water supply to Dilla University was approximately about 37.5^{o}C (as shown in Appendix B-3) even though the measurements was taken in the summer, which is the coldest season of the year around this area. It would not be to exaggerate that this value of water temperature is less than its value that it would be in the winter, the hottest season. Therefore, the drinking water of the university is not suitable.

However, drink this water as it is has many advantages such as loss of weight shading, assisting with nasal and throat congestion, diminishing menstrual cramps, body detoxification, prevention of premature aging, acne, dandruff and pimples, promoting hair growth, preventing dandruff, and enhancing digestion (Patel, 2015). Drinking hot/warm water also has the disadvantages of containing soluble contaminants, injuring of the intestinal lining, sleep disturbances, damaging kidneys, increasing blood volume (resulting in hypertension), scalding of mouth, etc (Patel, 2015).

In addition, studies have shown that most of time hot/warm water is recommended during coldest season when the body characterizes very less temperature than 37^{o}C. Nevertheless, suggested water temperature for better hydration of body, according to Hosseinlou, (2013) and *WHO*, is 16^{o}C, with recommended consumption rate of approximately 2 liters per day.

Gedeo zone, where more than 28% coffees supply in Ethiopia, is one of highly populated part of the country and found in the altitudes ranging from 1268-2993 meters above sea level. Piling-up of coffee during its harvesting is common for traditional drying process due to scarcity of enough land around this area, because of high population density of 699.84 people per km^2 (CSA 2007), is one the problem against coffee quality. Therefore, piling-up coffee remains drying problem around the society.

Tomato is one of vegetable crops that is consumed in every household and grown in different parts of Ethiopia. Ambecha et al., (2013) and Meniga & Muthyalu, (2014) studied that lack of tomato storage facility is one of the major challenges which results in products spoilage and its price falls quite significantly during peak harvesting season. These indicate that to process the tomatoes to another form (such as powder) to last it long, the drying system remains the problems in different parts of the country where tomatoes are abundantly produced.

1.3. The Objective

1.3.1. General objective

The general objective of the thesis is to investigate the geothermal energy at Gedeo and Gujji Zones for food (agricultural products) drying and cooling of drinking water by vapor absorption refrigeration system.

1.3.2. Specific objectives

The specific objectives of this study are

- To measure the average temperature of drinking water supply of Dilla University and geothermal sources such as '*Barsiso/Chombe'*, and '*Wallame'* hot springs.
- To estimate amount of heat to be removed from drinking water supply of DU.

- To estimate of moisture to be removed from assumed value of 500 kg of different agricultural products such as tomatoes, coffee, beans, and maize and their required final temperature & moisture after drying.
- To collect the meteorological data such as average air temperature, wind speed, and relative humidity around DU.
- To conduct heat and mass transfer analysis of drying system for different crops such as tomatoes, coffee, beans, and maize and VAR systems using geothermal water as energy sources.
- To analyze each components of both drying for estimated values of moisture amount to be removed from different crops and VAR systems for estimated values of heat to be removed from drinking water of the University.
- To investigate the optimization parameters of the two systems for better effectiveness.
- To analyzes cost of the two systems.

1.4. The scope of study

The thesis basically covers analyses of agricultural products (food) dryer and VARS powered by "Barsiso/Wallame" geothermal source. Average moisture contents in 500 kg of each of the crops such as tomatoes, maize, beans, and coffee at their matured stage are evaluated, their required moisture contents enable for safe storage reviewed and based on which their respective drying systems are analyzed.

In addition, it covers analyzing and sizing of major components done for vapor absorption refrigeration system for the total capacity of cooling load of 66,000 liters (*as per average consumption rate of DU*) of water per day.

1.5. Significance of study

Successful and practical implementation of the study will primarily solve the problems of unsuitable drinking water of DU and then challenges against coffee drying process in the society.

In addition, this work may help us in reducing appreciable consumptions of electric power that would be needed if vapor compression refrigeration system is used to cool drinking water.

Furthermore, the study will help us to reduces wastage of perishable food items such as tomatoes and the likes.

1.6. Organizations of the study

This thesis contains six chapters. The first chapter introduces brief history about what geothermal energy is and its applications as in the case of the world and Ethiopia. In this chapter the problem statements, objectives, and the scope of study are briefly explained.

The second chapter presents the literature review that focuses on recent technology development and application of direct use of geothermal energy. Furthermore, this chapter contains discussions on heat transfer and pressure drop characteristics through the tube bank, thermal properties of some crops, and absorption refrigeration system powered by means of different sources of thermal energy. The third chapter explains data collection methods and thermodynamic & mathematical analyses used, in designing the components of drying and VAR systems respectively.

Fourth chapter of the thesis divided in to three subparts; contains results & discussions of the two systems. Furthermore, chapter five contains cost analysis of VARS and chapter six contains conclusions & recommendations. Finally, References, Property tables and charts used in the thesis are listed at the ends.

1.7. Limitations of the study

The present study was limited to the following points:

- The capital cost of the systems is high, therefore it was not able to implement and take an experimental data of the systems.
- Data collected (measured) from “Barsiso/Chombe” and “Wallame” geothermal sources were for only three weeks and one day respectively. This was due to high cost and tiresome transportation to the areas.
- As was reported in the introduction and literature survey parts of the paper, limitations to find different literatures and materials related to this field of study somewhat hinders the study.

CHAPTER-TWO

LITERATURE REVIEW

2.1. Introduction

Drying of agricultural products is a very important process in avoiding wastage that will results from fungal and micro bacterial attack. We know that drying as energy intensive process, is means of oldest and common food preservation technique by reducing the moisture contents of the products.

As studied by many researchers, drying of agricultural products can be obtained by utilizing different types of energies. Solar and geothermal energies are some of the renewable energy sources that are used for prominent and efficient energy solar drier.

Open sun drying in which the products receives short wavelength during major part of the day and air circulation, is simplest process where exposing of the products directly to the sun allows solar radiation to be absorbed by the materials and as a result, required quality standards are not fulfilled by using this methods. Uses of solar dryers have been emerged in drying of agricultural products to significantly reduce or eliminate the losses and enhance productivity.

Unlike drying, refrigeration system is used to maintain agricultural products, foods, and medicines at required temperature below the ambient air temperature. It is used in all stages of the chain, from food processing, to distribution, retail and final consumption in home, agro processing industry, and other similar industries. Refrigeration has become an essential to slow the physical, microbiological and chemical activities that cause deterioration in foods.

According to Shet et al., (2012), in addition to progressive reduction of installation, maintenance cost and energy consumptions of low grade energy and environmental friendly ammonia-operated absorption systems, its potential replacement of high grade energy, CFC, and HCFC operated vapor compression systems, have been extensively paid attention in recent years.

In other hand, geothermal energy as one of the renewable energies have been utilized for direct applications such as agricultural drying systems, heat pumps, space heating, bathing, swimming, and refrigeration systems. Here after, brief history on direct uses of geothermal energy for dryer and VARS as studied by different researchers, the methods based on which they designed &

operate, and the research gaps identified through existing systems are explained one by one in the following sub-sections of chapter two.

2.2. Worldwide Geothermal Energy Direct Application

Direct applications of geothermal source of energy; rather than using indirect applications by converting to the electrical form of energy, involve immediate use of consisted heat and according to Sanja et al,. (2011), different types of direct heat use have been technically and economically proven during the last centuries. Works of Sanja et al,. (2011), shown in (Table 1), explains major areas of direct utilization of this energy over 65 countries worldwide in which thermal energy consumptions are estimated to be at least 162,000 TJ/yr which is equals to 45,000 GWh/yr, saving 11.4 million ton of energy every year.

Table 1. Summary of the various worldwide geothermal energy direct-use categories, 1995-2005

Name of direct consumptions type	Capacity, MWt			Utilization, TJ/yr			Capacity Factor		
	2005	2000	1995	2005	2000	1995	2005	2000	1995
1. Geothermal heat pumps	15,.723	5,275	1,854	86,673	23,275	14,617	0.17	0.14	0.25
2. Space heating	4,158	3,263	2,579	52,868	42,926	38,230	0.40	0.42	0.47
3. Greenhouse heating	1,348	1,246	1,085	19,607	17,864	15,742	0.46	0.45	0.46
4. Aquaculture pond heating	616	605	1,097	10,969	11,733	13,493	0.56	0.61	0.39
5. Agricultural drying	157	74	67	2,013	1,038	1,124	0.41	0.44	0.53
6. Industrial uses	489	474	544	11,068	10,220	10,120	0.72	0.68	0.59
7. Bathing and swimming	4,911	3,957	1,085	75,289	79,546	15,742	0.49	0.64	0.46
8. Cooling/snow melting	338	114	115	1,885	1,063	1,124	0.18	0.30	0.31
9. Others	86	137	238	1,045	3,034	2,249	0.39	0.70	0.30
Total	27,825	15,145	8,664	261,418	190,699	112,441	0.30	0.40	0.41

According to Nguyen, (2015), the thermal energy required for rice drying system designed in the Former *Yugoslav Republic of Macedonia* is 136 kilowatt hours per ton of wet weight, while the same system for tomato in *Greece* requires 1450 kilowatt hours per ton of wet weight.

Geothermal energy has been used to dry a wide range of agricultural products, such as rice, wheat, tomatoes, onions, cotton, chilies and garlic. General data and information of direct use of geothermal energy studied by Sanja et al., (2011); Nguyen, (2015) shall be given as follows.

A small-scale tomato drying plant (Figure 3) located in *Nea Kessani, Xanthi in Greece* started operating in 2001. Tomatoes are dried using geothermal hot water at 59 °C in a 14 m long rectangular tunnel dryer of 1.0 m wide and 2.0 m high. Similarly, a pilot-scale geothermal drying system for the pre-drying of cotton was designed and tested in *Nea Kessani*, *Xanthi* in 1991 and 1992. The test results demonstrated that cotton can be dried in specially designed tower drier using geothermal water.

Chilies and garlic are important to the economy of Thailand, where both fresh and dried products can be used for nutrition purpose. In this country, chillies and garlic are dried in cabinet driers (Figure 4), 2.1 m wide, 2.4 m long and 2.1 m high. Each dryer has 36 trays placed in two compartments with a total capacity of 450 kg of chillies or 220 kg of garlic.

For the dryer of Thailand geothermal hot water at about 80°C circulates through a cross-flow heat exchanger 100 mm wide, 500 mm long and 300 mm high, enabling a constant air flow of 1.0 kg/s to pass through the 10.5 m^3 drying chamber. The required air temperatures are 70°C for chillies and 50°C for garlic, with drying times and hot water flow rates of about 46 hours at 1.0 kg/s for chillies, and 94 hours at 0.04 kg/s for garlic. The total energy consumed is 13.3 MJ/kg of water evaporated for chillies and 1.5 MJ/kg of water evaporated for garlic. This type of dryer has relatively low running costs and can be used in any weather conditions.

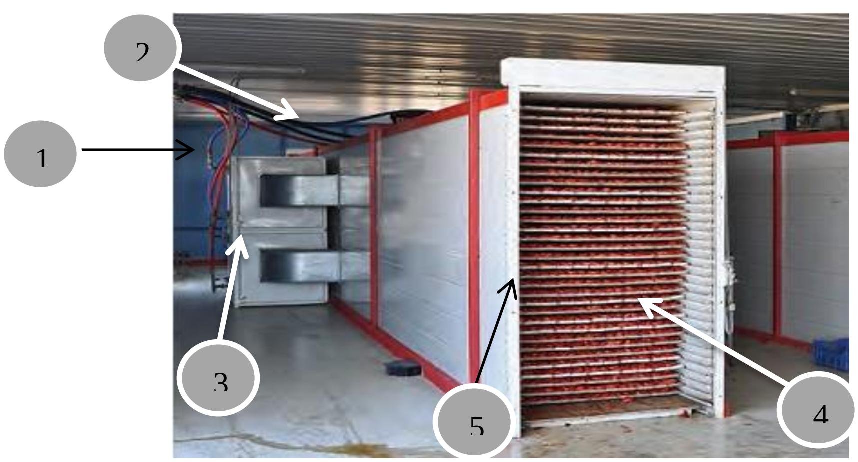

1. Inlet (back side; not visible)
2. Fan (back side; not visible)
3. Geothermal heat exchanger
4. Compartment (trays)
5. Outlet

Figure 3: Tomatoes loaded on drying racks in Greece (Sanja et al., 2011; Nguyen, 2015).

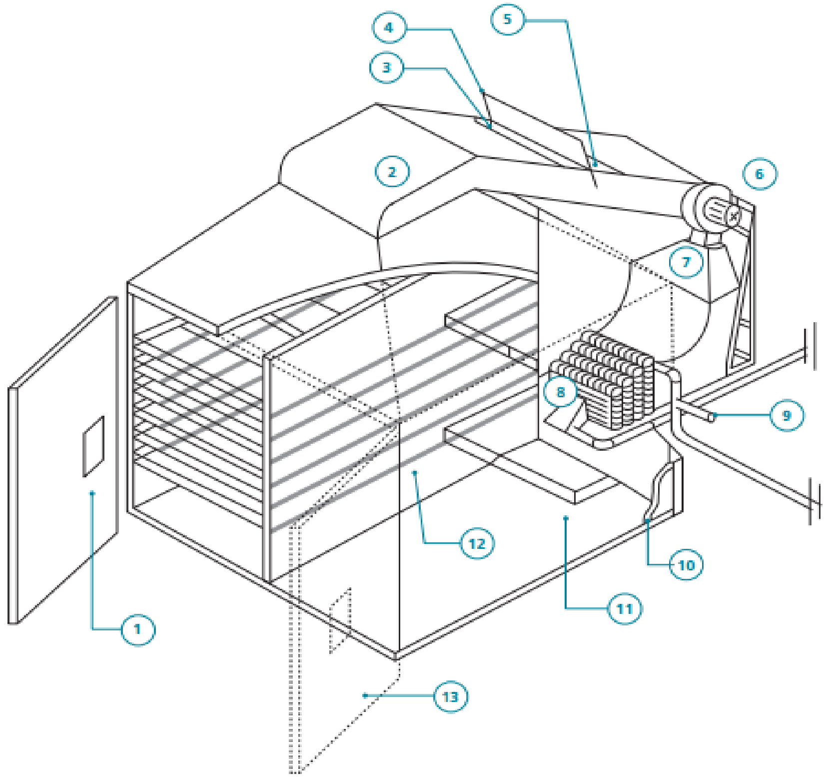

1. Window
2. Return air duct
3. Exhaust opening
4. Valve
5. Inlet
6. Centrifugal fan
7. Air duct
8. Heat exchanger using hot water
9. Hot water taps
10. Insulated walls
11. Grills
12. Shelf for putting grills
13. Door

Figure 4: Cabinet dryer for drying chilies and garlic in Thailand (Nguyen, 2015)

Water from a geothermal well is used for the direct heating of a rice drying plant in the Kotchany geothermal field in *Yugoslav Republic of Macedonia*. The capacity of the dryer (Figure 5) is 10 tons per hour with a heating capacity of 1360 kW. Air from outside, which has a temperature of 15°C and relative humidity of 60%, is heated to about 35°C in a water to-air heat exchanger. The temperatures of the inlet and outlet geothermal water are 75 and 50°C, respectively. The heated air is blown into the drying zone to dry the rice, which moves downwards through the drier at constant velocity. There is gravitation mixing as the grain column moves downwards. The temperature of the heated air is kept below 40°C to prevent cracking of the rice. The rice is dried to decrease the moisture content from 20 - 14 % and then air-cooled.

A fruit dryer (Figure 6) using geothermal energy was designed by Lund and Rangel, (1995) and installed in the Los Azufres geothermal field in *Mexico*. The dryer is 4.0 m long, 1.35 m wide and 2.3 m high with concrete walls, a timber ceiling and roof, and a reinforced concrete floor. It contains two containers with 30 trays each and has a capacity of about one ton of fruit per drying cycle.

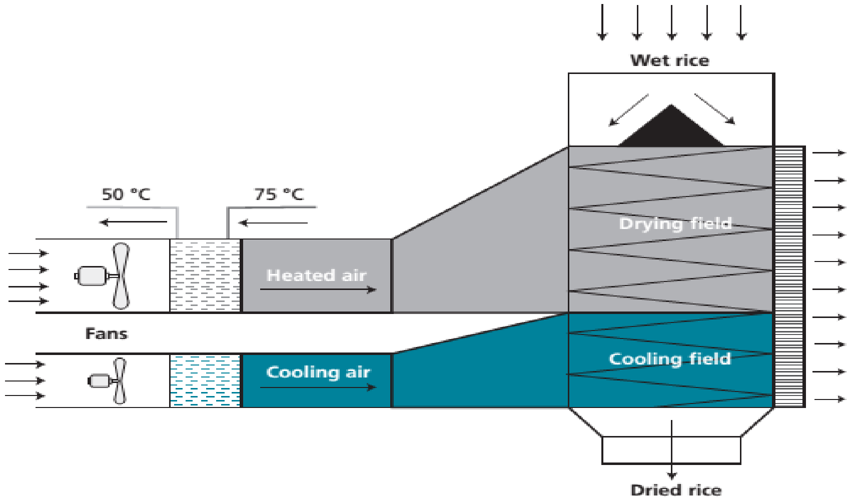

Figure 5: Convective geothermal rice dryer (Sanja et al., 2011; Nguyen, 2015)

Energy consumption is 10 kW at a geothermal water flow rate of 0.03 kg/s. The drying chamber is kept at a temperature of 60°C and reduces the moisture content of fruit from 80 - 20 % in 24 hours. Cascading can be used to boost efficiency and reduce the cost of producing and utilizing the geothermal resource.

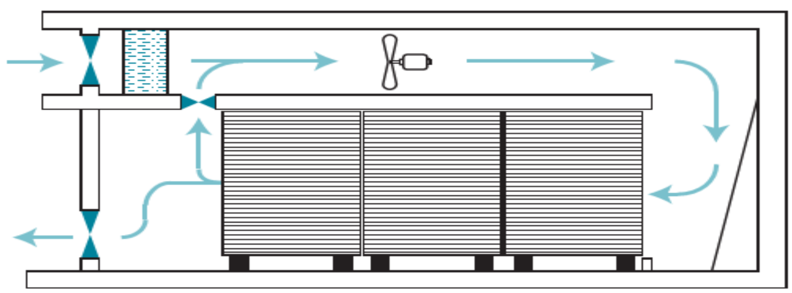

Figure 6: Fruit dryer using geothermal energy in Los Azufres, Mexico (Nguyen, 2015)

Indonesia has the greatest potential geothermal resources in the world. Geothermal energy can be used to dry several of the crops available in the area, such as coffee berries, tea, rough rice, beans and fishery products. A specially designed geothermal dryer (Figure 7) is being used to dry beans and grain in the *Kamojang* geothermal field of *West Java*. Geothermal steam from a well, at about 160 °C, is used to heat air for the drying process. The air is blown through a geothermal tube-bank heat exchanger where it is heated before being blown into the drying chamber, consisting of four trays. The heat transfer rate in the geothermal exchanger is one kW. The air flow velocity ranges from 4-9 m/s and the drying temperature from 45-60 °C. The drying time depends on the moisture content of the raw material.

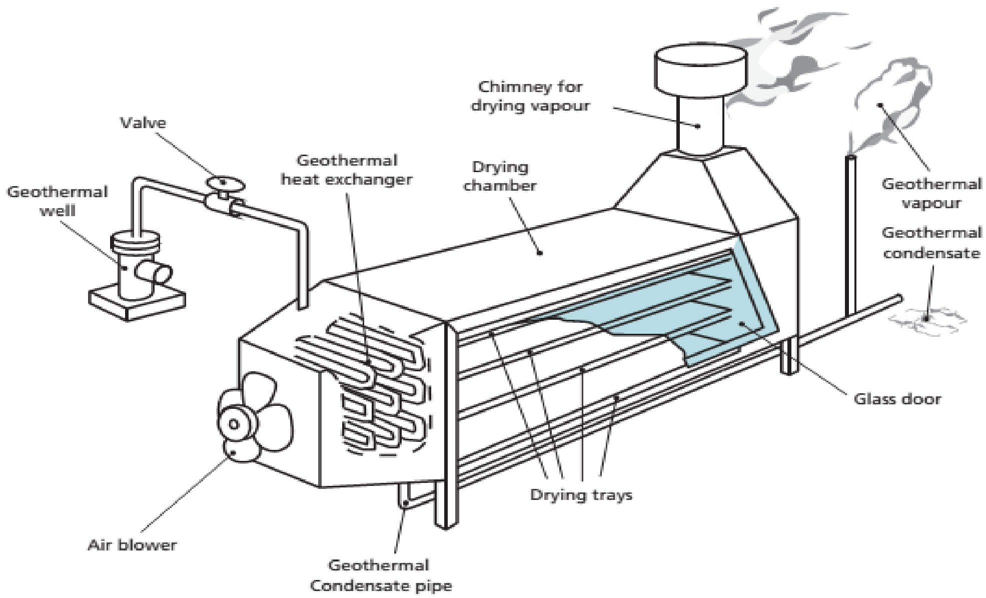

Figure 7: Geothermal dryer for drying beans and grains (Nguyen, 2015)

Example of food drying in developed countries such as in *Western Nevada, United States of America*, is a large-scale onion and garlic drying facility. Continuous conveyor belt dryers approximately 3.8 m wide and 60 m long (Figure 8) are fed 3,000–4,300 kg/hr. of wet onions. The capacity of the dryers varies from 500 to 700 kg per hour of dried onions, reducing the moisture content of the onions from 85 to about 4 percent after 24 hours of drying.

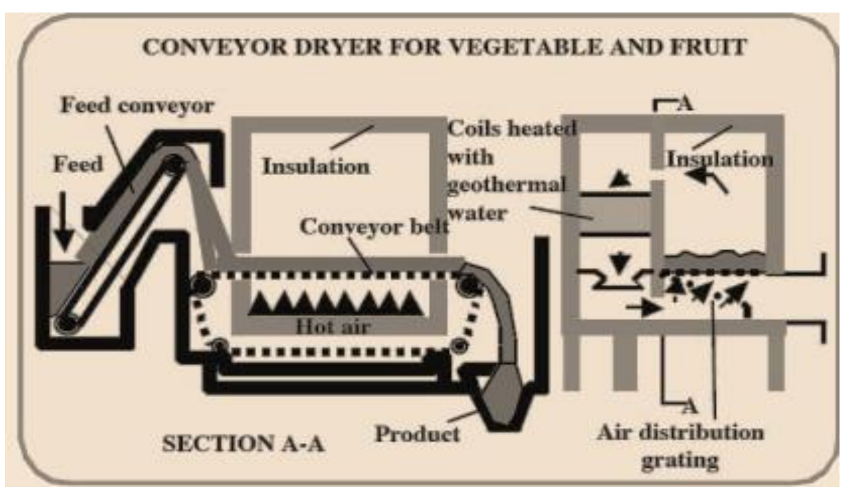

Figure 8: Conveyor dryer for vegetables and fruits (Sanja et al., 2011; Nguyen, 2015)

It is well known that grain drying consumes a significant amount of energy annually. These drying processes can easily be adapted to geothermal energy. A deep-bed dryer (batch dryer) commonly used for drying grains (Figure 9) consists of a fan that blows air through a geothermal heat exchanger, where it is heated. The hot air is then distributed uniformly to the product through the perforated floor. The temperature of the hot air is controlled by adjusting the flow rate of geothermal hot water.

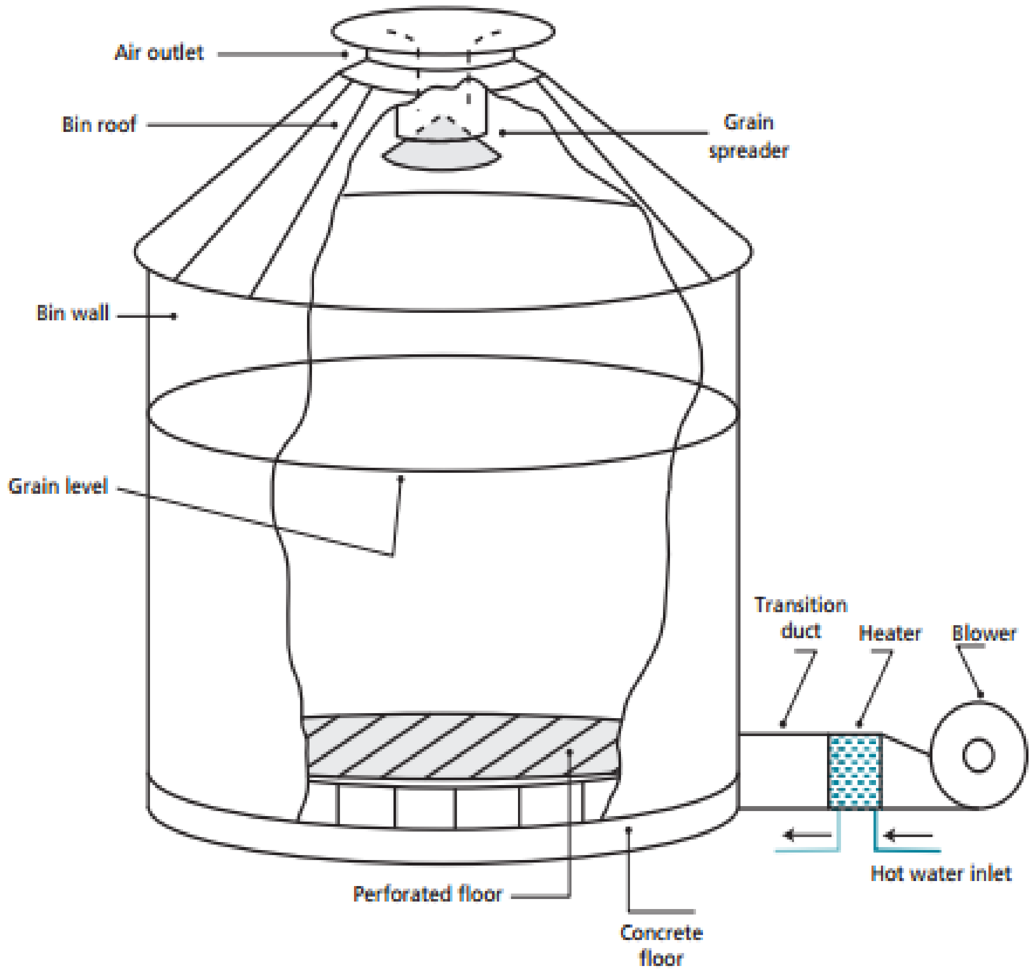

Figure 9: Batch grain dryer using geothermal energy (Nguyen, 2015)

Fish is dried in a two-step process: i) primary drying in a rack tunnel dryer (Figure 10) or conveyor dryer (Figure 11) for 24–40 hours at a drying temperature of 20–26°C, to reduce the moisture content from 80 to 55 percent; and ii) secondary drying in containers for three days at a temperature of 22–26 °C, resulting in a moisture content of about 15 percent.

The drying temperature of some grains can approach 90°C, but moderate temperatures of 50–60°C with relative humidity of about 40% is adequate for drying other product. For example, the drying temperature of coffee berries is about 50–60°C, that for rice must be maintained below 40°C to prevent cracking. The moisture content of dried grains should be in the range of 12–13 % to prevent mould growth and spoilage.

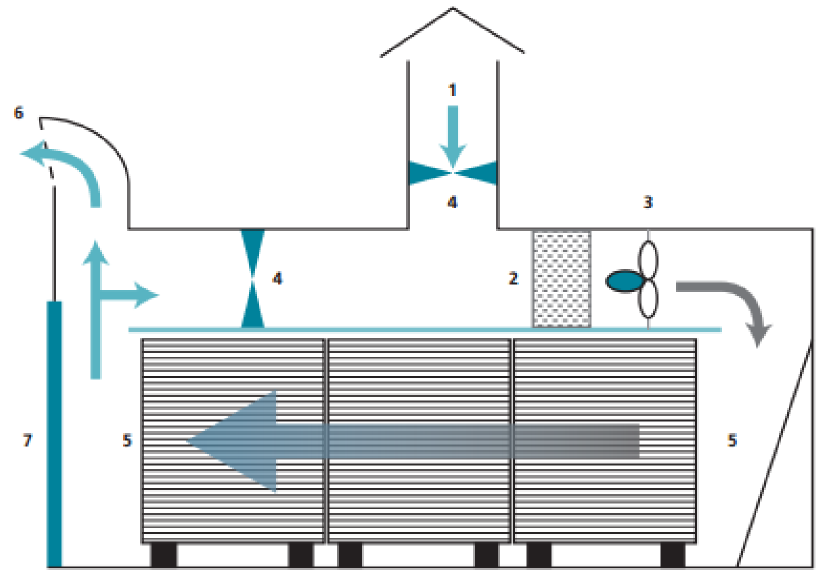

1. Air inlet
2. Geothermal heat exchanger
3. Fan
4. Adjustable valves
5. Pallets withtrays
6. Air outlet
7. Door

Figure 10: Rack tunnel dryer using geothermal energy for fish drying (Nguyen, 2015)

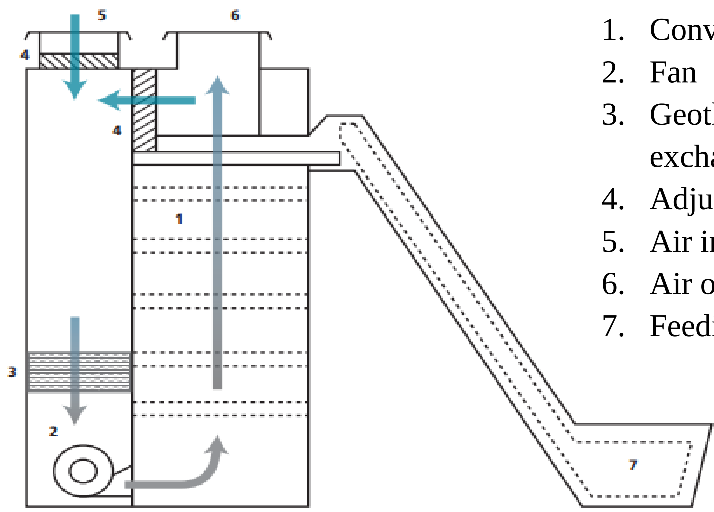

1. Conveyor
2. Fan
3. Geothermal heat exchanger
4. Adjustable valves
5. Air inlet
6. Air outlet
7. Feeding conveyor

Figure 11: Conveyor dryer using geothermal energy for fish drying (Nguyen, 2015)

An example of a large-scale industrial operation that uses geothermal energy is seaweed and fish drying in *Iceland*. Indoor drying has been applied for more than 35 years in regions where geothermal energy is available. Salted fish, cod heads, cod backbones, small fish and stock fish are among the products most commonly dried in this way. About 20 companies across Iceland dry fish using geothermal hot water and steam. One company drying seaweed has an annual capacity of 2,000–4,000 tons using geothermal hot water, and the drying of pet food is an emerging industry, with annual production currently about 500 tons.

Bączek, (2015) has made investigation on geothermal energy in VARS and concluded from his results that geothermal energy sources starting from temperature of 50 ^{o}C can be used in VARS and it leads to a reduction of electricity consumption and reduction of the negative impact of the cooling factors on the natural environment.

Geothermal energy supplies are generally more stable and accessible than those of other renewable resources such as wind and solar energy can be used to heat greenhouses while simultaneously providing freshwater to irrigate the greenhouse crops. Soil heating using geothermal sources inside a greenhouse makes it possible to extend the growing season and maintain a constant soil temperature to increase yields mainly to cultivate carrots and cabbages. This can be obtained by passing geothermal water through a grid of corrugated polypropylene pipes (Figure 12) spaced horizontally and buried to the ground at designed dimensions where the inlet and outlet of hot water is in the direction of arrow.

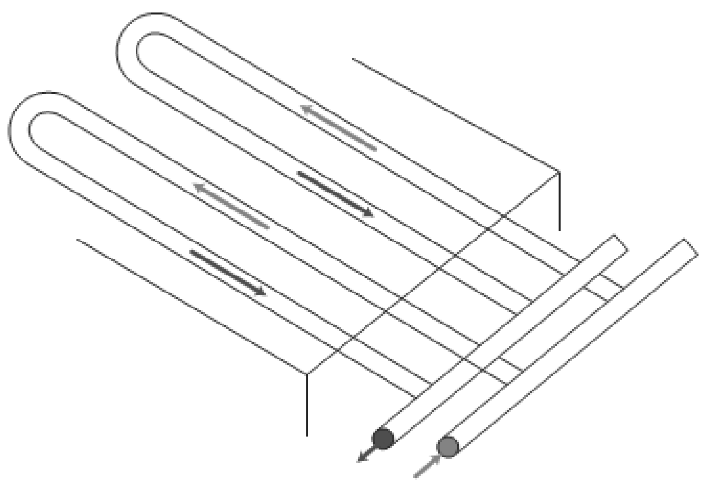

Figure 12: Heating pipe distribution for a soil warming system inside a greenhouse (Nguyen, 2015)

Furthermore, geothermal energy has been used in aquaculture (even in colder climates) in such way that freshwater exchanges heat with environmental friendly geothermal source to obtain suitable temperature for fish farming as shown in Figure 13.

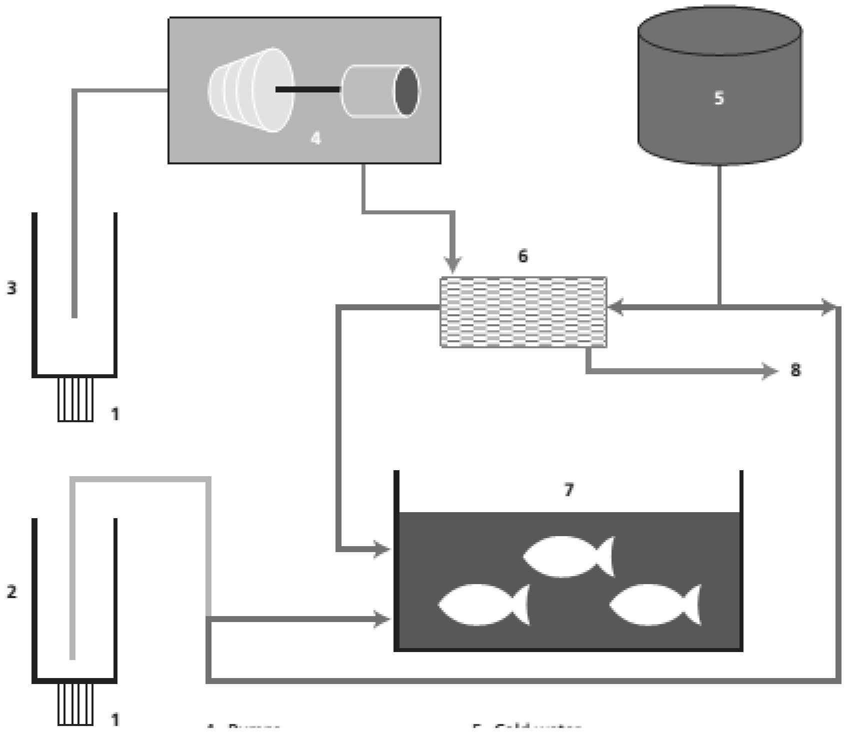

Figure 13: Fish farming using geothermal energy (Nguyen, 2015)

2.3. Development of geothermal energy applications in Ethiopia

According to energy sector report of Ethiopia, energy consumption in the country is low in terms of per capita, and underdeveloped in terms of structure. It is made up of less than 1% of electricity, about 5.4% of hydrocarbon fuels, and the rest percent is from traditional biomass fuels. Most of the petroleum products are consumed in the transport sector, whereas household energy comprises primarily of biomass fuels. About 40 million tons of fuel wood and 8 million tons of agro-residue are consumed annually. An important source of rural fuel supply is animal droppings.

The country currently has approximately 4,500 MW of installed generation capacity of which approximately 90% of the installed generation capacity is from hydropower while the remaining 8% and 2% is from wind and thermal sources respectively (Kassu, 2018). Geothermal share is contributed by the existing *Corbetti*, *Tulu Moye, and* Aluto Langano Geothermal Pilot Power Plants (Kebede et al., 2010).

The energy conversion efficiency of geothermal energies is low, at 10-15%, so that the released thermal energy is much larger than the obtained electrical energy. But thermal energy does not cost anything, so low energy conversion efficiency does not hurt. However, the total concession package agreed on between the Ethiopian government and the project stakeholders allows for the development of 1020 MW of geothermal energy at the respective sites (Yewendwossen, 2017).

As explained by Kebede & Solomon, (2016), Ethiopia has started long-term geothermal exploration in 1969 that its inventory of the possible resource areas within the Ethiopian sector of the East African Rift system, over the years has been built up, as reflected in surface hydrothermal manifestations. The inventory work in the highland regions of the country is not complete but the rift system has been well covered. Of the about 120 localities within the rift system that are believed to have independent heating and circulation systems, about two dozen, *Aluto-Langano* and *Tendaho geothermal field* are judged to have potential for high enthalpy resource development, including for electricity generation.

According to Kebede et al., (2010), detailed geological, geochemical and geophysical surveys were carried out in the Langano area during the late 1970s and early 1980s and based on the results showed, two wells (LA3 and LA6) drilled on Aluto volcano produced 36 and 45 ton per hour, geothermal fluid at greater than 300 ^oC along a fault zone oriented in the NNE-SSW direction. Two wells drilled as offsets to the West (LA4) and East (LA8) of this zone produced 100 and 50 ton per hour, respectively. As a result, a 7.3 MW pilot geothermal plant was installed in 1999 at Aluto Langano geothermal field as shown in Figure 12.

The Tendaho geothermal field (Figure 13) is another plant carried out in the Tendaho area with economic and technical support from Italy where, three deep wells about 2100 m and three shallow exploratory wells about 500 m being drilled and yielded a temperature of over 250 ºC can supply enough steam to operate a pilot power plant of about 5 MW, and the potential of the deep reservoir is estimated about 20 MW (Kebede et al., 2010).

Figure 14: One of the discharging wells (LA-3) of the Aluto-Langano Geothermal Field, total depth and maximum temperature of 2.3 km and 320°C, respectively (Kebede et al.,2010).

Abaya, Corbetti, Tulu Moye, Dofan and Fantale are more important areas where a number of prospects have been subjected to surface investigation: geology, geochemistry and geophysics and the shallow subsurface have been investigated by drilling at a few of the prospects.

2.1. Review on heat transfer and pressure drop characteristics of air flow over tube bank in cross flow

Heat transfer and fluid flow in tube bundles represents an idealization of many industrially-important processes. Cross flow heat exchangers are some of the processes in industry where through tube bundles (in-line and staggered arrangements of tubes as shown in Figure 29) either hot or cold fluid flow is supplied. Heat exchangers with tube bundles in cross flow are of a major operating interest in many chemical and thermal engineering processes (Ishak, 2013).

Ishak, (2013) studied that average Nusselt number, *NU* and therefore heat transfer coefficient, *h* increases with an increase in the free stream velocity, *V* of the air flow and the heat flux supply. Average Nusselt number, increases with increase in Reynolds number R_E, however, increasing linear pressure drop will affect the strength of joints of tubes. This increase may be due to variations in the air properties, as the air density decreases with an increasing temperature.

Prasetya, (2017) studied design of drying cocoa beans and concluded that the temperature during the drying process in the chamber should be maintained at constant temperature of 62 ^{o}C to avoid case hardening of the crop. However, this needs additional study as only maintaining chamber temperature would not be solution for the problem of case hardening.

Figure 15: One of the shallow wells (TD-5) of the Tendaho Geothermal Field, total depth and maximum temperature of 516 m and 253°C, respectively (Kebede et al.,2010).

2.2. Thermal properties of different crops

Quality of most of agricultural products and crops (*especially oily seeds*) are negatively affected by amount of moisture they contains and temperature they stored. Thermal properties of crops depend on these factors and therefore, they have to be known in order to develop the thermal processes and equipment needed for storage, drying, heating, and cooling (Ince et al., 2008). Some of thermal properties collected for some of agricultural product through different literatures are summarized in Table 2 and more details on this can be found in (ASHRAE, (2006).

Tomatoes

It can be consumed in the form of either fresh or processed in to another form such as into paste, puree, ketchup and powder. Tomatoes may be dried by sun but the end product is infested with dirt (Abdulmalik, (2014). Based on ASHRAE, (2006), heat capacity of mature green tomatoes is approximately C_{pp}= 4.02 kJ/kg.^{o}C.

Beans

It is a type of agricultural product that is to be consumed in original form as well as processed in to another form. The processed form of beans, its powder is used to prepare *shuro wot* in Ethiopia. From ASHRAE, (2006), heat capacity of beans is approximately C_{pp}=3.99 kJ/kg.^{o}C.

According to Firmansyah et al., (2018), the critical temperature in drying coffee beans is 50 °C. This is because the drying temperature above 50 °C can lead to physical phenomenon called case hardening which leads to damage coffee beans. The recommended temperature for drying is about 45 °C and the heat capacity of coffee, C_{pp}= 1.4 kJ/kg.^{o}C.

As per the studies done by Pimenta et al., (2018); Siagian et al., (2017) drying and storage conditions, can influence the quality of coffee beans and therefore, well-conducted drying can produce high-quality coffee. According to their literatures, high moisture content of coffee at matured stage (60-70%) can be removed using temperatures range of (40-60^{o}C). This consequently reduces the risk of infestation by microorganisms; reducing the occurrence of enzymatic fermentation, preserving quality and nutritive value, and ensuring germinate power.

Maize

Maize is an all-important crop which provides an avenue for making various types of foods. Every part of the maize plant has economic value: the grain, leaves, stalk, tassel, and cob can all be used to produce a large variety of food and non-food products.

According to Bola et al., (2013), initial moisture content of the matured maize (*with specific heat capacity approximately of 1.8 kJ/kg^{o}C*) to be dried is 35% and the final desired moisture content for the maize to preserve without damage is 13%. In addition, Arku et al., (2012) studied and concluded that specific heat capacity of maize is found in the range from 1.6891-3.2247 kJ/kg. ^{o}C.

2.3. Vapor compression versus Vapor absorption refrigeration system

In VCRS saturated vapor refrigerants are used to be compressed in the compressor by means of mechanical work input in expense of high grade energy (electricity). Ideal vapor-compression refrigeration cycle (P-h and T-s diagram shown in Figure 16) contains four of the steady-flow processes with basic assumptions to be made.

One of the assumptions is that temperature of the refrigerant after expansion device drops below the temperature of the refrigerated space/medium. Therefore, to have heat transfer at a reasonable rate, a temperature difference of 5-10°C should be maintained between the refrigerant and the medium to be freeze (Boles et al., 2006).

Another form of refrigeration, which becomes economically attractive when there is a source of inexpensive thermal energy (*such as geothermal, solar, and waste from cogeneration or process steam*), involves the absorption of a refrigerant by a transport medium (*absorbent*) where liquid is compressed instead of compressing vapor and the working principle of this system is discussed in chapter three.

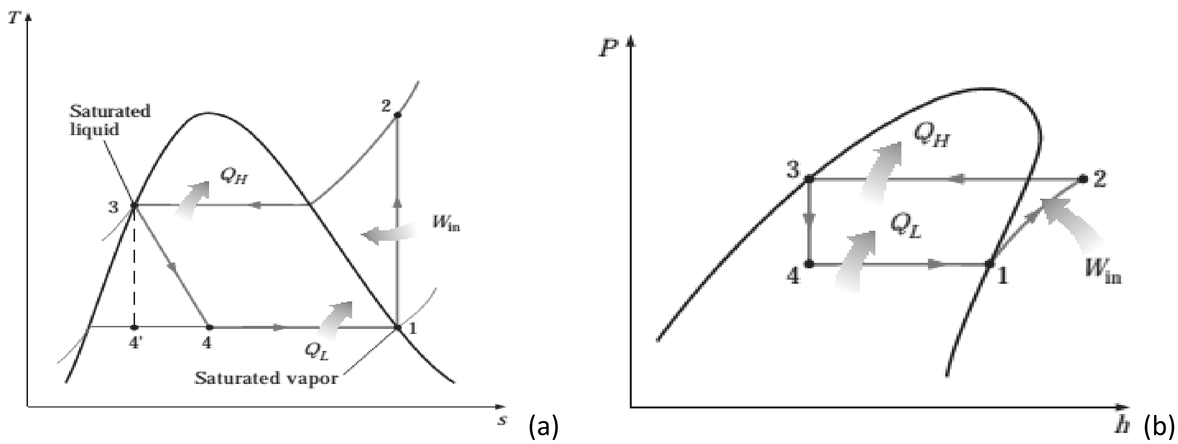

Figure 16: T-s (a) and P-h (b) ideal vapor-compression refrigeration cycle diagram.

Vapor compression system is similar with absorption refrigeration system whereas the only difference between them is compressor of the former is replaced by absorber, solution pump and generator of the later as shown by hidden block in Figure 31.

Since mid-17th century between the two World wars, which was marked by the disclosures of the two companies in the field of refrigeration; Electrolux in Sweden and Servel in the USA, many working fluid pairs are considered for absorption systems of which over 40 refrigerant compounds and 200 absorption compounds have been developed as indicated in the comprehensive study by (Srikhirin et al., 2001; Labus et al., 2012; Ullah et al., 2013).

According to Labus et al., (2012), in the last three decades following the Montreal and Kyoto protocol due to increase in depleted area of ozone hole that was being reported as grown from 1.1 km^2 in 1979 to 22.4 km^2 in 1987 by NASA, (2019), absorption technology has become more prominent as a possible alternative to the protection of ozone layer depletion. The use of environmental friendly working fluids and low grade energy makes this equipment very interesting for further research and development.

Nevertheless, currently the most common working fluids with practical application in absorption systems are H_2O-NH_3 and LiBr-H_2O. A water-lithium bromide pair, which has been used in absorption equipment since 1950s, has the advantages of high safety, volatility ratio, affinity, stability and latent heat. However, the minimum chilled water temperatures in the absorption system with H_2O-LiBr is around 5°C since water (*refrigerant*) freezes at below 0°C and require very low pressures (*vacuum*).

In other hand, ammonia-water pair, which has been in use since the 18th century is used for refrigeration applications in the range from 5ºC down to -60 ºC (Labus et al., 2012). However, Corrosive property of ammonia to metals such as copper and copper alloys, as reviewed by Srikhirin et al., (2001) and Ullah et al., (2013), inhibits the use of copper tubes which is widely available in the market.

Happening of corrosion when temperature of generator more than 200 ^{o}C, limitation in using for moving operation (locomotives and fishing boats) because of flowing problem, and complexity of its design when dephlegmator (or use of rectifier as ammonia-water pair is volatile) in the generator required are challenges over its wide applications as discussed by (Ullah et al., 2013).

2.4. Vapor absorption system powered by different sources of energy

Based on Ullah et al., (2013), 35% percent of incident solar powers falling on a formal photovoltaic collector generate electricity in a silicon-based PV system where, 65% of it is converted into heat energy. In contrast, it is described that a thermal system is capable of absorbing more than 95% of incident solar radiation, depending on the medium. This is one of the reasons that make great attention on thermally driven refrigeration system.

Many authors such as Anand et al., (2016) and Vazhappilly et al., (2013) have extensively analyzed the utilizations of process steam and exhaust gases from engine respectively to vaporize the ammonia refrigerant as alternative sources of heat input to the generator.

The results obtained by Anand et al., (2016) show that COP along with *exergy efficiency* increases with the heat source temperature at constant evaporator, condenser, and absorber temperature. In addition to this, another result has been obtained being COP as well as exergy efficiency increases with an increase in the evaporator temperature at constant generator, condenser, and absorber temperature.

Also results from thermodynamic analysis of ammonia–water absorption system using solar energy done by *Srikanth et al., (2012)* indicate that, the COP of cycle slightly decreases by increasing the concentration of ammonia at constant generator temperature and pressure.

2.5. Agricultural Products and Existing Drying Systems in Gedeo and Gujji Zones

These two ethnic groups were engaged in different but complementary economic activities, with the Guji being agro-pastoralists and the Gedeo settled agriculturalists. Their economic activities and sharing of separate ecological niches enabled them to create a kind of symbiotic relationship. Even in some conflicts, they co-existed by resolving disputes locally using customary conflict resolutions.

These two Cushitic groups (people of Gede'o and Guji) mainly are depend on *ensete* as their basic staple in securing degree of food but grow mixture of crops such as Maize, wheat, barley, haricot beans, fruits, coffee and some vegetables depending on land elevation (Kanshie, 2002; Wu, 2018). Open sun drying process of removing moisture is the common traditional drying method used in these societies to dry coffee and other crops.

2.6. Conclusions from Literature Reviews

2.6.1. Heat and Mass Transfer of Drying Systems

Generally, from all the dryer types briefly explained during the reviews of literature, it can be concluded as; in order to attain the final required moisture of the agricultural products in the compartments, air states can be summarized in to three.

Atmospheric air coming through inlet at state (1) with ambient conditions exchanges heat with hot geothermal sources flowing across (1'-2'). After convective heat transfer in the cross-flow heat exchanger (1-2), heated air then contains enough energy to remove moisture contents of the products in the drying compartments in the form of mass transfer (2-3) as shown in Figure 17.

Chilies and garlic dryer of Figure 4 with 10.5 m^3 compartment volume can holds 450 kg of chillies or 220 kg of garlic. Cross flow heat exchanger occupying the volume of 0.015 m^3 converts atmospheric air temperature to 70 °C for chillies and 50 °C for garlic. For this system energy rate of 36 kW and 0.98 kW in case of chillies and garlic, respectively should be transferred from 80 ^{o}C circulating hot source.

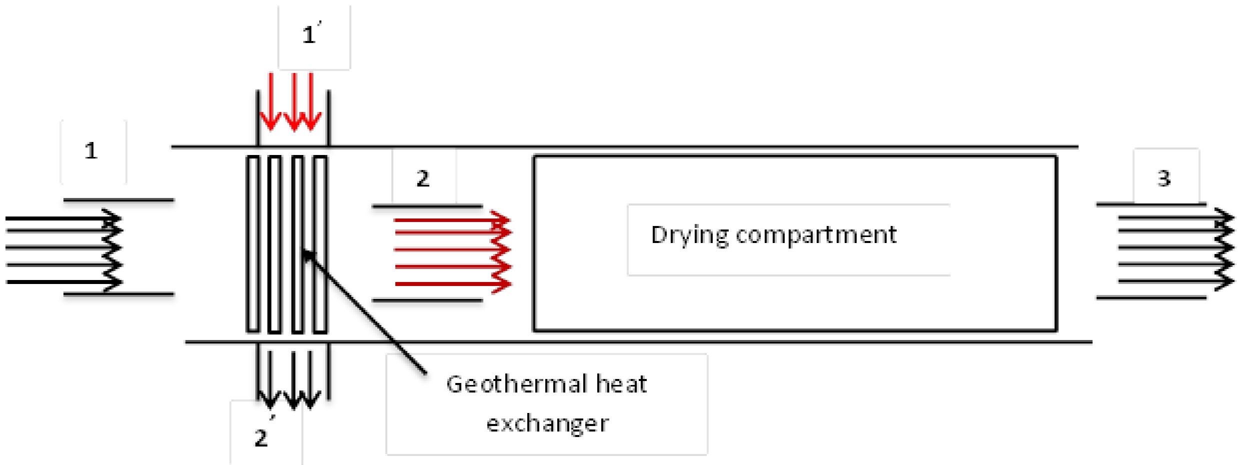

Figure 17: The working principle of drying system

Rice dryer of Figure 5 designed for 10 tons with heat transfer rate of 1360 kW. In this area, ambient air of 15°C with 60% relative humidity is heated to about 35°C in cross flow heat exchanger. Hot source is changed from 75 to 50°C to decrease the moisture content of rice from 20-14 % and then air-cooled.

A fruit dryer of Figure 6 designed by *Lund and Rangel* has the volume of 12.42 m^3 made of concrete walls, a timber ceiling and roof, and a reinforced concrete floor has a capacity of about 1000 kg of fruit per 24 hours and energy rates of 10 kW at geothermal water flow rate of 0.03 kg/s.

One kW of heat transfer in tube-bank heat exchanger of beans and grain dryer of Figure 7 operating at geothermal steam from a well, at about 160 °C is used to heat air from atmospheric conditions to 45-60 ^{o}C. Air flow velocity across cross flow ranges from 4-9 m/s and drying time depends on the moisture content of the raw materials.

Calculating logarithmic mean temperature difference in tube bank heat exchanger is compulsory along with energy conservation. Thus, rate of heat removed from geothermal hot fluid in heat exchanger is equals to amount of heat added to air flowing across the bank. In addition, mass conservation principle should be applied to mass transfer from materials in the compartment to heated air in the form of moisture removed.

From above systems it can be concluded that the same volume of compartment can hold different amounts of mass of different products. In addition, different types of agricultural products requires different rates of hear energy transfer and hot source flow rates. The dryer can be used in any weather conditions.

Furthermore, it has also been identified from the previous systems that different crops (agricultural products) require different drying temperatures and other properties of some of the products have been discussed. Thermal properties of agricultural product shown in Table 2 are basic parameters required in the design analysis of dryer.

It has to be remembered that if a refrigerated space is to be maintained at 16 °C, for example, the temperature of the refrigerant in the evaporator should be maintained at about 5 °C (*the case of design of this paper*).

Table 2: Thermal properties of some agricultural products

No.	Crop types	Thermal properties			Reference(s)
		Specific heat, (kJ/kg^{o}C)	Conductivity, (W/m^{o}C)	Diffusivity, m^2/s (10^{-7})	
1.	Tomatoes	4.02	-	-	*Ashrae, (2006*)
2.	Coffee	1.4	-	-	*Ashrae, (2006*)
3.	Maize	1.6891 - 3.2247	-	-	*Ashrae, (2006*), Bola et al., (2013)
4.	Beans	3.99	-	-	*Ashrae, (2006*)
5.	Corns	1.4868 - 2.4224	0.1194 - 0.2474	1.111 - 1.371	*Ince et al.,(2008*)
6.	Soybean	1.3934 - 3.1976	0.0980 - 0.2276	0.8268 - 1.496	*Ince et al.,(2008*)
7.	Sunflower	0.8649 - 1.9302	0.0929 - 0.2099	2.325 - 3.695	*Ince et al.,(2008*)
8.	Wheat	1.0792 - 5.5336	-	-	Cao, (2010)

2.7. Research Gaps

Dryer and vapor absorption refrigeration systems reviewed so far were analyzed only for thermal energy with high temperature values. But, analyses of dryer powered by geothermal sources of 50^{o}C have never been done.

Different literatures on the developments of geothermal energy direct applications in Ethiopia shows that no analysis has been made on different types of thermal systems powered by geothermal energy in the country.

CHAPTER-THREE

DATA COLLECTIONS AND ANALYSES OF THE TWO SYSTEMS

3.1. Data Collections

3.1.1. Day and night temperature data of hot springs

Although temperature values are the subjects of the study, other measurements were also taken repeatedly for “Barsiso” hot springs (near Dilla) were on turbidity, p^H, conductivity, and temperature. An instruments/devices used for measurement are shown in Figure 18. But, only temperature measurement of “Wallame” hot spring was taken.

Nephelometer or turbidimeter (a) measure turbidity of water in *FNU* (Formazin Nephelometric Units), P^H meter was used to measure acidity/basicity of water (b) Conductivity, the ability of

(a)

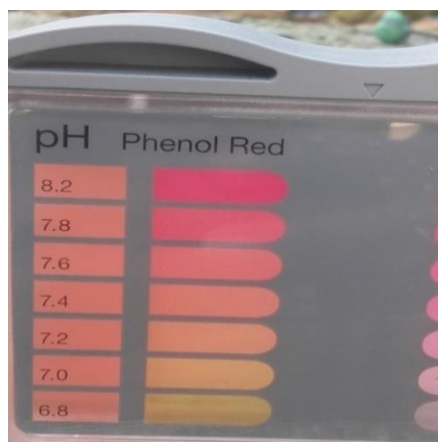

(b)

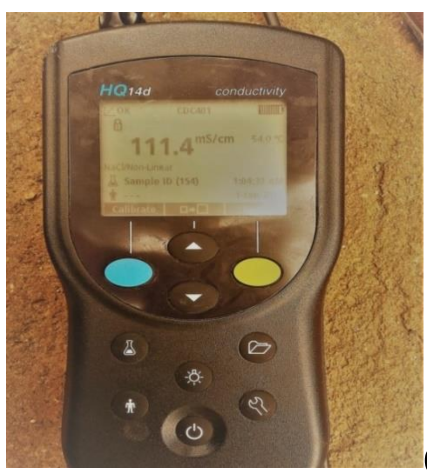

(c)

Figure 18: Instruments used for measurements of water properties

water to conduct or transmit heat, electricity, or sound in *ms/cm* (*millimhos per centimeter*) (c) as shown in Figure 18 were used in collecting measurements.

It was measured from Barsiso/Chombe that 7.4, 1.23 FNU, 111.4 ms/cm, and 54 ^oC (*average*) for p^H, turbidity, conductivity, and temperature, respectively. The average temperature measurements of Wallame show that 88.25 ^oC of the source. Daily and hourly temperature data recorded for these springs and presented in Appendix B-4 & B-5 are also shown from Figure 19-23.

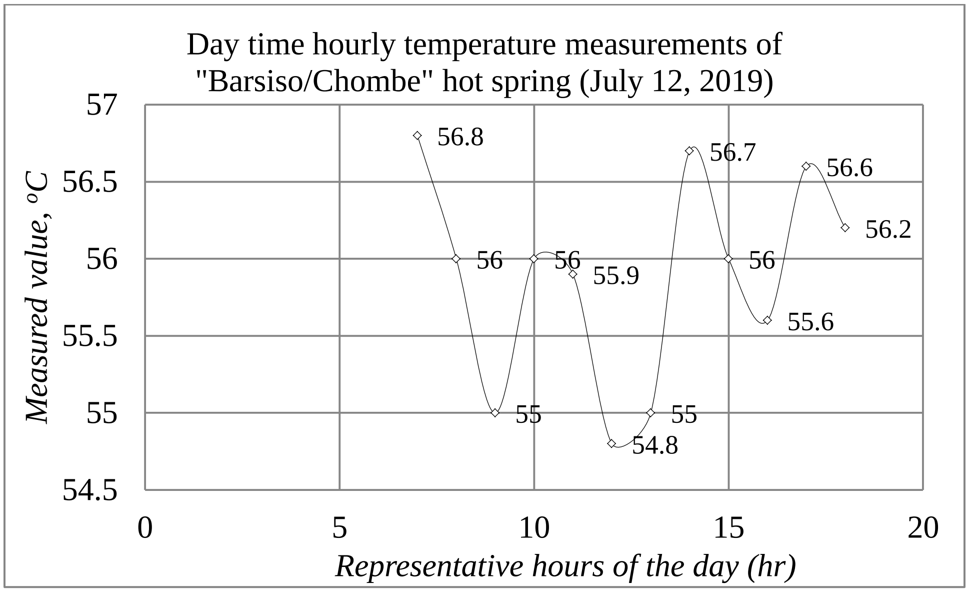

Figure 19: Day time temperature measurement of "Barsiso/Chombe" hot spring

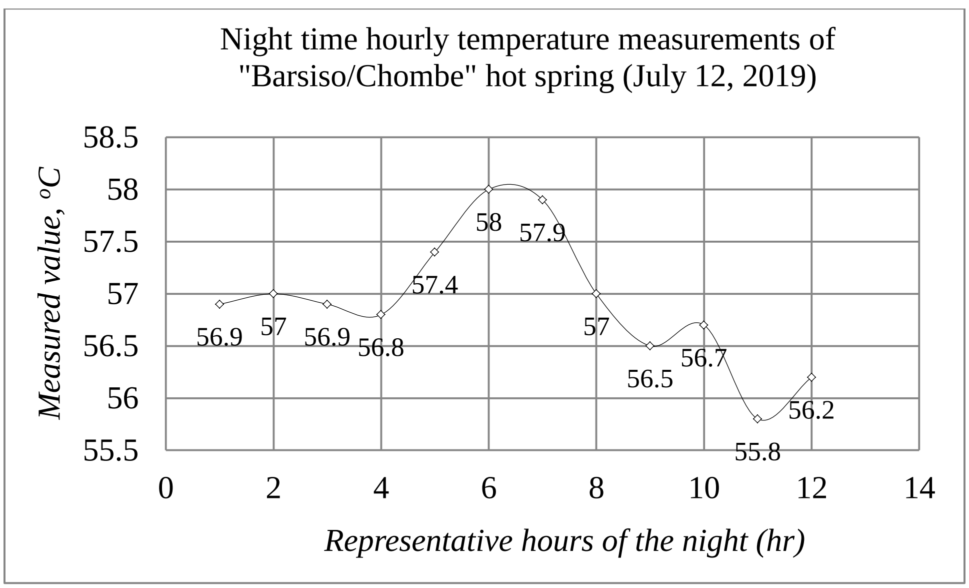

Figure 20: Night time temperature measurement of "Barsiso/Chombe" hot spring

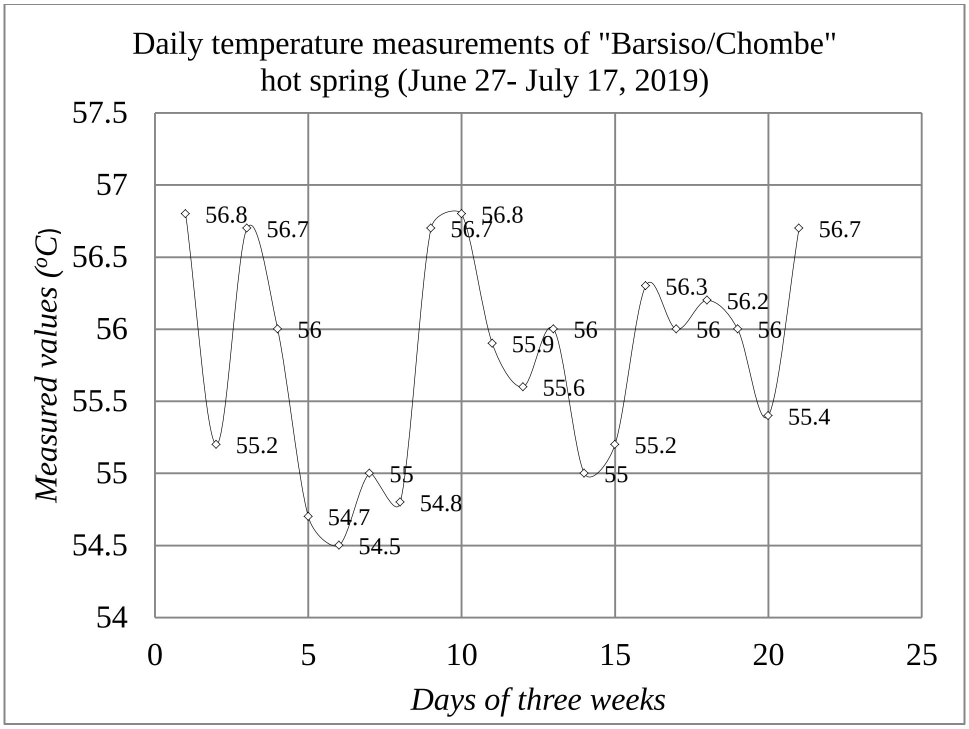

Figure 21: Daily temperature measurements of "Barsiso/Chombe" hot spring for three weeks

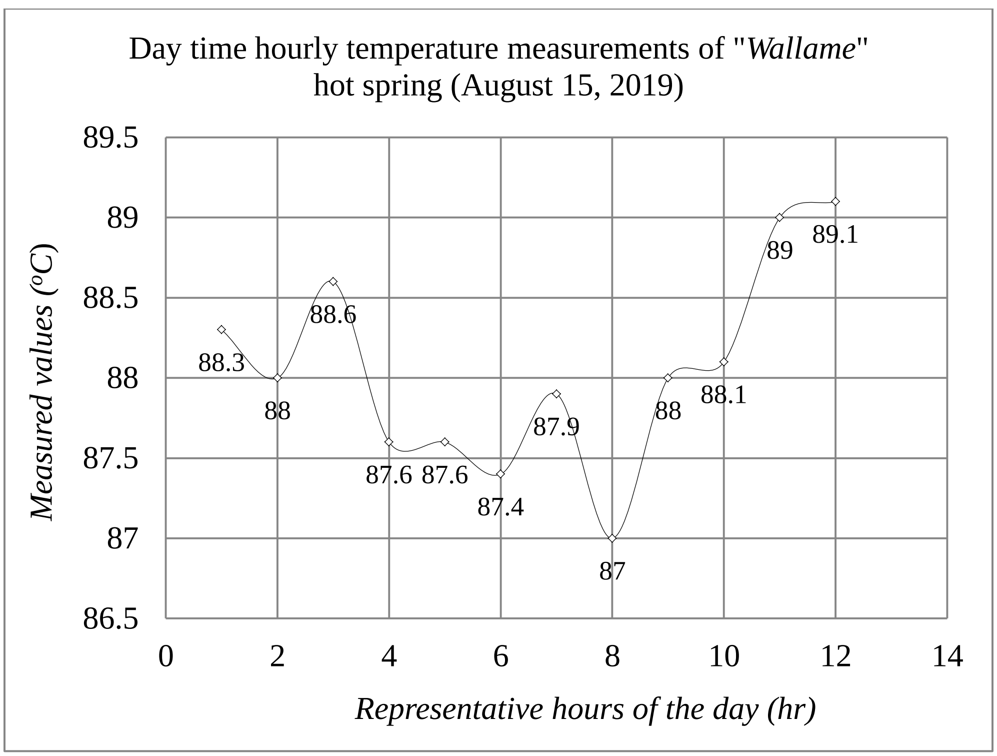

Figure 22: Day time temperature measurement of "Wallame" hot spring

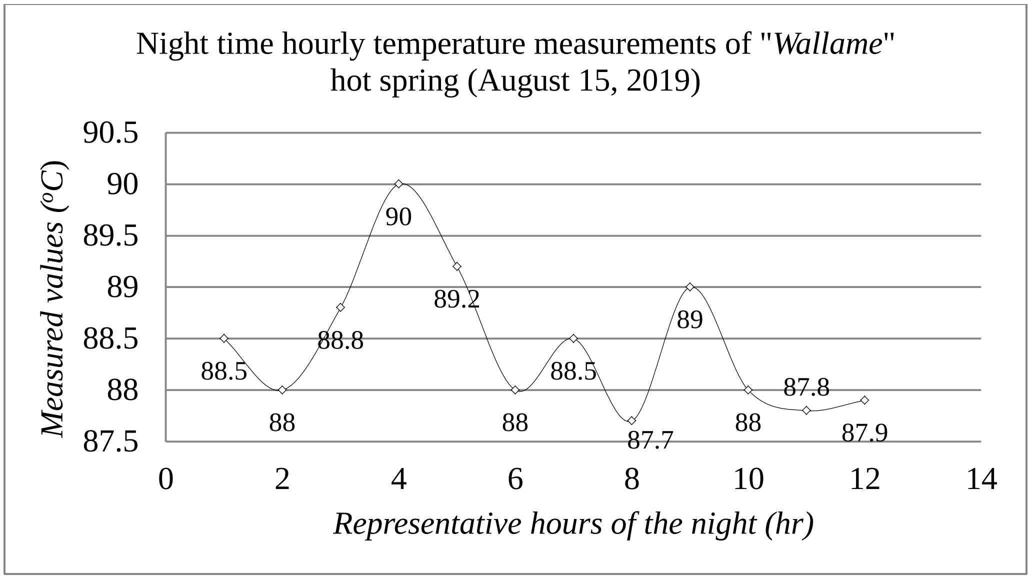

Figure 23: Night time temperature measurement of "Wallame" hot spring

3.1.2. Water and meteorological data

Quantifying climatic data have great effect in load calculations in the design of thermal systems such as refrigeration, air-conditioning, and drying system. Weather data of environment for Dilla are collected from Meteorological agency and drinking water temperature measurements of the University are taken for about three weeks. Averaged daily temperature data recorded at the water faucet are given in figure 24.

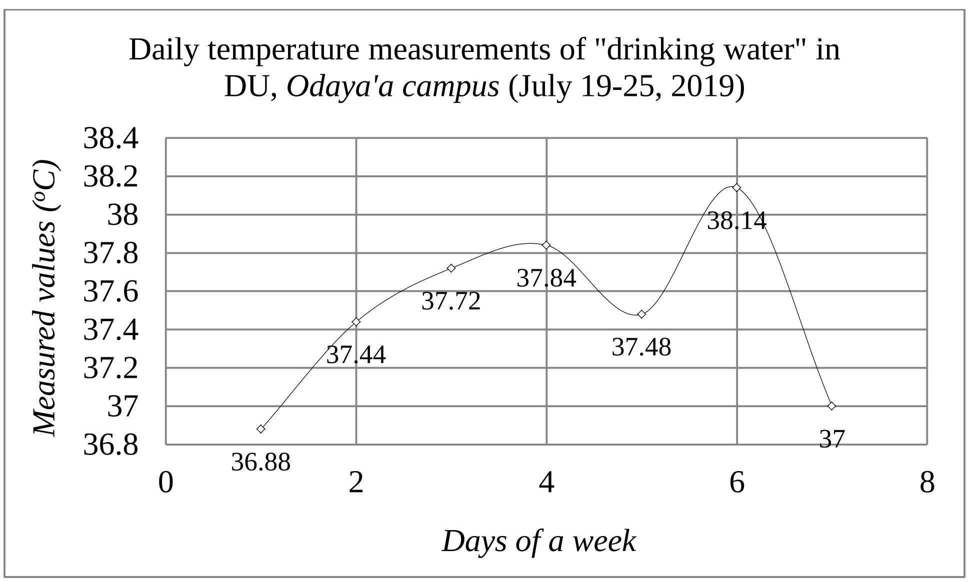

Figure 24: Daily temperature measurements of "drinking water" in DU, Odaya'a campus

Ambient air of the area has an average value of temperature 20.5 ^{o}C, wind speed 0.6 m/s, and relative humidity of 58% whereas average temperature of drinking water was about 37 ^{o}C and tabulated in (Appendices B-1 up to B-5).

3.2. Thermodynamic analysis of drying system

3.2.1. Heat transfer in flow across single hollow cylinder and tube banks

First part of this project deals with the design of drying system, the system which uses heat energy available in the geothermal water. Ambient air is forced by the help of fan across the tube banks through which hot water is flowing. Shape of dryer as shown in Figure 25 is selected for its simplicity in construction and design analysis.

Generally, working principle is in such way that ambient air is forced to pass across tube bank heat exchanger and heat transfer from geothermal water to air happened. Now, these air will take out the moisture from crops (agricultural products) placed on sieved shelving drying compartment.

Heat transfer coefficients in tubes of shell-and-tube heat exchanger involve both internal flow through the tubes and external flow over the tubes. So the analysis of both flows is required in the design of heat exchanger of such type.

Consider the control volume around a single tube with inlet and outlet conditions as shown in Figure 26 that has elements of internal flow convection (the heating water), external flow convection (cross flow of air over a tube), and conduction heat transfer (through the tube wall).

This may be modeled by use of a circuit analogy as applied to the heat transfer relations as shown in Figure 27, from which heat transfer rate may be computed by equation (1) using given inlet air & water temperatures and equivalent resistances of an equations (2-5).

$$\dot{Q} = (T_{w,\ hot\ in} - T_{a,\ cold\ in})/R_{eq} \tag{1}$$

$$R_{eq} = R_{air} + R_{wall} + R_{hot,\ w} \tag{2}$$

Air side thermal resistance $R_{air} = 1/(h_{air}A_{out})$ (3)

Wall conducting resistance $R_{wall} = \ln\left(\frac{d_{out}}{d_{in}}\right)/2\pi k_{wall}L$ (4)

Water-side thermal resistance $R_{hot,\ w} = 1/(h_{water}A_{in})$ (5)

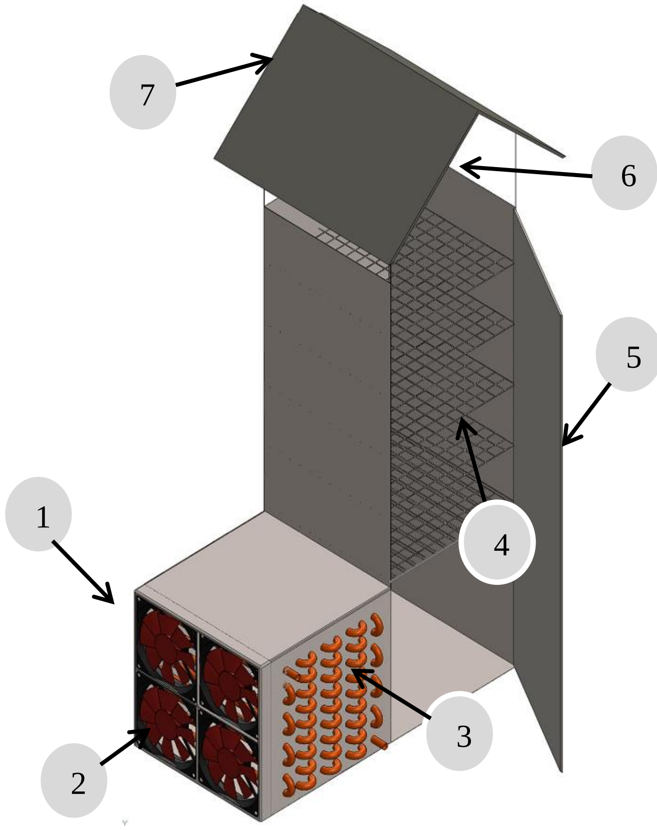

1. Inlet
2. Fans
3. Tube banks (heat exchanger)
4. Shelving (trays)
5. Door
6. Outlet
7. Lid (tap)

Figure 25: The three dimensional view of drying system

Because of the complexity of the flow patterns, it is difficult to handle analytical investigations for such the flow across tube. This has been studied by numerous investigators and only correlations for the average heat transfer coefficients have been developed experimentally.

Average Nusselt number correlations Nu for a flow of different Reynolds number across the tube, by Churchill and Bernstein as studied by Bergman et al., (2011) are given in equations (6-8).

$$\mathrm{Nu} = 0.3 + \frac{0.62 R_E^{1/2} P_r^{1/3}}{[1+(0.4/P_r)^{2/3}]^{1/4}}\left[1+\left(\frac{R_E}{282{,}000}\right)^{5/8}\right]^{4/5} \quad (6)$$

Where, Reynolds number $R_E > 400{,}000$ and P_r is Prandtl number (*at mean temperature*)

$$\mathrm{Nu} = 0.3 + \frac{0.62 R_E^{1/2} P_r^{1/3}}{[1+(0.4/P_r)^{2/3}]^{1/4}}\left[1+\left(\frac{R_E}{282{,}000}\right)^{1/2}\right] \quad (7)$$

Where, $10{,}000 < R_E < 400{,}000$

$$\mathrm{Nu} = 0.3 + \frac{0.62 R_E^{1/2} P_r^{1/3}}{[1+(0.4/P_r)^{2/3}]^{1/4}} \quad (8)$$

Where, $R_E < 10{,}000$

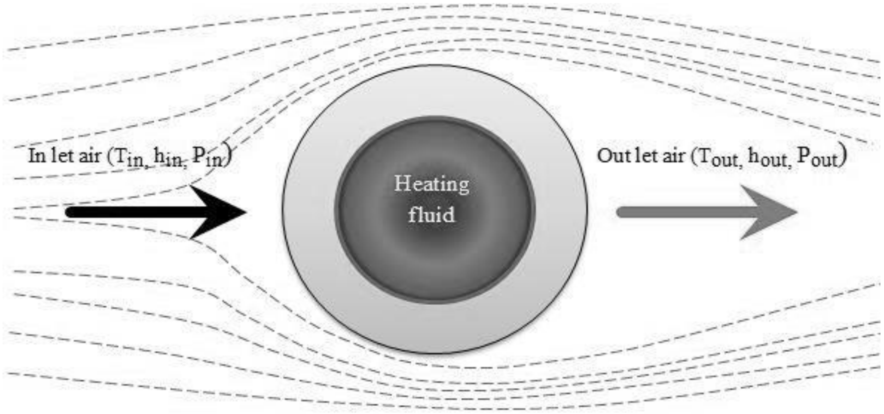

Figure 26: Control volume for the fluid flow over the tube.

Reynolds number can be calculated as given in equation (9) where the characteristics diameter of cylindrical tube is to be taken as outer diameter of the tube.

$$R_E = VD/\nu \quad (9)$$

Where, V is uniform velocity of fluid approaching the tube (*m/s*).

D is characteristics diameter and v is dynamic viscosity of flow (m^2/s).

It is known that the boundary layer remains laminar for about $R_E = 2x10^5$ but turbulent for the Reynolds number greater than this. The fluid approaching the tube branches out and encircles the cylinder, forming boundary layer that wraps around the cylinder as shown in Figure 26. The fluid particles will became a complete stop at stagnation point, where high pressure created and the pressure will decrease with flow direction while fluid velocity increases.

The nature of the flow across cylinder strongly affects the total drag coefficient, C_D (both *friction drag* and the *pressure drag* can be significant). The high pressure at stagnation point and the low pressure on the opposite side in the wake produce a net force on the body in the flow direction that need to be considered during design of fixing tube banks.

In addition to equations (6-8), empirical correlations for the average Nusselt number for forced convection across the cylindrical tube and non-cylindrical structure, by *Zukauskas and Jacob*, are given in Table 3.

Heat transfer surface area A_S for single cylindrical tube is as given in equation (11) and the rate of heat transfer $\dot{Q}$ can be determined from the Newton's law of cooling as given in equation (12) and the properties of fluid will be evaluated at mean temperature, T_f given by equation (10).

$$T_f = (T_S + T_\infty)/2 \tag{10}$$

$$A_S = \pi DL \tag{11}$$

$$\dot{Q} = hA_S(T_S - T_\infty) \tag{12}$$

Where, T_S is surface tube temperature in ^oC, T_∞ is air stream temperature in ^oC, L is tube length in m, h is average heat transfer coefficient in $W/m^2.K$ or ($W/m^2.^oC$).

Table 3: Empirical correlations for the average Nusselt number (Boles, 2006).

Cross-section of the cylinder	Fluid	Range of Reynolds number	Nusselt number correlations
Circle 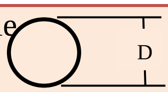	Gas/liquid	0.4-4 4-40 40-4000 4000-40,000 40,000-400,000	$Nu=0.989Re^{0.330}Pr^{1/3}$ $Nu=0.911Re^{0.385}Pr^{1/3}$ $Nu=0.683Re^{0.466}Pr^{1/3}$ $Nu=0.193Re^{0.618}Pr^{1/3}$ $Nu=0.027Re^{0.805}Pr^{1/3}$
Square 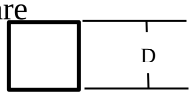	Gas	5000-100,000	$Nu=0.102Re^{0.675}Pr^{1/3}$
Square tilted 45^o 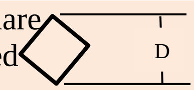	Gas	5000-100,000	$Nu=0.246Re^{0.588}Pr^{1/3}$
Hexagon 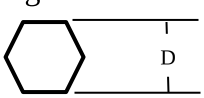	Gas	5000-100,000	$Nu=0.153Re^{0.638}Pr^{1/3}$
Hexagon tilted 45^o 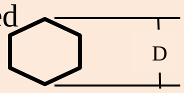	Gas	5000-19,500 19,500-100,000	$Nu=0.160Re^{0.638}Pr^{1/3}$ $Nu=0.0385Re^{0.782}Pr^{1/3}$
Vertical plate 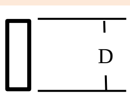	Gas	4000-15,000	$Nu=0.228Re^{0.731}Pr^{1/3}$
Ellipse 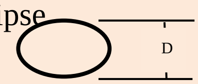	Gas	2500-15,000	$Nu=0.248Re^{0.612}Pr^{1/3}$

For example, if it is given that: 10-cm-diameter steam pipe at surface temperature of 110^{o}C, passing open area against the winds blowing at a velocity of 8 m/s at 1 atm and 10^{o}C. In order to determine *rate of heat loss per unit length*, equations (6), (7), and (8) in addition to suitable correlation from Table 3 can be used.

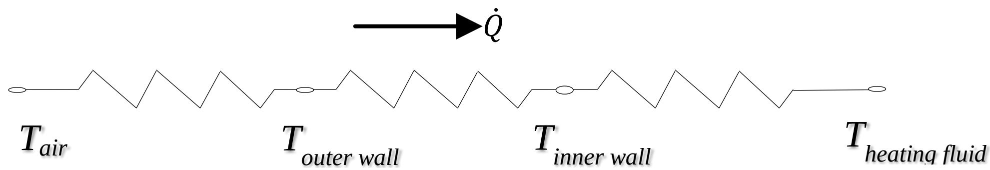

Figure 27: Equivalent resistance circuit analogy

Air properties are evaluated at mean temperature of 60^{o}C from (Appendix A-1), k = 0.02808 W/m.^{o}C, v = 1.896x10^{-5} m^2/s, Pr =0.7202. Reynolds number became, R_E = 4.219x10^4 and Nusselt number, Nu = 124. Evaluating values, Nu = (hD)/k, h=34.8 W/m^2.^{o}C and finally, $\dot{Q}$ =34.8(3.14) (0.1) (110-10) = 1.10 kW

Note that the equations presented so far were from the perspective of flow over a single tube. However, in the case of tube banks, the number of tubes per row (N_T) must be taken into account to determine the total heat transfer through that tube row.

Heat transfer to or from a bank (*or bundle*) of tubes in across flow is relevant to numerous industrial applications, such as steam generation in a boiler or air cooling or air heating in the air conditioning system. One fluid moves through the tubes while the other moves over the tubes in a perpendicular direction with velocity V. The geometric arrangement is shown schematically in Figure 28.

We have seen that heat transfer rate from hot fluid in the tube to the air flow across the tube depend of the Reynolds number of the flow, the Prandtl number of the flow, and a coefficients that are empirically determined based on the heat exchanger geometry and tube arrangements. These factors are used to determine the Nusselt number. The Nusselt number is used to calculate the convective heat transfer coefficient (*h*) which is used to quantify the heat energy transferred from the tube wall to air (*Q*).

Of the four heat transfer models; Grimison, modified Grimison, Zhukauskas, and the Kays & London models whose comparison done in Hammock, (2011), *Zhukauskas* model published in 1972 and has been reported to be accurate to within ±15% (between calculated and measured value) is selected as per design of drying sytem.

For the average convective heat transfer coefficient with tubes at uniform surface temperature, from experimental results more recently, *Zukauskas* has proposed correlations of the form:

$$\mathrm{Nu} = \frac{\mathrm{hD}}{\mathrm{k}} = \mathrm{C}(\mathrm{R_E})^{\mathrm{m}}(\mathrm{P_r})^{\mathrm{n}}\left(\frac{\mathrm{P_r}}{\mathrm{P_{rs}}}\right)^{0.25} \tag{13}$$

Where, P_{rs} = Prandtl number evaluated at tube surface temperature, C, m, and n are generic scalar variables depend on Reynolds number and tube arrangements or bank geometry.

Heat transfer relations based on empirical data for both arrangement types (*aligned and staggered*), including turbulent phenomena in the correlations (*such as vortex shedding*), are summarized in Table 4.

When tube banks are used in heat exchangers, the flow over the tubes in the second subsequent rows of tubes is different from the flow over a single tube. Even in the first row the flow is modified by the presence of the neighboring tubes. The extent of modification depends on the spacing between the tubes.

Due to this reason, the heat transfer also differs between a single tube and tube banks. It is for this reason that a correction for the number of tubes in the heat exchanger is presented. This correction is to account for the front-row tube being coated by a relatively smooth boundary layer formed by an undisturbed free stream; however, successive downstream tubes benefit from augmented heat transfer due to the eddies of the turbulent wake created by upstream tubes (Hammock, 2011).

Two arrangements of the tubes are aligned and staggered (Figure 29). If the spacing is very much greater than the diameter of the tubes, correlations for single tubes can be used. Correlations for flow over tube banks when the spacing between tubes in a row and a column is not much greater than the diameter of the tubes have been developed for use in heat-exchanger applications.

As per the scope of this study, the heat transfer relations for in-line arrays (*aligned*) tube arrangement are used in the analysis of heat transfer. It is clear that heat transfer from banks of tubes depends on the flow conditions, tube geometries, and tube arrangements.

Tubes are usually placed in a shell (thus the name called *shell-and-tube heat exchangers*). Arrangements of the tubes in the bank are characterized by the transverse pitch S_T, longitudinal pitch S_L, and the diagonal pitch S_D. As the flow enters the bank, the flow area will be reduced from A_1 to A_T between the tubes and then flow velocities increases.

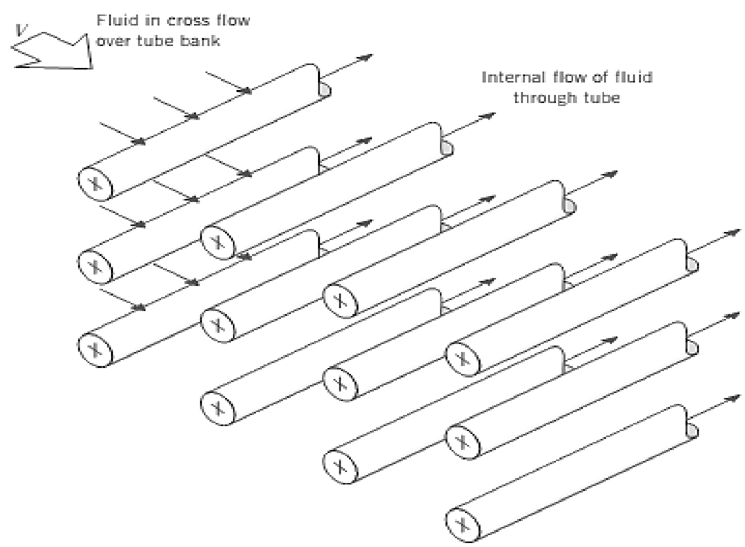

Figure 28: Schematic of tube bank in cross flow

$$A_1 = S_T L \tag{14}$$

$$A_T = (S_T - D)L \tag{15}$$

In staggered tube arrangement, the velocity may increase further in the diagonal region. Thus the flow is characterized by the maximum velocity created, and therefore the Reynolds number also evaluated at maximum velocity.

From conservation of mass requirement for steady incompressible flow; in the case of inline arrangement tube banks and staggered of $2A_D > A_T$, the maximum velocity is derived (Appendix A-6) and given in equation (16). Similarly, for staggered tubes arrangement of $2A_D < A_T$, the maximum velocity is derived (Appendix A-6) and given in equation (17).

$$V_{max} = V.\frac{S_T}{(S_T - D)} \tag{16}$$

$$V_{max} = \frac{S_T}{2(S_T - D)} V \qquad (17)$$

As known before, as long as Nusselt number and heat transfer coefficients calculated from correlations given in Table 3 and using equation 13, then heat transfer rate can be determined from newton law of cooling using equations 19 through 20.

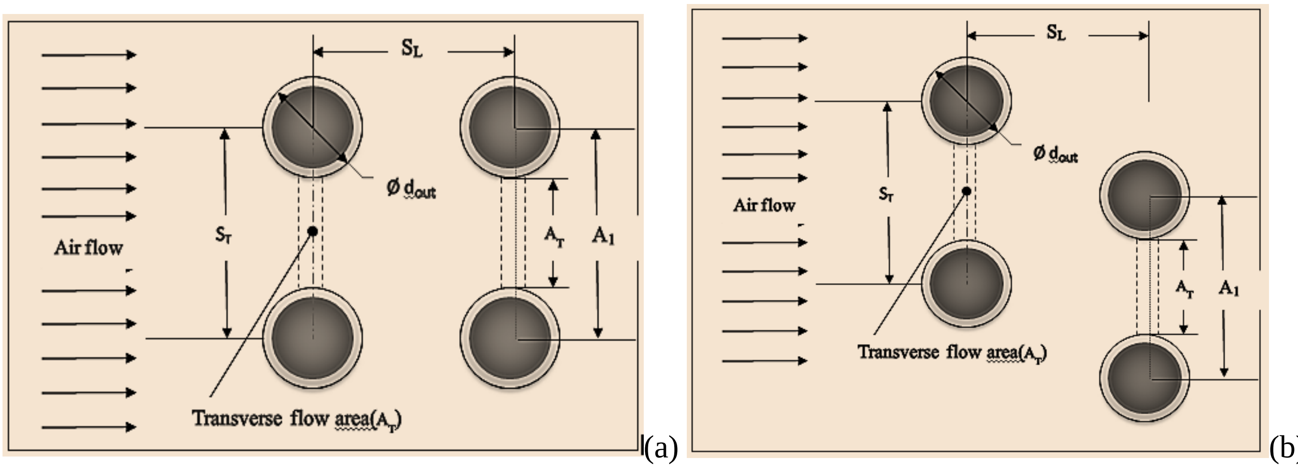

Figure 29: Aligned (a) and Staggered (b) tube arrangement free body diagrams

Table 4: Nusselt number correlations for cross flow over tube banks for $N_L > 16$ and $0.7 < Pr < 500$ by Zukauskas (Boles, 2006).

Arrangement	Range of Reynolds number	Correlations
In-line	0-100	$Nu = 0.9R_E^{0.4}\ Pr^{0.36}(Pr/Prs)^{0.25}$
	100-1000	$Nu = 0.52R_E^{0.5}\ Pr^{0.36}(Pr/Prs)^{0.25}$
	$1000\text{-}2\text{x}10^5$	$Nu = 0.27R_E^{0.63}\ Pr^{0.36}(Pr/Prs)^{0.25}$
	$2\text{x}10^5\text{-}2\text{x}10^6$	$Nu = 0.033R_E^{0.8}\ Pr^{0.4}(Pr/Prs)^{0.25}$
Staggered	0-500	$Nu = 1.04R_E^{0.4}\ Pr^{0.36}(Pr/Prs)^{0.25}$
	500-1000	$Nu = 0.71R_E^{0.5}\ Pr^{0.36}(Pr/Prs)^{0.25}$
	$1000\text{-}2\text{x}10^5$	$Nu = 0.35(S_T/S_L)^{0.2}R_E^{0.6}\ Pr^{0.36}(Pr/Prs)^{0.25}$
	$2\text{x}10^5\text{-}2\text{x}10^6$	$Nu = 0.031(S_T/S_L)^{0.2}R_E^{0.8}\ Pr^{0.36}(Pr/Prs)^{0.25}$

However, the average Nusselt number relations presented in Table 4 collected from Boles, (2006) are for tube banks with 16 or more rows. However, those relations can also be used for tube banks with rows less than 16 provided that they are modified as given by equation (18) where correction factor F from Boles, (2006) for flow with $R_E > 1000$ is given in Table 5.

$$N_{UD,NL} = F\, N_{UD} \tag{18}$$

Table 5: Correction factor F to be used in above equation from Zukauskas. (Cengel, 2004)

N_L	1	2	3	4	5	7	10	13
In-line	0.70	0.80	0.86	0.90	0.93	0.96	0.98	0.99
staggered	0.64	0.76	0.84	0.89	0.93	0.96	0.98	0.99

The total number of tubes taken for the analysis as per this thesis are ($N = N_L x N_T$=8x8= 64). Therefore, the heat transfer surface area, volumetric flow rate, and air mass flow rate are given in equations (19), (20) and (21), respectively. Logarithmic mean temperature difference in tube bank heat exchanger is calculated using equations (22), (22 a), and (22 b).

$$A_S = N\pi DL \tag{19}$$

$$\dot{V} = V(N_L \pi DL) \tag{20}$$

$$\dot{m} = \rho_i \dot{V} \tag{21}$$

$$\Delta T_{ln} = \frac{\Delta T_e - \Delta T_i}{\ln\left(\frac{\Delta T_e}{\Delta T_i}\right)} \tag{22}$$

$$\Delta T_e = T_{w,\ hot\ in} - T_{air,out} \tag{22 a}$$

$$\Delta T_i = T_{hot,\ out} - T_{a,\ cold\ in} \tag{22 b}$$

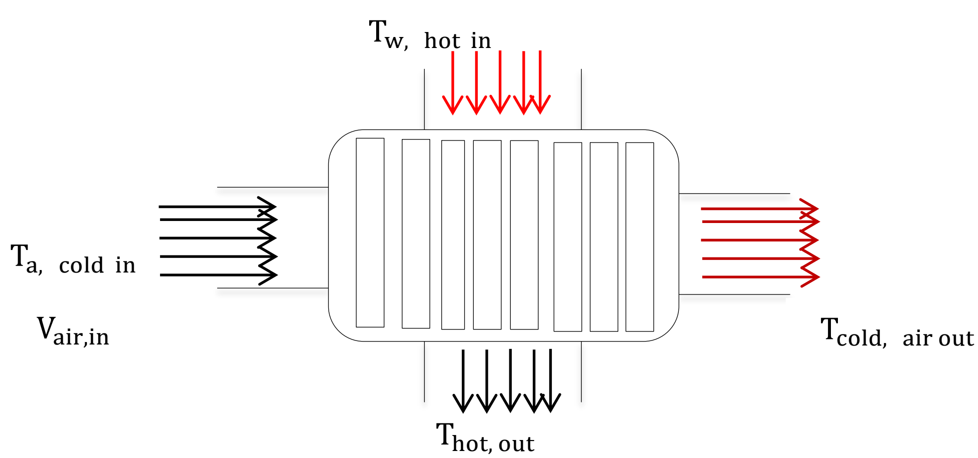

Figure 30: Free body schematic for tube bank heat exchanger (Top view)

Where, $T_{w,\ hot\ in}$ is tube surfaces temperature taken to be equal to hot inlet source temperature, $T_{air,out}$ is air exit temperature must be equal to the required temperature in the drying chamber

$T_{hot,\,out}$ is the exit hot water temperature that could be used for other purposes if cascade system is applied, $T_{a,\ cold\ in}$ is ambient air temperature.

Finally, heat transfer rate from tube bank to the air flowing across is given as equation (23). In other word, drying can be obtained through two stages, namely *heating* and *drying*. Therefore, heat energy required by crops/grains to be dried is their summation.

$$Q = hA_S\Delta T_{ln} \tag{23}$$

$$Q_D = Q_{heat\ up} + Q_{evaporate} \tag{24}$$

$$Q_{heat\ up} = m_p C_{pp}(T_{air,out} - T_{air,in}) \tag{25}$$

$$Q_{evaporate} = m_r h_{fg}/\mathrm{time} \tag{26}$$

$$Q_D = \dot{m}_a(h_{after} - h_{before}) \tag{27}$$

3.2.2. Pressure drops in the tube bank and pumping power

Major pressure loss, ΔP_{maj} of hot fluid flowing due to friction, inside the tube bank is calculated by Darcy-Weisbach equation which is valid for fully developed, steady-state, and incompressible flow given by:

$$\Delta P_{maj} = \lambda\rho_i L V_f^{\,2}/2d_i \tag{28}$$

Where, λ is Darcy-Weisbach friction coefficient, ρ_i is density of geothermal water, L is total length of tube, V_f is velocity of fluid, and d_i is inner tube diameter. The friction coefficient λ for not laminar flow can be calculated by the Colebrook equation as given in equation (29).

$$1/\lambda^{\frac{1}{2}} = -2\log[2.51/(R_E\,\lambda^{\frac{1}{2}}) + (k/D_h)/3.72] \tag{29}$$

Where R_E is Reynolds number of the flow, *k* = roughness of duct, pipe/tube surface (*m*), and D_h is hydraulic diameter (*m*).

In addition to the Moody-type friction loss computed for the length of pipe, curved structures will add additional head loss of the system called minor losses ΔP_{min} given by:

$$\Delta P_{min} = k_L\,V^2/2g \tag{30}$$

Where, local loss coefficients, k_L for different types of structures (*curves/ shapes*) are given in (Appendix A-14). As per the case of drying system design in this paper, this value is taken as 0.2. Based on the sum of two pressure losses ΔP_D, the mechanical power required, $P_{m,D}$ and then electrical power consumptions $P_{el,D}$ will be calculated using equations (32) and (33), respectively.

$$\Delta P_D = \Delta P_{maj} + \Delta P_{min} \quad (31)$$

$$P_{m,D} = (\dot{V}_h \rho g \Delta P_{dry})/3.6x10^6 \quad (32)$$

$$P_{el,D} = P_{m,D}/\eta_m \quad (33)$$

3.2.3. Parameters to be known

For the design of crop drying system, the parameters basically to be known, according to (Afuar et al., 2016), (Prasetya et al., 2017), and (Firmansyah et al., 2018) are

a) *Capacity of the system* (M): -it is drying capacity in *kg* and taken based on the total production per day of given crops.
b) *Temperature of the hot water*:-is the value of the hot source temperature in the area and it vary with depth in the same area.
c) *Flow rates of the source*: -different geothermal sources of water (steam) have different mass flow rate and the design of thermal equipment greatly depends on it.
d) *Average speed of air*: - blowing of air across tube bundle is required in order forced convection to takes place as a result the temperature of forced air will be raised to the required value.
e) *Temperature of drying chamber*: -value of temperature under which water content from the crops can evaporates without damaging it. This value will vary with types of crops (grains) which the system will be designed for.
f) *Humidity ratio of air*: -temperature at which air exists from tube bank affect the humidity ratio of air and these values have to be maintained based on the nature of crops.
g) Initial and final moisture contents of crops

Average values of moisture available are different from one crop to another. For example, tomatoes at its matured stage contain about 97.5% of moisture by mass and it must be reduced to about 26% for safe storage. The purpose of drying coffee beans is to reduce the water content contained in coffee beans from the initial moisture content of about 65% to reach the standard water content of about 11-12% with drying temperature between 45 & 50 ^{o}C.

h) *Specific heat capacity of crops, foods, air, water, etc. (heat capacity)*

Thermal properties of foods must be known to perform the various heat transfer calculations involved in designing storage and refrigeration equipment and estimating process times for refrigerating, freezing, heating, or drying of foods. Thermal property models for some of food components, water, and ice are developed by ASHRAE Handbook, (2006) for temperature range of (-40 to 150 ^{o}C).

i) Total length of pipeline

The distance from source to the drying system is the main factor to be considered because of energy loss. The type of materials of pipe, insulator, and coating used have great meanings in accounting heat loss and designing for output temperature of pipe that is used as input for the system.

j) *Total time required* indicates how long the crops should dry under given chamber temperature

k) Moisture to be removed (M_r)

As grain dries, it releases its moisture into the drying air and consequently loses weight. The weight of grain after drying may be found using equation (35) and the mass of moisture to be removing also given in equation (34).

$$M_r = M \text{ x } H_{r_1} - H_{r_2}/(1 - H_{r_2}) \qquad (34)$$

Where, M_r= moisture to be removed (*kg*)

M = drying capacity (*kg*)

H_{r_1}= initial water content (%)

H_{r_2}= Final water content (%).

$$W_2 = W_1 - M_r \qquad (35)$$

Where, W_1 = Weight of wet grain (*kg*)

W_2 = Weight of dried grain (*kg*)

l) Mass flow rate of air

Calculating mass of air and its rate required to reduce water content from initial humidity to final humidity through the drying chambers is compulsory.

$$M_a = M_r/(H_{r_1} - H_{r_2}) \qquad (36)$$

$$\dot{m}_a = M_a/t \qquad (37)$$

Where, M_a = quantity of air required (*kg*)

$\dot{m}_a$ = air flow rate (*kg/s*)

t = time taken for drying (*s*)

3.3. Thermodynamic analysis of VARS

3.3.1. Introduction

Second part of this project deals with the design of single stage and single effect vapor absorption refrigeration system, the system uses of ammonia-water as refrigerant–absorbent pair with components comprised of a generator, a condenser, an absorber, an evaporator, a solution heat exchanger (to enhance COP), a throttling device, a pressure reducing valve, and a pump; similar to that of developed by Anand et al., (2016) and Shukla et al., (2015) which uses process-steam from the industries as energy input.

Line diagram of the developing system, presented in Figure 31, shows the flow direction of refrigerant and solution with geothermal hot water used as source of energy input to the generator.

3.3.2. Working Principle

The refrigerant in the solution gets vaporized and leaves the solution at high pressure as long as it is heated by hot water circulating through the tube coiled in the generator. The high pressure and the high temperature refrigerant then enters the condenser, where it is condensed by rejecting heat of condensation at this pressure, and it enters the capillary tube and then into the evaporator where it produces the cooling effect.

In other hand, weak solution left over the generator will flow back to absorber through pressure reducing valve. Furthermore, vapor refrigerant from the evaporator will be absorbed by weak solution in the absorber; releasing heat of absorption to the environment and strong solution will be formed. Finally, the strong solution in the absorber has to be pumped to the generator by small power solution pump. The cycle will repeat again and again whenever there is constant supply of heat in the generator and strong solution pumped from absorber.

Discussions presented below give clues about methods through which the design of each components of VARS to be carried out.

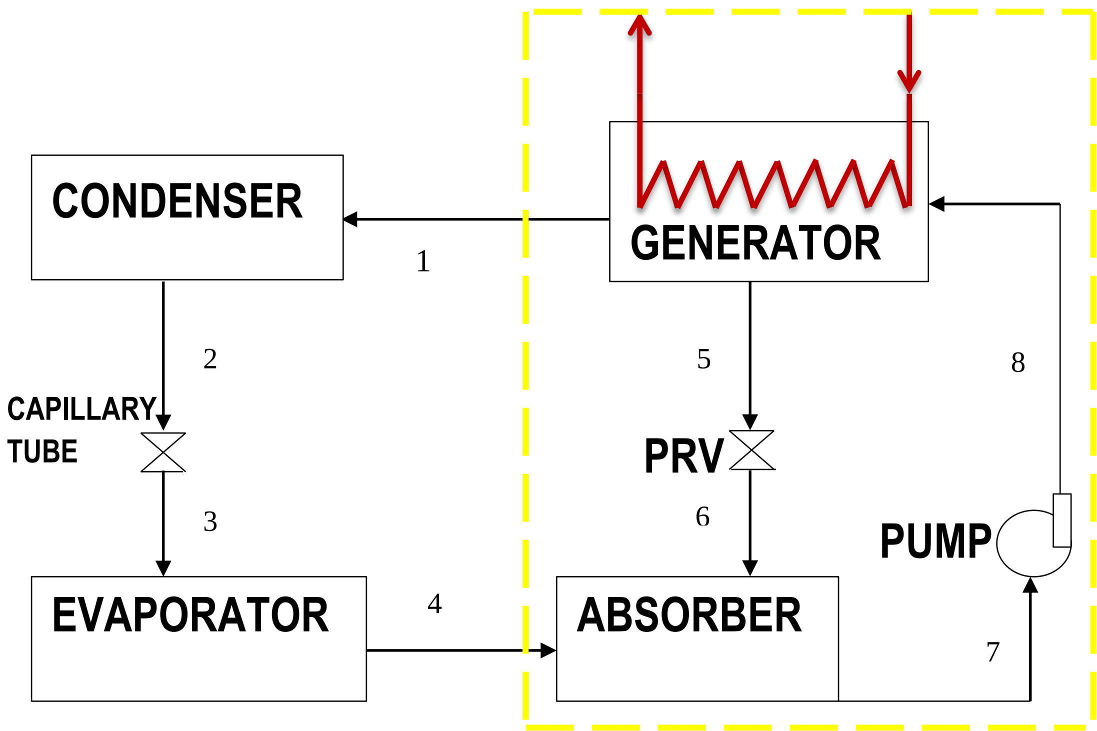

Figure 31: A schematic view of a single-effect and single stage ammonia–water vapor absorption refrigeration system.

3.3.3. Ammonia-water as working pair

Ammonia, the compound consisting of one atom of nitrogen and three atoms of hydrogen (*designated as* NH_3), is colorless chemical substance that has pungent odor and an alkaline or soapy taste. This substance when inhaled suddenly, brings tears into the eyes has lighter weight than air. Liquid ammonia has the freezing and boiling point of −77.7 and −33.3 °C, respectively with latent heat of vaporization of 1370 J per gram.

As refrigerant, ammonia is able to fulfill required properties such as: ozone and environmental friendly, low boiling temperature, vaporization pressure lower than atmospheric, high heat of vaporization, non-flammability and non-explosive. It can be used in the field of refrigeration technology of thermal sources with temperature less than 100 ^{o}C. Consequently, ammonia-water pair (*with a chemical formula of* NH_3-H_2O) is considered for the system analyzed in this thesis.

3.3.4. General assumptions

In order to carry out the analysis for this system, assumed conditions are listed below:

- All components are in steady state conditions
- Pressure drops (head difference) are negligible in all components
- Pump efficiencies is 90%
- Absorber temperature is the same as that of the condenser temperature
- Refrigerant leaving the generator is saturated vapor with the mass fraction of (90%) ammonia at condenser temperature, weak solution (38%), and strong solution (42%).
- The liquid refrigerant leaving the condenser is saturated liquid at condenser temperature
- The refrigerant vapor leaving an evaporator is saturated vapor at evaporator temperature
- Strong solution leaving the absorber is saturated at absorber temperature
- Weak solution leaving the generator is saturated at generated temperature
- Tube in the generator delivering hot spring is vertically coiled in helical form as this helps to enhance heat transfer due to centrifugal forces created in the flow will generate a secondary flow, normal to the primary direction of flow, with circulatory effects, that increases both the friction factor and the rate of heat transfer *(Sandeep et al., 2008)*.

3.3.5. Operating conditions and size of the system

In order to proceed to the analysis of size of each components of the system, operating conditions of the system, based on the required drinking water amount in Dilla University, nature of hot springs available and ambient conditions of the surrounding are listed as follows.

Concentration of NH3 in refrigerant circuit, x_r = 0.90

Concentration of NH3 in strong solution, x_S = 0.42

Concentration of NH3 in absorbent, x_w = 0.38

Temperature of the evaporator compartment, T_{comp} = 16℃

Temperature of refrigerant in the evaporator tube, T_E = 6℃

Generator Temperature, T_G = 50℃ (*if "Barsiso" source used*)

Generator Temperature, T_G = 83℃ (*if "Wallame" source used*)

Temperature of the Condenser outside and Absorber, T_C = T_A= 20.5℃ (*Appendix B-3*)

Generator or condenser pressure, P_S = 10.7 bar

Evaporator pressure, P_E = 4.7 bar

In addition to those parameters described above, based on amount of water recommended by science is approximately two liters of water per day per person. According to data collected from university website, Dilla University has over 30,000 students and 3000 staff members. This will give the total volume of water to be cool every day is 66,000 liters.

i. The refrigeration capacity

An average consumption rate per day of drinking water in DU is approximately 66,000 liters and has initial average measured temperature of $T_{w,\ initial}$ = 37.5 ^{o}C (Appendix B-3). This amount of water has to be converted to recommended final temperature $T_{w,\ final}$ = 16^{o}C. Therefore, the capacity $\dot{Q}_{tot}$ of system to be designed can be obtained from equation (38).

$$\dot{Q}_{tot} = mC_P(T_{w,initial} - T_{w,final})/t_{tot} = Q_E \quad (38)$$

Where, m is amount of water in (*kg*), t_{tot} is time taken to cool water (*sec*), and C_P is specific heat capacity of water (4.186 kJ/kg.°C).

ii. Enthalpy-concentrations charts

At the exiting of the generator, vapor refrigerant flowing to the condenser at generator temperature, t_K = 50 ^oC and pressure, P_K = 10 bar has the enthalpy at this state (1) evaluated as h_1. At state (2), for known values of generator pressure and the refrigerant concentrations of $x_r = 0.9$, temperature of saturated liquid refrigerant after condenser and its enthalpy at the inlet to the expansion device is, $t_{C,O}$ and h_2.

Assuming isenthalpic expansion in capillary tube, $h_3 = h_2$. Furthermore, state (4) of refrigerant after evaporator at t_E = 6 ^oC and P_E = 2 bar will have enthalpy of h_4. Finally, $h_5 = h_6$ and $h_7 = h_8$ will be evaluated at corresponding temperatures and compositions.

iii. Mass flow rates

Three types of mass flow are refrigerant mass flow, $\dot{m}_r$ through the refrigerant circuit, weak solution mass flow, $\dot{m}_w$ back to absorber through pressure relief valve and strong solution mass flow, $\dot{m}_s$ to the generator through the pump.

The mass flow of refrigerant can be determined by writing heat extracted rate Q_E in the evaporator compartment, by applying energy balance on evaporator, as written in equation (39).

$$Q_E = \dot{m}_r(h_4 - h_3) \tag{39}$$

Where, Q_E is taken as refrigeration capacity (*kW*), h_4 is enthalpy of the saturated vapor refrigerant at evaporator temperature and pressure (*by drawing tie-line*), and h_3 is enthalpy of the saturated liquid refrigerant equals to h_2, enthalpy of *saturated liquid state* evaluated at condenser pressure and concentration x_r from *enthalpy-concentration* diagram.

Applying steady-state mass balance (the conservation of mass) across the absorber, using equation (40) and re-writing in terms of concentrations as given in equation (41), mass flow of weak and strong solution can be calculated.

$$\dot{m}_s = \dot{m}_r + \dot{m}_w \tag{40}$$

$$x_S\ \dot{m}_s = x_r\ \dot{m}_r + x_w\ \dot{m}_w \tag{41}$$

Where, x_S, x_r and x_w are concentrations of ammonia in strong solution, refrigerant circuit, and weak solution respectively.

iv. Condenser, its finned surfaces and fans

The condenser is heat exchanging surfaces (device or unit) that used to condense a refrigerant (*ammonia in this case*) from its gaseous to its liquid state, by cooling it at generator pressure. Heat of condensation is energy amount to be removed from gaseous refrigerant at high pressure and then to convert refrigerant in to liquid state at the same pressure.

Air-cooled (natural convection and forced convection types), water-cooled, and evaporative classifications of condenser are based on their way of removing heat from the refrigerant flowing in the tube.

Forced air-cooled condenser; Serpentine type of condensers used in this thesis employs a fan or blower to move air over the condenser coil at a certain velocity and it is most commonly used in the refrigeration industry. The condenser coil is of the finned type in order to enhance heat transfer where the fins in such coils are closely spaced.

Amount of energy removed from refrigerant (heat of condensation) applying first law of thermodynamics, Q_C can be either the product of refrigerant flow rate and enthalpy differences, as given in equation (42) or the product of logarithmic mean temperature difference Δt_m**,** with overall heat transfer coefficient U**,** and effective heat transferring area of condenser A_C , equation (44).

$$Q_C = \dot{m}_r(h_1 - h_2) \tag{42}$$

Where, $\dot{m}_r$= refrigerant flow rate (*kg/s*)

h_1= enthalpy of saturated ammonia vapor entering the condenser (*kJ/kg*)

h_2= enthalpy of saturated ammonia liquid exiting the condenser (*kJ/kg*)

Equation (42) can be modified as:

$$Q_C = \dot{Q}_v\rho(C_p\Delta t) \tag{43}$$

Where $\dot{m}_r = \dot{Q}_v \rho$ (43 a)

$\Delta h = C_p \Delta t$ (43 b)

Where, $\dot{Q}_v$ is volumetric flow of air (*m³/s*), ρ is density (*kg/m³*)

$$Q_C = UA_C \Delta t_m \quad (44)$$

Where, $A_C = n\pi D_o L$ (*44 a*)

n = number of tubes

D_o= tube diameter (*mm*)

L= tube length (*cm*)

Heat-exchangers arrangements of condenser may be taken as multiple rows of either staggered or in-line arranged tubes which will be called tube banks. The tube bank may or may not be integrated with fins. Volumetric flow of forced air flowing across bank with velocity of u_∞ is given as:

$$\dot{Q}_v = (FA)u_\infty \quad (45)$$

$$FA = \pi {D_E}^2/4 \quad (45\ a)$$

Where, FA = face area of finned condenser tubes.

D_E = effective diameter (including tubes and fins surface)

Refrigerant-side heat transfer coefficient inside tubes as given by Akers, Deans and Crossef when the condensation rate or the length of tube is large and R_E>20,000 will be:

$N_U = \frac{h_i D_i}{k_f} = 0.026(P_r)^{1/3}(R_E)^{0.8}$, Where, $R_E = \frac{D_i \dot{m}}{\mu_f A_i}$ and $P_r = \frac{C_p \mu_f}{k_f}$. (*46*)

Note that: ammonia properties are to be evaluated at mean temperature of ammonia t_{am}. Δt_r is refrigerant-side temperature drop which is equals to change in refrigerant temperatures before and after condenser.

$$t_{am} = t_c - \Delta t_r/2 \quad (47)$$

Similarly, average *air-side* heat transfer a coefficient for the forced convection across a tube is given by Grimson’s as:

$$\mathrm{Nu} = \frac{h_o D_E}{k} = 0.193(P_r)^{1/3}(R_E)^{0.618}\text{ , where, } \mathrm{R_E} = \frac{\mathrm{D_E \rho u}}{\mu_a} \text{ and } \mathrm{P_r} = \frac{\mathrm{C_p \mu}}{\mathrm{k}_a}. \qquad (48)$$

Hence, *air properties* are to be evaluated at mean temperature of air t_a. Surface area temperature rise Δt_a, can be calculated from the following relations.

$$\mathrm{t_a = t + \Delta t_a/2} \qquad (49)$$

$$\mathrm{Q_C = \dot{Q}_v \rho C_p \Delta t_a} \qquad (50)$$

Temperature of air leaving the condenser and logs mean temperature will be calculated as:

$$\mathrm{\Delta t_m = (t_c - t) - (t_c - t_{a2})/\ln(t_c - t)/(t_c - t_{a2})} \qquad (51)$$

$$\mathrm{t_{a2} = t + \Delta t_a} \qquad (51\ a)$$

Heat transfer from condenser in terms of finned surface area can be written as:

$$\mathrm{Q_C = U_t A_t \Delta t_m} \qquad (52)$$

Where overall heat transfer coefficient U_t; neglecting the metal-wall resistance, based on the total fin-side surface area is given by:

$$\frac{1}{\mathrm{U_t A_t}} = \frac{1}{\mathrm{h_i A_i}} + \frac{1}{\mathrm{h_o A_t \eta_f}} \qquad (53)$$

$$\frac{1}{\mathrm{U_t}} = \frac{1}{\mathrm{h_i}}\left(\frac{\mathrm{A_t}}{\mathrm{A_o}}\right)\left(\frac{\mathrm{A_o}}{\mathrm{A_i}}\right) + \frac{1}{\mathrm{h_o \eta_f}} \qquad (53\ a)$$

Where, $\mathrm{A_t/A_o}$ is ratio of finned surface area to outside bare tube bank surface area and η_f is finned surface efficiency.

Values assumed for condenser tube banks are

Forced air velocity of, u_∞= *6 m/s*

Forced air volumetric flow of, $\dot{Q}_v$= 6 *m³/s*

Number of tubes in the bank, n = 48

Outer diameter, D_o= 2 *cm*

Inner diameter of tube D_i = 1.5 *cm*

Length of tubes, *L*= 50 *cm*

Ratio of finned surface area to outer bare surface of bank is A_t/A_o = 20

Mean temperature to evaluate ammonia properties (equation 32) is t_{am} = 40°C. The properties of ammonia evaluated at *40°C* from ammonia table will be:

μ_f = 1.219x10^{-4} kg/m.s C_p = 4.932 kJ/kg°C k_f = 0.4464 w/m°C ρ = 579.4 kg/m^3

Similarly, mean temperature of air t_a (equation 49) is t_a= 30.5°C. A*ir properties* evaluated at 30.5°C from air table will be:

μ = 1.8680x10^{-5} kg/m.s C_p = 1.0065 kJ/kg°C $k = 0.026341$ w/m°C ρ = 1.1649 kg/m^3

Temperature of air leaving the condenser (equation (51 a) and log mean temperature equation (51) will be: t_{a2}= 40.4 °C and Δt_m= 17.73 °C.

v. Condenser Fan

Because natural convection will not produce sufficient airflow and heat transfer over a reasonably sized condenser, a fan must be employed to keep the air moving. Power consumed by fan is negligible as compared to other power consuming devices. This power is directly related to the air pressure drop across the condenser and the volume flow rate of the air.

vi. Capillary tube analysis

Fixed restriction-type device made of long and narrow tube connecting the condenser directly to the evaporator. It is used to reduce pressure from high condenser pressure to low evaporator one, and to regulate the refrigerant flow from the high-pressure liquid line into the evaporator at a rate equal to the evaporation rate in the evaporator.

The refrigerant enters the capillary tube in sub cooled liquid state, and with continuous flowing of this liquid the pressure will drop, while the temperature remains constant. When this pressure drops to a level lower than the pressure of vaporization for the refrigerant, some of liquid will evaporate in a process called flash process, then the two-phase flow process begins proceeds to the tube exit.

The pressure drop is due to:

a) Viscosity, resulting in frictional pressure drop Δp_F.

b) Acceleration (when flashing of liquid refrigerant into vapor), resulting in momentum pressure drop $\Delta \mathrm{p_A}$.

Therefore, the total pressure drop; which must be equal to the difference in pressure at the two ends of the tube is the summation of the above and mathematically,

$$\Delta \mathrm{p} = \Delta \mathrm{p_F} + \Delta \mathrm{p_A} \tag{54}$$

For a given state of refrigerant, the pressure drop is directly proportional to the length and inversely proportional to the bore diameter of the tube. Therefore, the sizing of tube implies the selection of bore and length to provide flow for the given condenser and evaporator pressures.

a) Design Principle used

The principle of designing capillary tube discussed in *Arora, (2006)* based on methods as proposed by *Stocker* & *Hopkins* and *Cooper et al.* is used as per the scope of this project.

Let capillary of bore diameter *D* and cross-sectional flow area *A* with a saturated liquid state of refrigerant entering at given rate of $\dot{m}_r$ is known. Step decrements in pressure are then assumed and the corresponding required increments of length calculated which, when summed up will give the complete length of tubing for a given pressure drop Δp.

The condenser and evaporator temperatures are t_k and t_c, and the corresponding pressures are p_k and p_c respectively. Let dividing this temperature drop in to a number of *n* sections, the corresponding pressure drops will be Δp_1, Δp_2, Δp_3, Δp_4, ... Δp_n (as shown in Fig. 32).

Isenthalpic, shown by line *c*-*n* and adiabatic (fanno-line) shown by line *c*-*a* expansions are the two approaches to design where the actual practice expansion takes place adiabatically with pressure drop, the volume increases and an increase in kinetic energy is obtained from decrease in enthalpy.

Assumptions used to analyze the flow through adiabatic capillary tube:-

1. The capillary tube inner diameter and surface roughness are constant.

2. The capillary tube is perfectly insulated.

3. Pure refrigerant is flowing through the capillary tube (*i.e. refrigerant is free of oil*).

4. One dimensional and steady state flow.

5. The flow is homogeneous in the two-phase region.

6. Flash point lies on saturated liquid line (*i.e. the metastable flow region phenomena is not considered*).

7. The capillary tube is horizontal (*i.e. the influence of gravity is ignored*).

8. The capillary tube is adiabatic (*i.e. there is no heat transfer process in and out of tube*).

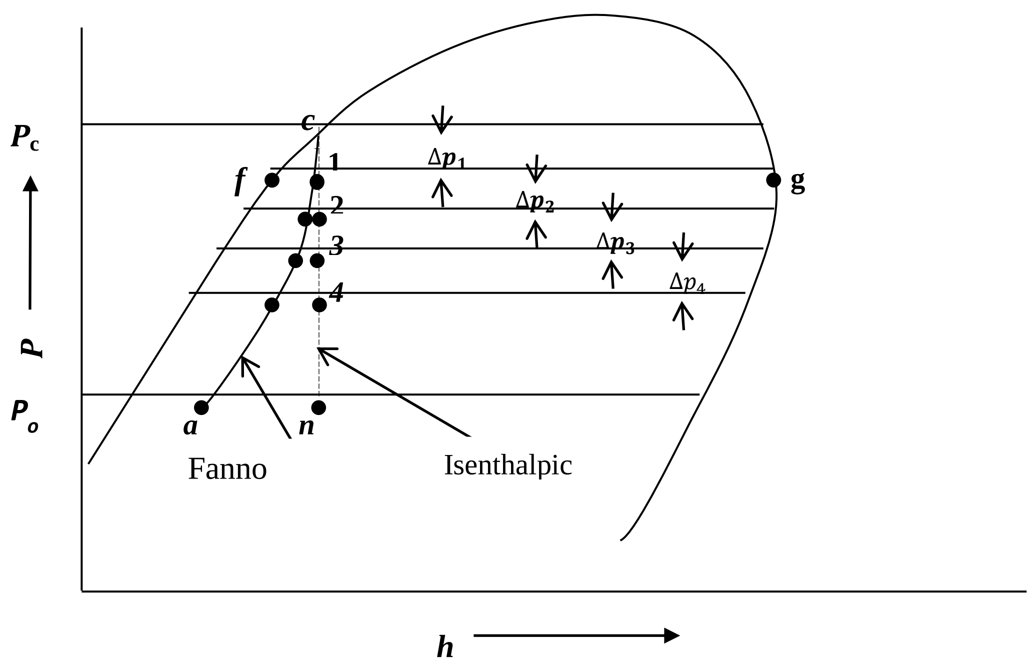

Figure 32: Incremental pressure drops in a capillary tube

b) Design steps

1. Determine the quality at the end of the decrement for isenthalpic flow. For example, quality and specific volume at the end of first section:

$$x_1 = (h_c - h_{f_1})/h_{fg_1} \tag{55}$$

Where, x_1= quality at the end of first section and h_c=constant enthalpy (kJ/kg)

$$v_1 = v_{f_1} + x_1(v_{g_1} - v_{f_1}) \tag{56}$$

Where, v_1= specific volume at the end of first section (m^3/kg)

v_{f_1}= specific volume of saturated liquid (m^3/kg)

v_{g_1} = specific volume of saturated vapor (m^3/kg)

2. Equation for determining the velocities is derived from continuity equation.

Rate of mass flow in to the section of tube corresponding to step decrements in pressure is equals to its rate out of that section. Mathematically,

$$\dot{m}_{in} = \dot{m}_{out} \tag{57}$$

Up on rearranging and modifying equation (57), the following equations will be derived.

$$\frac{u_k A}{v_k} = \frac{u_1 A}{v_1} = \frac{u_n A}{v_n} = \dot{m} \text{ (Constant)} \tag{58}$$

$$\frac{u}{v} = \frac{\dot{m}}{A} = G \text{ (Constant, mass velocity)} \tag{59}$$

$$u = vG \tag{60}$$

$$\Delta h_1 = \frac{u_1{}^2 - u_C{}^2}{2} \tag{61}$$

Applying equations (55-61) to *n*-sections of tubes based on isenthalpic approach, the corresponding velocities will be obtained and summarized in table below.

Table 6: Steps for calculations of velocities and enthalpy changes for isenthalpic flow

section	h (constant)	*x*	$10^3(v)$ m^3/kg	u=G*v*	Δh (kJ/kg)
k	h_c	$x_c = 0$ ($h_c = h_{fc}$)	$v_c = v_f + x_c(v_g - v_f)$	$u_c = Gv_c$	0.0
1	"	$x_1 = (h_c - h_{f1})/h_{fg1}$	$v_1 = v_{f1} + x_1(v_{g1} - v_{f1})$	$u_1 = Gv_1$	$\Delta h_1 = \frac{u_1{}^2 - u_C{}^2}{2}$
2	"	$x_2 = (h_c - h_{f2})/h_{fg2}$	$v_2 = v_{f2} + x_2(v_{g2} - v_{f2})$	$u_2 = Gv_2$	$\Delta h_2 = \frac{u_2{}^2 - u_1{}^2}{2}$
3	"	$x_3 = (h_c - h_{f3})/h_{fg3}$	$v_3 = v_{f3} + x_3(v_{g3} - v_{f3})$	$u_3 = Gv_3$	$\Delta h_3 = \frac{u_3{}^2 - u_2{}^2}{2}$
4	"	$x_4 = (h_c - h_{f4})/h_{fg4}$	$v_4 = v_{f4} + x_4(v_{g4} - v_{f4})$	$u_4 = Gv_4$	$\Delta h_4 = \frac{u_4{}^2 - u_3{}^2}{2}$
5	"	$x_5 = (h_c - h_{f5})/h_{fg5}$	$v_5 = v_{f5} + x_5(v_{g5} - v_{f5})$	$u_5 = Gv_5$	$\Delta h_5 = \frac{u_5{}^2 - u_4{}^2}{2}$
….	….	…..	…..	…	…
n	"	$x_n = (h_c - h_{fn})/h_{fgn}$	$v_n = v_{fn} + x_n(v_{gn} - v_{fn})$	$u_n = Gv_n$	$\Delta h_n = \frac{u_n{}^2 - u_{n-1}{}^2}{2}$

3. For fanno line (*actual/adiabatic flow*), enthalpy will not be constant and then the calculations for quality, specific volume, velocity, and enthalpy may be repeated until the corresponding

values of h are equals to its values in the preceding iterations. The first three iterations procedures *for example*, are listed in the following tables.

Table 7: Fanno 1(first iteration)

section	h	x	$10^3(v)$ m^3/kg	u (m/s)	Δh (kJ/kg)
k	h_C	$x_C= 0$	$v_C=v_f$	$u_C=Gv_C$	0.0
1	$h_{11}=h_C- \Delta h_1$	$x_{11}=(h_{11}-h_{f1})/h_{fg1}$	$v_{11}=v_{f1}+ x_{11}(v_{g1}-v_{f1})$	$u_{11}=Gv_{11}$	$\Delta h_{11}=\frac{{u_{11}}^2-{u_{k1}}^2}{2}$
2	$h_{21}=h_C- \Delta h_2$	$x_{21}=(h_{21}-h_{f2})/h_{fg2}$	$v_{21}=v_{f2}+ x_{21}(v_{g2}-v_{f2})$	$u_{21}=Gv_{21}$	$\Delta h_{21}= \frac{{u_{21}}^2-{u_{11}}^2}{2}$
3	$h_{31}=h_C- \Delta h_3$	$x_{31}=(h_{31}-h_{f3})/h_{fg3}$	$v_{31}=v_{f3}+ x_{31}(v_{g3}-v_{f3})$	$u_{31}=Gv_{31}$	$\Delta h_{31}= \frac{{u_{31}}^2-{u_{21}}^2}{2}$
4	$h_{41}=h_C- \Delta h_4$	$x_{41}=(h_{41}-h_{f4})/h_{fg4}$	$v_{41}=v_{f4}+ x_{41}(v_{g4}-v_{f4})$	$u_{41}=Gv_{41}$	$\Delta h_{41}= \frac{{u_{41}}^2-{u_{31}}^2}{2}$
5	$h_{51}=h_C- \Delta h_5$	$x_{51}=(h_{51}-h_{f5})/h_{fg5}$	$v_{51}=v_{f5}+ x_{51}(v_{g5}-v_{f5})$	$u_{51}=Gv_{51}$	$\Delta h_{51}= \frac{{u_{51}}^2-{u_{41}}^2}{2}$
…	…	…	…	…	…
n	$h_{n1}=h_C- \Delta h_n$	$x_{n1}=(h_{n1}-h_{f5})/h_{fg5}$	$v_{n1}=v_{fn}+ x_{n1}(v_{g5}-v_{fn})$	$u_{n1}=Gv_{n1}$	$\Delta h_{n1}= \frac{{u_{n1}}^2-{u_{(n-1)1}}^2}{2}$

Table 8: Fanno 2(second iteration)

Section	h	x	$10^3(v)$ m^3/kg	u (m/s)	Δh (kJ/kg)
c	h_C	$x_C= 0$	$v_C=v_f+x_k(v_g-v_f)= v_f$	$u_C=Gv_C$	0.0
1	$h_{12}=h_C- \Delta h_{11}$	$x_{12}=(h_{12}-h_{f1})/h_{fg1}$	$v_{12}=v_{f1}+ x_{12}(v_{g1}-v_{f1})$	$u_{12}=Gv_{12}$	$\Delta h_{12}= \frac{{u_{12}}^2-{u_{c2}}^2}{2}$
2	$h_{22}=h_C- \Delta h_{21}$	$x_{22}=(h_{22}-h_{f2})/h_{fg2}$	$v_{22}=v_{f2}+ x_{22}(v_{g2}-v_{f2})$	$u_{22}=Gv_{22}$	$\Delta h_{22}= \frac{{u_{22}}^2-{u_{12}}^2}{2}$
3	$h_{32}=h_C- \Delta h_{31}$	$x_{32}=(h_{32}-h_{f3})/h_{fg3}$	$v_{32}=v_{f3}+ x_{32}(v_{g3}-v_{f3})$	$u_{32}=Gv_{32}$	$\Delta h_{32}= \frac{{u_{32}}^2-{u_{22}}^2}{2}$
4	$h_{42}=h_C- \Delta h_{41}$	$x_{42}=(h_{42}-h_{f4})/h_{fg4}$	$v_{42}=v_{f4}+ x_{42}(v_{g4}-v_{f4})$	$u_{42}=Gv_{42}$	$\Delta h_{42}= \frac{{u_{42}}^2-{u_{32}}^2}{2}$
5	$h_{52}=h_C-\Delta h_{51}$	$x_{52}=(h_{52}-h_{f5})/h_{fg5}$	$v_{52}=v_{f5}+ x_{52}(v_{g5}-v_{f5})$	$u_{52}=Gv_{52}$	$\Delta h_{52}= \frac{{u_{52}}^2-{u_{42}}^2}{2}$
…	…	…	…	…	…
n	$h_{n2}=h_C-\Delta h_{n1}$	$x_{n2}=(h_{n2}-h_{fn})/h_{fg5}$	$v_{n2}=v_{f5}+ x_{n2}(v_{gn}-v_{fn})$	$u_{n2}=Gv_{n2}$	$\Delta h_{n2}= \frac{{u_{n2}}^2-{u_{(n-1)2}}^2}{2}$

Table 9: Fanno 3 (third iteration)

Section	*h*	*x*	$10^3(v)$ m^3/kg	u (m/s)	Δh (kJ/kg)
c	h_C	$x_C = 0$	$v_C = v_f + x_k(v_g - v_f) = v_f$	$u_C = Gv_C$	0.0
1	$h_{13} = h_C - \Delta h_{12}$	$x_{13} = (h_{13} - h_{f1})/h_{fg1}$	$v_{13} = v_{f1} + x_{13}(v_{g1} - v_{f1})$	$u_{13} = Gv_{13}$	$\Delta h_{13} = \frac{u_{13}^2 - u_c^2}{2}$
2	$h_{23} = h_C - \Delta h_{22}$	$x_{23} = (h_{23} - h_{f2})/h_{fg2}$	$v_{23} = v_{f2} + x_{23}(v_{g2} - v_{f2})$	$u_{23} = Gv_{23}$	$\Delta h_{23} = \frac{u_{23}^2 - u_{13}^2}{2}$
3	$h_{33} = h_C - \Delta h_{32}$	$x_{33} = (h_{33} - h_{f3})/h_{fg3}$	$v_{33} = v_{f3} + x_{33}(v_{g3} - v_{f3})$	$u_{33} = Gv_{33}$	$\Delta h_{33} = \frac{u_{33}^2 - u_{23}^2}{2}$
4	$h_{43} = h_C - \Delta h_{42}$	$x_{43} = (h_{43} - h_{f4})/h_{fg4}$	$v_{43} = v_{f4} + x_{43}(v_{g4} - v_{f4})$	$u_{43} = Gv_{43}$	$\Delta h_{43} = \frac{u_{43}^2 - u_{33}^2}{2}$
5	$h_{53} = h_C - \Delta h_{52}$	$x_{53} = (h_{53} - h_{f5})/h_{fg5}$	$v_{53} = v_{f5} + x_{53}(v_{g5} - v_{f5})$	$u_{53} = Gv_{53}$	$\Delta h_{53} = \frac{u_{53}^2 - u_{43}^2}{2}$
…	…	…	…	…	…
n	$h_{n3} = h_C - \Delta h_{n2}$	$x_{n3} = (h_{n3} - h_{fn})/h_{fgn}$	$v_{n3} = v_{fn} + x_{n3}(v_{gn} - v_{fn})$	$u_{n3} = Gv_{n3}$	$\Delta h_{n3} = \frac{u_{n3}^2 - u_{(n-1)3}^2}{2}$

In such way, iterations may be repeated as long as the differences in *h* values of the preceding iterations become very small or zero.

4. Taking the values of all parameters from final iterations, calculate friction factor *f*, viscosity μ, and Reynolds number R_e at every steps *(from* Niaz and Davis correlations)

$$f = 0.324/R_e^{0.25} \quad (62)$$

$$\mu_1 = (1 - x_1)\mu_f + x_1\mu_g \quad (63)$$

$$R_e = \frac{\rho u D}{\mu} = \frac{GD}{\mu} \quad (64)$$

5. Similarly, taking the values of all parameters from final iteration, determine Pressure drop due to acceleration and friction

From momentum equation, pressure drop due to acceleration can be derived as:

$$Adp = -\dot{m}du \quad (65)$$

$$\int Adp = \int -\dot{m}du \ (\textit{Integrating both sides})$$

$$\Delta p_A = \frac{\dot{m}}{A}(u_k - u_1) = G\ (u_k - u_1) \quad (66)$$

Pressure drop due to friction will be calculated from equation (67).

$$\Delta p_F = \Delta p - \Delta p_A \tag{67}$$

6. Finally, determine incremental in length from:

$$\Delta p_F = \frac{\rho f \Delta L u^2}{2D} \tag{68}$$

$$= \frac{\rho u f u \Delta L}{2D} = \frac{G}{2D} f u \Delta L$$

Where, ΔL is increment in length that is to be designed, u and f are mean values of velocity and friction factor respectively.

vii. Evaporator analysis

The evaporator is heat exchanging surfaces that transfer the heat from the substance to be cooled to the refrigerant, thus removing the heat from the substance. The heat energy to be removed from substances in the evaporator is at low pressure; hence, called heat of evaporation.

It is part in the compartment of domestic compression refrigeration system where the substance to be cooled is placed. In case of large refrigeration plants and central air conditioning plants, the evaporator is also known as the chiller since these systems are first used to chill the water, which then produces the cooling effect.

Using the steady flow energy equation on the evaporator of system, cooling effect (*heat of vaporization* Q_E or Q_{eva}) is given as the product of the refrigerant flow rate and enthalpy differences equation (69). In addition, it is the product of logarithmic mean temperature difference $\Delta \boldsymbol{t_m}$, with overall heat transfer coefficient U, and effective heat transferring area of evaporator A_E, as given in equation (70).

$$Q_E = \dot{m}_r(h_4 - h_3) \tag{69}$$

Where, $\dot{m}_r$= refrigerant flow rate (*kg/s*)

h_4=enthalpy of saturated ammonia vapor exiting the evaporator (kJ/kg)

h_3= enthalpy of saturated ammonia liquid entering the evaporator (kJ/kg)

$$Q_E = U A_E \Delta t_m \tag{70}$$

Where, $A_E = n\pi DL$

n =number of tubes

D=tube diameter (*mm*)

L=tube length (*cm)*

Air inlet to evaporator has temperature value of 20.5 ^oC (*ambient air around the university*); air outlet temperature is assumed to be 16 ^oC, and evaporator temperature of 6 ^oC. The logarithmic mean temperature difference across this heat exchanger with natural air convection across its surface is calculated as follows.

θ_1= (20.5-6) ^oC = 14.5 ^oC

θ_2 = (16-6) ^oC = 10 ^oC

$\Delta t_m = \theta_1 - \theta_2 / \ln(\theta_1 / \theta_2)$

Δt_m = (14.5-10) / ln (14.5/10)

Δt_m = 12.5 ^oC

viii. Generator analysis

A device used for boiling of strong aqua ammonia solution more than the boiling point of ammonia to produce vapor refrigerant. As per scope of this thesis, geothermal water source is used for supplying heat for the strong solution in the generator. However, any sources of heat energy (such as waste heat from industry, solar heat, etc.) can be used to heat the solution. Due to its resistance against the effect of ammonia, mild steel may be used because other nonferrous materials like copper and brass are attacked by ammonia (Tangka & Kamnang, 2008).

Designing procedure is based on the principle of *energy conservation*. Taking the summation of energy input to the generator should be equal to sum of energy removed as given in equation (71).

Energy to be added is from hot source Q_G and strong solution at state 8, $\dot{m}_s h_8$. In contrast, energy removed from generator is by means of vapor refrigerant at state 1, $\dot{m}_r h_1$ and weak solution flowing back to the absorber $\dot{m}_W h_5$.

$$Q_G + \dot{m}_s h_8 = \dot{m}_r h_1 + \dot{m}_W h_5 \qquad (71)$$

From equation (71), required energy from hot source, Q_G in order to produce vapor refrigerant at required flow rate is unknown and the equation can be rearranged as:

$$Q_G = \dot{m}_r h_1 + \dot{m_W} h_5 - \dot{m}_s h_8 \tag{72}$$

based on which the size of heat exchanger in the generator is to be designed.

Fourier's law for heat transfer to the radial direction from hot water flowing through a long hollow cylindrical tube of length L, inner and outer radius of r_i and r_o, respectively (shown in Figure 23) is as given in equation 73.

$$q_r = -kA_r \frac{dT}{dr} \tag{73}$$

However, if the tube is exposed to a convection environment on its inner and outer surfaces, the equation will be modified to:

$$Q_G = (T_H - T_{atm}) \Big/ \frac{1}{h_i A_i} + \frac{\ln(r_o/r_i)}{2\pi k L_c} + \frac{1}{h_o A_o} \tag{74}$$

Hot water from geothermal sources at an average temperature of T_H is flowing through long hollow cylindrical tube of known inner and outer diameters, d_i and d_o, respectively. Heat transfer coefficients inside and outside of tube; h_i and h_o are also known.

Therefore, applying equation (74) and evaluating all known parameters, total length of tube, L_C required can be computed. Otherwise, for the given length of tube L_C, and known properties of tube material, the diameter of tube could be part of the problem.

ix. Absorber analysis

Applying energy balance in the absorber (*shown by equation 75*); sum of heat energy added by means of saturated vapor refrigerant from evaporator ($\dot{m}_r h_4$) and weak solution from generator ($\dot{m_W} h_5$) is equals to sum of energy rejected by means of strong solution flowing out to the generator ($\dot{m}_s h_7$) and heat of absorption rejected (Q_A) during mixing in the absorber. The equation is then rearranged in to equation (76).

$$\dot{m}_r h_4 + \dot{m_W} h_9 = \dot{m}_s h_{10} + Q_A \tag{75}$$

$$Q_A = \dot{m}_r h_4 + \dot{m_W} h_6 - \dot{m}_s h_7 \tag{76}$$

x. Pressure relief valve analysis

Pressure relief valve is connected with high pressure and low pressure lines (between generator and absorber pressure). It consists mainly of poppet loaded by a spring of stiffness $k_{rv.}$ The poppet is pushed by the spring to rest against its seat in the valve housing as shown in figure 33. The spring is pre-compressed by an adjustable pre-compression distance $x_{o.}$ When valve is not operating, spring pre-compression force ($k_{rv}x_o$) pushes the poppet against its seat. Seat also produces equal seat reaction force $F_{SR.}$

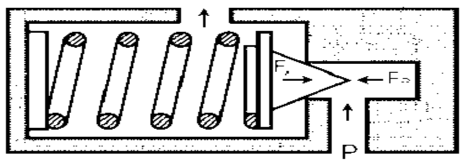

Figure 33: A simple direct-operated pressure relief valve

Neglecting the jet reaction forces, the motion of the poppet is governed by the spring force, the seat reaction force, and the pressure force. The poppet rests against its seat as long as the pressure force is less than spring force. The two forces are equal as given by equation (77), when the pressure reaches the value called cracking pressure P_r.

$$\mathrm{F_P} = \mathrm{A_P P_r} = \mathrm{k}_{rv}\mathrm{x_o} \qquad (77)$$

Where k_{rv} = Spring stiffness (*N/m)*

$\mathrm{x_o}$ = Spring pre-compression distance (*m)*

$\mathrm{P_r}$ = Cracking pressure (*N/m²)*

$\mathrm{A_P}$ = Poppet area subjected to pressure; for seated poppet, ($\frac{\pi {d_p}^2}{4} = \frac{\pi d^2}{4}$), (*m²)*

d = Circular poppet seat diameter (*m)*

When the pressure force (PA_p) exceeds the spring force ($k_{rv}x_o$); further increases in cracking pressure, the poppet displaces, opening the path from the inlet port to the drain port, with a pressure P_T, where seat reaction forces will be zero.

The conical poppet is one of the frequently used designs of poppet valves. When the poppet rests against its seat, the contact line is a circle of diameter *d* (which is equals to the diameter of inlet area) and the force acting on the spring, F_d is as given in equation (78). The poppet is subjected to a pressure force, F_P is as given by equation (79).

$$F_d = (\pi d^2/4)\Delta P_{min} \tag{78}$$

$$F_P = (\pi {d_P}^2/4)\Delta P_{max} \tag{79}$$

If the poppet is displaced by distance x_o, the fluid is allowed to flow through the opened area A_t. This area A_t consists of the side area of the truncated cone (*abce*) shown in figure 34, whose left base is of diameter d and right base is of diameter d_p is derived as written by equations 80-82.

$$\overline{ab} = x\sin(\alpha/2) \tag{80}$$

$$d_P = d - 2x\sin(\alpha/2)\cos(\alpha/2) \tag{81}$$

$$A_t = \frac{\pi}{2}(d + d_P)\overline{ab} \ = \pi x\sin(\alpha/2)\{d - x\sin(\alpha/2)\cos(\alpha/2) \tag{82}$$

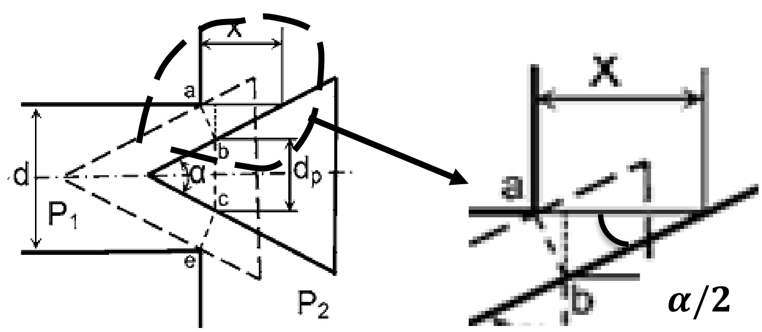

Figure 34: A conical poppet valve.

The area of conical poppet subjected to the pressure force F_P is of diameter d_p and given by equation 83.

$$A_P = \frac{\pi {d_P}^2}{4} = \frac{\pi}{4}\{d - 2x\sin(\alpha/2)\cos(\alpha/2)\}^{\,2} \tag{83}$$

Where A_t = Throttle area (m^2)

d_P = Diameter of circular poppet area subjected to the pressure (*m*)

x = Poppet displacement *(m)*

α = Cone vertex angle *(rad)*

ΔP_{min} = Pressure difference in generator and absorber when poppet not opened (*N/m²*)

ΔP_{max} = Pressure difference in generator and absorber when poppet opened (*N/m²*)

A_p and A_t can be calculated for conical poppet of standard vertex angle α and inlet diameter d. the results can be plotted in the graph by calculating the areas in non-dimensional form relative to inlet area A_i and plotted versus the relative poppet displacement (x/d). The throttle area, A_t, being the minimum cross-sectional area of the stream tube, should be less than or equal to the inlet area, $A_i=0.25\pi d^2$. For practical applications poppet displacement can be taken as, $x=0.2d$ (Rabie, 2009).

For the given inlet diameter d of poppet seat, displacement x can be calculated. Moreover, area A_P of circular poppet subjected to the pressure when poppet moves x displacement will be evaluated which is used to calculate pressure force to be acting on the valve. Finally, evaluating known parameters in equation (77), spring stiffness k_{rv} (*N/m*) will be part of the problem.

xi. Pumps

A. Solution pump and its geometry

This is one of basic components of *VARS*, which is since energy supplied to them, sometimes called *energy absorbing device* according to Cimbala et al., (2006) and resulting in an increase in fluid pressure.

Either *Rotodynamic type* in which the mutual dynamic action between the rotor and the working fluid forms their basic principle of operation or *positive displacement type* in which volume of chambers changes periodically with the rotation of crank shaft and allow the fluid to displace from the suction line to the delivery line by the successive expansion and contraction of the pumping chambers, can be used to increase the energy of the liquid flowing through them.

The reciprocating motion of piston by means of crank mechanism provides consistent variation of operating chamber volume. Working principle of positive displacement pump (Figure 35), which is designed as per the scope of this thesis, is summarized as follows.

1. During its expansion, the volume of pumping chamber which is connected to the suction line will increase from V_{min} to V_{max} result in geometric volume of chamber V_g. Vacuum pressure developing inside the chamber through piston backward movement forces the solution from absorber to be sucked in through suction and opened *valve 1*. (discharge valve closes preventing return flow of pumped fluid)
2. When the volume of the chamber reaches its maximum value, the chamber is separated from the suction line (*valve 1* will be closed and *valve 2* opened).
3. During the contraction period, the chamber is linked with the pump delivery line through *valve 2*. The fluid is then displaced to the pump exit line and is acted on by the pressure necessary to overcome the exit line resistance.
4. The delivery stroke ends when the volume of the chamber reaches its minimum value V_{min}. Afterward, the chamber is separated from the delivery line (*valve 2* will be closed).
5. The cycle repeats again and again as long as there is mechanical power P_m (traditionally called *brake horse power*) supplied to the crankshaft that transfers the power to the connecting rod and then piston from electrical motor.

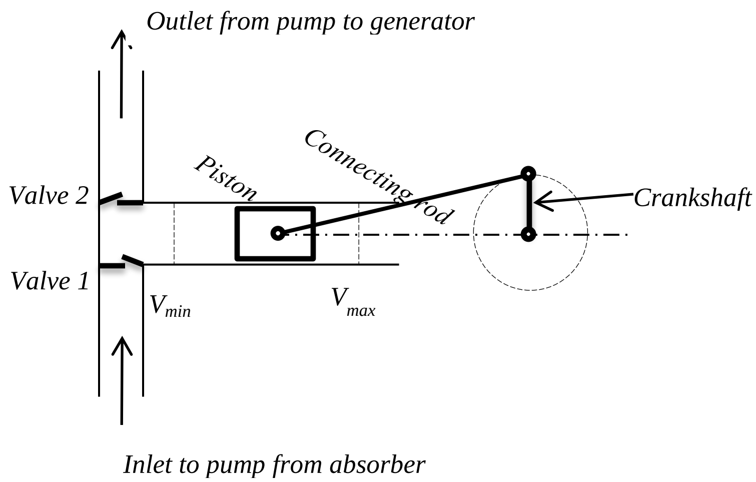

Figure 35: Single piston operated positive displacement pump

Analysis of single piston operated solution pump will be performed by utilizing mathematical equations 84-89.

$$\Delta P = P_G - P_A \tag{84}$$

ΔP= pressure rise (*Pa*), P_G= generator/condenser pressure (*Pa*), P_A= absorber/evaporator pressure (*Pa*)

$$\dot{V}_s = A_{p,cross} L_s N_S \tag{85}$$

$\dot{V}_s$= volumetric flow rate (m^3/s), $A_{p,cross}$ = cross-section (m^2), L_s = stroke length (*m*), V_g= geometric volume (m^3), N_S = shaft rotational speed, (s^{-1})

$$P_{m,s} = \dot{V}_s \rho g H_s / 3.6x10^6 \tag{86}$$

$P_{m,s}$= mechanical power (*kW*), ρ = density of solution (kg/m^3), g = gravitational acceleration (m/s^2), *and* H_s = Head (*m*)

$$P_S = P_h / \eta_p \tag{87}$$

$$P_{el,s} = P_h / \eta_{el} \tag{88}$$

Where, P_S = shaft power *kW*, η_p= pump efficiency %, $P_{el,s}$ = electrical power *kW*, η_{el}= motor efficiency%. It is clear that assuming ideal pump (neglecting all losses), the input mechanical power is equal to the increase in the fluid power (traditionally called *water horse power*) as given by equation (89).

$$P_h = \dot{V}_s (P_G - P_A) / (3.6x10^6) \tag{89}$$

B. Hot spring pump

Pumping system similar with solution pump can be selected to deliver hot spring from source to the generator of the system. So far, volumetric flow rate $\dot{V}_h$ with which hot spring should be supplied (*in order to maintain temperature of generator at* T_G) is assumed in the case of generator design.

When hot fluid flows in a helical coil tube in the generator, there is a significant pressure head losses against pump which are greater than those compared with in straight tube. Due to secondary flow induced by centrifugal forces that result from curvature of curved tubes and it also has an ability to enhance the heat transfer performance.

For known values of *length* and *diameter* of coiled tube in the generator, *pressure head* H_h that to be developed through hot water piping system will be determined.

As given by Pandey et al., (2014) major head loss due to friction of fluid flowing inside the coiled tube is calculated by *Darcy-Weisbach* equation (90) which is valid for fully developed, steady-state, and incompressible flow.

$$\Delta \mathrm{H_h} = \lambda_\mathrm{C} \rho \mathrm{L} \mathrm{V}^2 / 2\mathrm{d_i} \tag{90}$$

Where, λ_C is correction factor, ρ is density of geothermal water, L is total length of tube, V is velocity of fluid, and d_i is inner tube diameter.

For fully developed laminar flow, the roughness of the duct or pipe can be neglected and the friction coefficient depends only on the Reynolds Number and expressed as:

$$\lambda = 64/\mathrm{R_E} \tag{91}$$

The friction coefficient λ for not laminar flow can be calculated by the *Colebrook* equation as given by equation (93).

$$1/\lambda^{\frac{1}{2}} = -2\log[2.51/(\mathrm{R_E}\,\lambda^{\frac{1}{2}}) + (k/\mathrm{D_h})/3.72] \tag{92}$$

Where λ is Darcy-Weisbach friction coefficient, R_E is Reynolds number of the flow, k is roughness of duct, pipe/tube surface (*m*), and D_h is hydraulic diameter (*m*).

Since the friction coefficient is on both sides of the equation, it must be solved by iteration. Otherwise, if we know the Reynolds number R_E and the surface roughness k (Appendix A-8) or relative roughness **(**k/D_h**)**, the friction coefficient in the particular flow can be evaluated by using Moody Diagram (Appendix A-7).

However, friction coefficients correlations discussed so far are used only for straight duct/pipe; different friction factor developed by many authors can be used to determine friction coefficients of coiled tube. Friction factor developed by *Planck* for turbulent flow in the coiled tube is given below.

$$\lambda_\mathrm{C} = \lambda_\mathrm{S} + 0.01(\mathrm{d}/\mathrm{D})^{0.5} \tag{93}$$

Finally, mechanical power required $P_{m,h}$ and then electrical power consumptions $P_{el,h}$ of this pump are parts of the problems in hot spring pumping system (equation 94-95).

$$\mathrm{P_{m,h}} = (\dot{\mathrm{V}}_{\mathrm{h}}\rho \mathrm{g} \mathrm{H_h})/3.6\mathrm{x}10^6 \tag{94}$$

$$\mathrm{P_{el,h}} = \mathrm{P_{m,h}}/\eta_{\mathrm{m}} \tag{95}$$

3.3.6. COP

As it is expensive, occupy more spaces, and complex for design, VARS should be considered only when unit cost of thermal energy is very low relative to electricity. The COP of this system is defined as:

$$\mathrm{COP_{Absorption}} = \frac{\text{Desired utput}}{\text{Required input}} = \mathrm{Q_E}/\mathrm{Q_G} \tag{96}$$

Where electrical power input to the pump is negligible as compared to thermal energy supplied to the generator.

3.4. Equipment and materials to be used

Hot water distribution system in geothermal source pipelines has been investigated for last decades. Sanja, (2011), has made comprehensive studies on the materials used for source distributions. Thermal expansion of pipelines heated rapidly from ambient to geothermal fluid temperatures causes stress that must be accommodated by careful engineering design. As long as cost is considered, Sanja, (2011) explained that transmission distances of up to 60 km have proven economical for hot water by taking *Akranes project* in Iceland as an example.

Up to now, there is no special equipment on disposal, particularly constructed and produced for use in geothermal direct use projects. However, taking in to account corrosion and scaling caused by unique chemistry of geothermal fluids, different types of materials can be used for their installations.

Polyvinyl chloride is a low-temperature (maximum up to 60 ºC) rigid thermoplastic material. Chlorinated polyvinyl chloride is a higher temperature rated material with a maximum temperature rating up to 100 ºC. Fiberglass piping normally referred to as (fiberglass reinforced plastic) can be compounded to be serviceable to temperatures of up to 140 ºC.

In case galvanized steel used, Consideration should be given to the fact that the protective nature of the zinc coating is generally not effective above 60 ºC. Polyethylene, same chemical family (polyolefin) as poly-butylene is serviceable for temperature is only of 40 to 50 ºC. Sanja, (2011) also explained that carcinogenic nature of asbestos piping system, which has been used for many years, has ceased its production.

Buried, supported on concrete pipe supports as shown in Figure 36 and above ground, aesthetically more pleasing than aboveground as shown in Figure 37, are the two pipelines installations in source distribution.

Figure 36: Aboveground geothermal pipeline in Smokvica, Macedonia (Sanja et al., 2011)

Figure 37: Buried pipes installation (Sanja et al., 2011)

CHAPTER-FOUR

RESULTS AND DISCUSSIONS

4.1. Mathematical analysis of drying system

4.1.1. System sizing

In the drying system, geothermal hot water is allowed to circulate through banks of tube. Ambient air is forced horizontally perpendicular by the help of fan across to the tube banks through which hot water is circulating.

Mathematical analyses of the drying system for each of the following agricultural products (such as: tomatoes, coffee, beans, and maize) are done one by one.

Tube bank dimensions

a. Transversal pitch, (S_T): they are the horizontal distances between center to center of columns of the tubes in the bank. For mathematical analysis for thermodynamics of the bank, it is taken to be 5 cm.

b. Longitudinal pitch, (S_L): these, with equal value to the transversal pitch, are vertical distances between center to center of rows of the tubes in the bank are taken to be 5 cm.

c. Tube diameter, (D): diameter of (copper) tube is taken with its outer diameter of 1 cm.

d. Number of rows, (N_L): $N_L = 8$

e. Number of tubes per row, (N_T): $N_T = 8$

f. Tube length, (L): it is the horizontal distance of single tube which is equals to width of the compartments in which tube bank is placed. The value taken is equal to 1/2 m.

g. Total surface area, A_S =1.0054 m^2

Other parameters

Compartment Capacity also called dryer capacity is amount of crops in *kg* that are required to be dry in the system. In this thesis, capacity of 500 kg for each of matured crops is taken for the analysis of dryer.

Drying time is given period of time in hour for the crops to become dry to the final required specific humidity. In this thesis three time intervals, (*t= 6 hrs, t= 12 hrs, t= 24 hrs*) are used.

Ambient conditions in this area are taken based on the data collected. Atmospheric air is at temperature of 20.5 ^{o}C and relative humidity of 58% and average wind velocity of 0.4 m/s.

Logarithmic mean temperature of this air across the bank of tube will be evaluated from equation (22) and equals to ΔT_{ln}= 7 ^{o}C.

From psychometric chart (Figure 33), air with dry bulb temperature of 20.5 ^{o}C and 58% relative humidity (RH), after sensible heating in the tube bank, will have the following properties at outer temperature of 40 ^{o}C.

h_1= 42.5 kJ/kg at 58% RH, h_2= 65 kJ/kg with approximately 20% RH.

Now, reading of enthalpy change between airs flowing across hot surfaces of the bank, enable us to know its mass flow rate in kg/s through drying channel for different crop types.

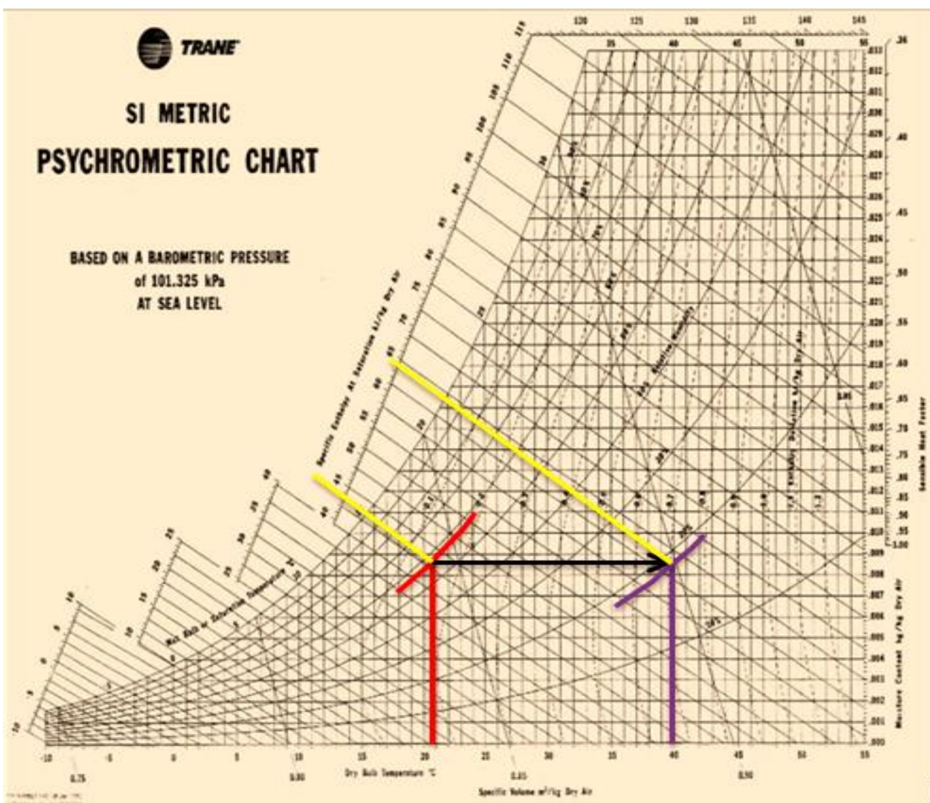

Figure 38: Psychometrics reading of air for the dryer

Enthalpies and relative humidity data of the air evaluated carefully at different temperature value from psychometric chart are presented in Table 10 and explained in Figure 39.

Table 10: Enthalpy and humidity of cross flow air from psychometric chart

Temperature (^{o}C)	Enthalpy (kJ/kg)	Relative humidity (%)
20.5	42.5	58
25	48	47.5
30	54.9	35
35	59.5	26.5
40	65	20
45	70	16
50	75	12
55	81	9

From the graph of Figure 39 it can be seen that as the temperature in the tube bank increases and then increases in temperature of cross flow air will result in increasing enthalpy (*shown by hidden line*) whereas relative humidity of air will be lowered (*shown by solid line*). Therefore, dry air with less humidity contents will be able to remove moisture contents of crops in the drying chamber.

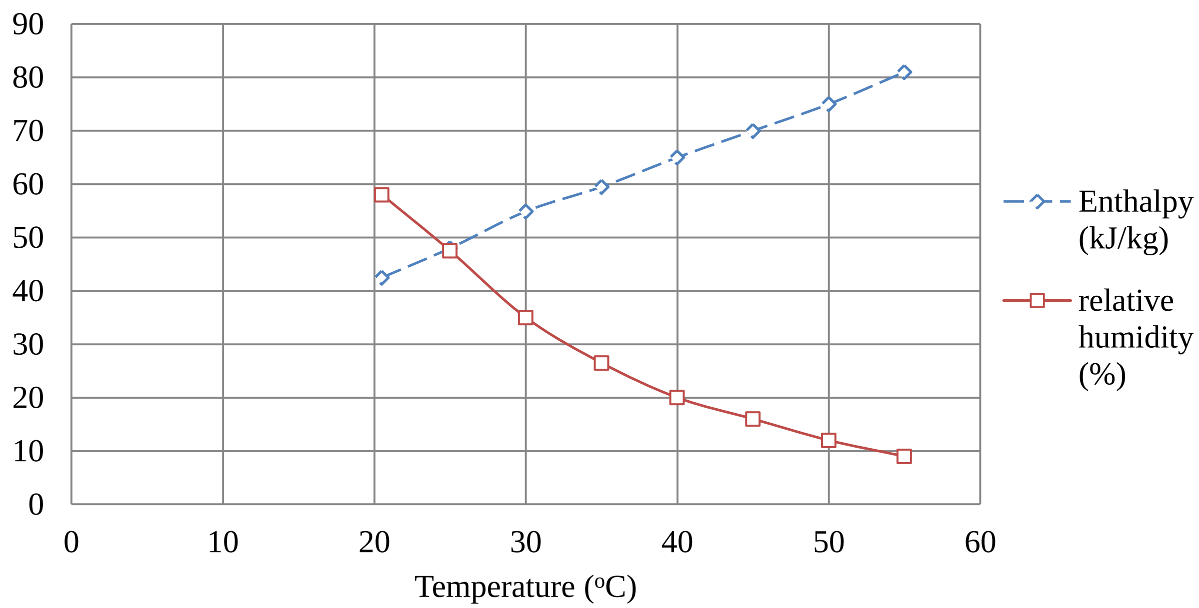

Figure 39: Temperature versus enthalpy & relative humidity of air

4.1.2. Tomatoes drying system

Properties of tomatoes required to estimate the amount of heat transfer rate for drying purposes at different time are presented as follows.

Heat capacity (kJ/kg^{o}C)	Possible drying temperature range (^{o}C)	Initial water content when matured (%)	Required humidity for better durability (%)	Latent heat of moisture at mean temperature (kJ/kg)
$\mathbf{C_{pp}}$= 4.02	50-70	H_{r_1}= 95.7	H_{r_2}=26	h_{fg}= 2357.7

Total amount of heat transfer rate equation (24), required for tomatoes to dry is summation of heat energy for heat-up equation (25) and evaporative heating equation (26). For known values of surface area of tube bank and logarithmic mean temperature difference of air across the bank, heat transfer coefficient *h* at different drying time is evaluated in equation (23). All the results found by applying equations (23-26) at three different time intervals are summarized in Table 11.

Table 11: Calculations summary of required parameters (case of tomatoes dryer)

Time (hr)	Heat required (kW)	Heat transfer coefficients (W/m^2.k)	Nusselt number	Reynolds number
6	53.22	370.54	146.56	26213
12	26.61	185.27	73.28	8723
24	13.30	92.63	36.64	2903

Time (hr)	Maximum air velocity V_{max} (m/s)	Optimum Air velocity V (m/s)	Mass flow rate of air m_a (kg/s)	Volumetric flow rate of air $\tilde{V}$ (m^3/s)
6	42.77	34.21	2.36	34.40
12	14.23	11.40	1.83	11.44
24	4.74	3.80	0.60	3.81

Taking air inlet velocity of 34.21 m/s for the case of tomatoes drying system, the effect of varying longitudinal and transversal pitch of tube bank on heat transfer coefficient is presented in Table 12. Thermal conductivity of air at ambient condition is k = 0.026065 W/m.^{o}C, dynamic viscosity, v = 1.6315x10^{-5} m^{2}/s and tube diameter of D_{out} = 0.01m

Table 12: Effect of longitudinal and transversal pitch in other parameters (case of tomato dryer)

Transversal and longitudinal pitch ($S_D = S_L$) in (m)	Maximum velocity (m/s)	Reynolds number	Nusselt number	Heat transfer coefficient
0.02	68.43	41941	197	513
0.03	51.32	31456	164	428
0.04	45.62	27961	152	397
0.05	**42.77**	**26213**	**146**	**382**
0.06	41.06	25165	142	372
0.07	39.92	24466	140	365
0.08	39.10	23966	138	361
0.09	38.50	23592	137	357
0.1	38.02	23300	136	354

It can be seen from the graph of Figure 40 that maximum velocity that results through tube bank increases with decreasing both pitches. This will results in increasing Reynolds number, Nusselts number, and heat transfer coefficient through the heat exchanger. Conversely, the opposite is true; increasing the gaps between tubes (pitches) result in decreasing Reynolds number, Nusselts number, and heat transfer coefficient through the bank.

One thing to be remarked is that decreasing of the transversal as well as longitudinal pitches is possible up to their values become equal with diameter of the tube. This is because; the evaluation of pitches distances in equations 16-17 is defined for their values greater than tube diameter. Otherwise, evaluation of pitches distance less than or equals to tube diameter will make the equations undefined.

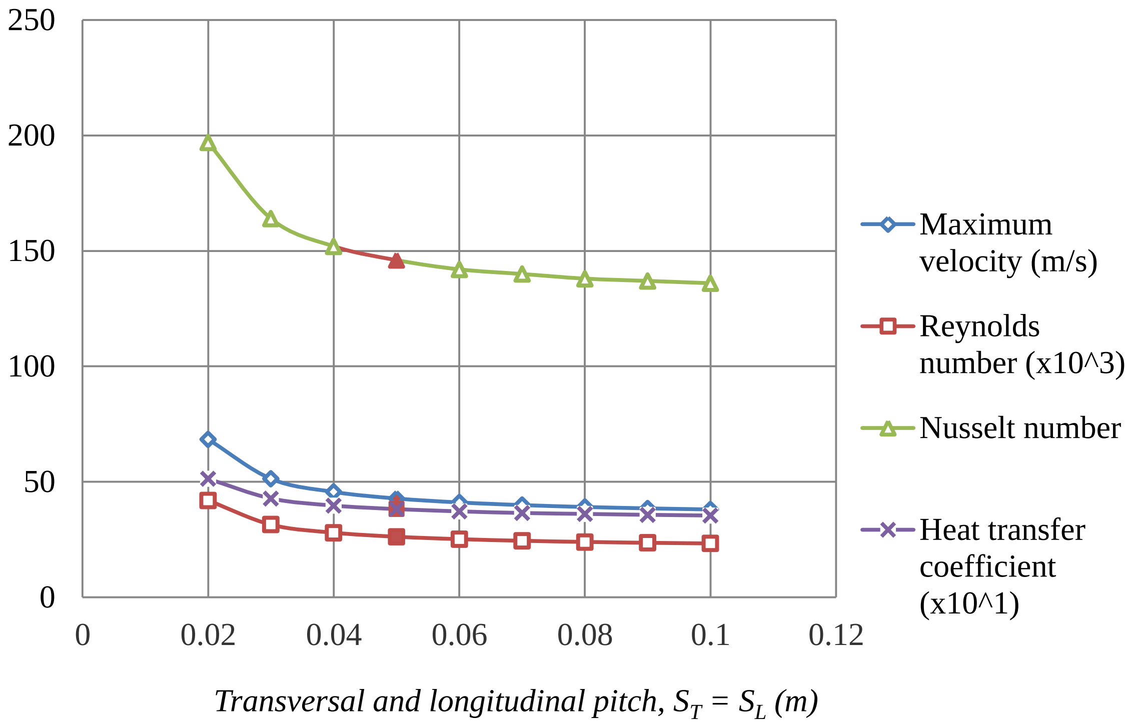

Figure 40: Effect of longitudinal and transversal pitch in other parameters (case of tomato dryer)

Drying time, how long it takes for the crops to dry is one of the factors that alter the operation parameters of the system. The effects of drying time in other parameters such as flow velocity of air, heat transfer rate from the tube bank, mass flow rates & velocity of the hot source, and pump power requirements are given in Table 13 and graphically shown in Figure 41.

Table 13: Effect of drying time in other parameters (case of tomatoes dryer)

Drying time (hr)	Inlet velocity (m/s)	Heat transfer rate (kW)	Mass flow rate of hot source (kg/s)	hot fluid velocity (m/s)	Pump power requirements (kW)
6	34.22	53.22	1.82	23.45	23.8
12	11.40	26.61	0.91	11.7	3.05
24	3.80	13.30	0.45	5.8	0.37

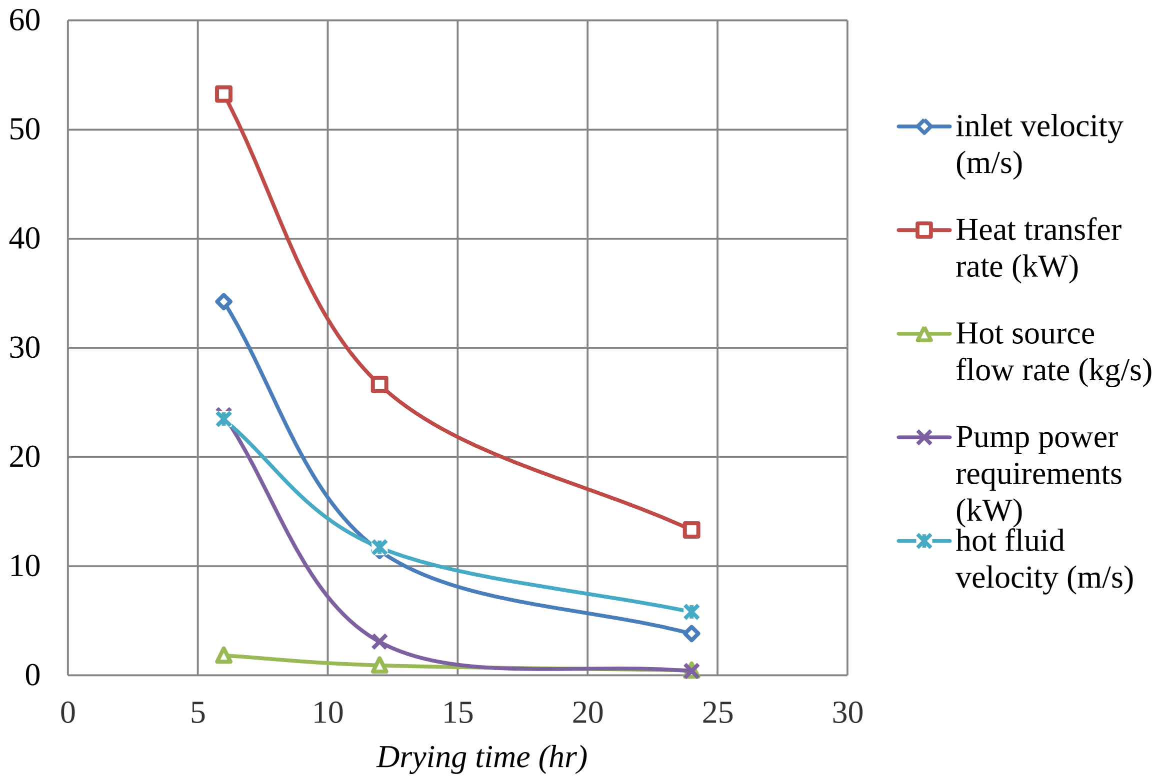

Figure 41: Effect of drying time in other parameters (case of tomatoes dryer)

It is clear from graph of Figure 41 that as drying time increases; the system needs air inlet velocity, heat transfer rate, hot source flow rate, pump power, and hot fluid velocity at minimum amount. The reverse is true that the short we need the crops to dry the greater will be forced air inlet velocity, hot source flow rate through the tube, pump power requirement, hot flow velocity, and then heat transfer rate.

4.1.3. Coffee drying system

The quality of the coffee beans may change due to changes in drying parameters such as temperature difference, drying time and remaining water content in coffee beans. The purpose of drying coffee beans is to reduce the water content contained in coffee beans from the initial moisture content of about 65% to reach the standard water content of about 11-12% (Firmansyah et al., 2018).

According to Firmansyah et al., (2018), the critical temperature drying coffee beans is 50 °C. This is because the drying temperature above 50 °C can lead to physical phenomenon called *case* *hardening* which leads to damage coffee beans. The recommended temperature for drying is about 45 ° C.

Properties of tomatoes required to estimate the amount of heat transfer rate for drying purposes at different time are presented as follows.

Heat capacity (kJ/kg^{o}C)	Possible drying temperature range (^{o}C)	Initial water content when matured (%)	Required humidity for better durability (%)	Latent heat of moisture at mean temperature (kJ/kg)
C_{pp}= 1.4	45-50	H_{r_1}= 65	H_{r_2}= 11	h_{fg}= 2357.7

Similar to that of tomatoes, total amount of heat transfer rate equation (24), required for tomatoes to dry is summation of heat energy for heat-up equation (25) and evaporative heating equation (26). For known values of surface area of tube bank and logarithmic mean temperature difference of air across the bank, heat transfer coefficient *h* at different drying time is evaluated in equation (23). All the results found by applying equations (23-26) are summarized below.

Table 14: Calculations summary of required parameters (case of coffee dryer)

Time (hr)	Heat required (kW)	Heat transfer coefficients (W/m^2.k)	Nusselt number	Reynolds number
6	33.75	235	93	12719
12	16.90	117	46	4233
24	8.44	59	23	1408

Time (hr)	Maximum air velocity V_{max} (m/s)	Optimum Air velocity V (m/s)	Mass flow rate of air m_a (kg/s)	Volumetric flow rate of air $\tilde{V}$ (m^3/s)
6	20.80	16.60	1.64	16.7
12	6.90	5.52	0.82	5.60
24	2.30	1.84	0.41	1.85

Table 15: Effect of longitudinal and transversal pitch in other parameters (case of coffee dryer)

SD = SL) in (m)	Maximum velocity (m/s)	Reynolds number	Nusselt number	Heat transfer coefficient (W/m^2.K)
0.02	33.20	20351	125	325
0.03	24.90	15263	104	271
0.04	22.14	13567	97	252
0.05	**20.754**	**12719**	**93**	**242**
0.06	19.924	12210	90	236
0.07	19.34	11871	89	232
0.08	18.974	11629	88	229
0.09	18.68	11447	87	226
0.1	18.45	11306	86	225

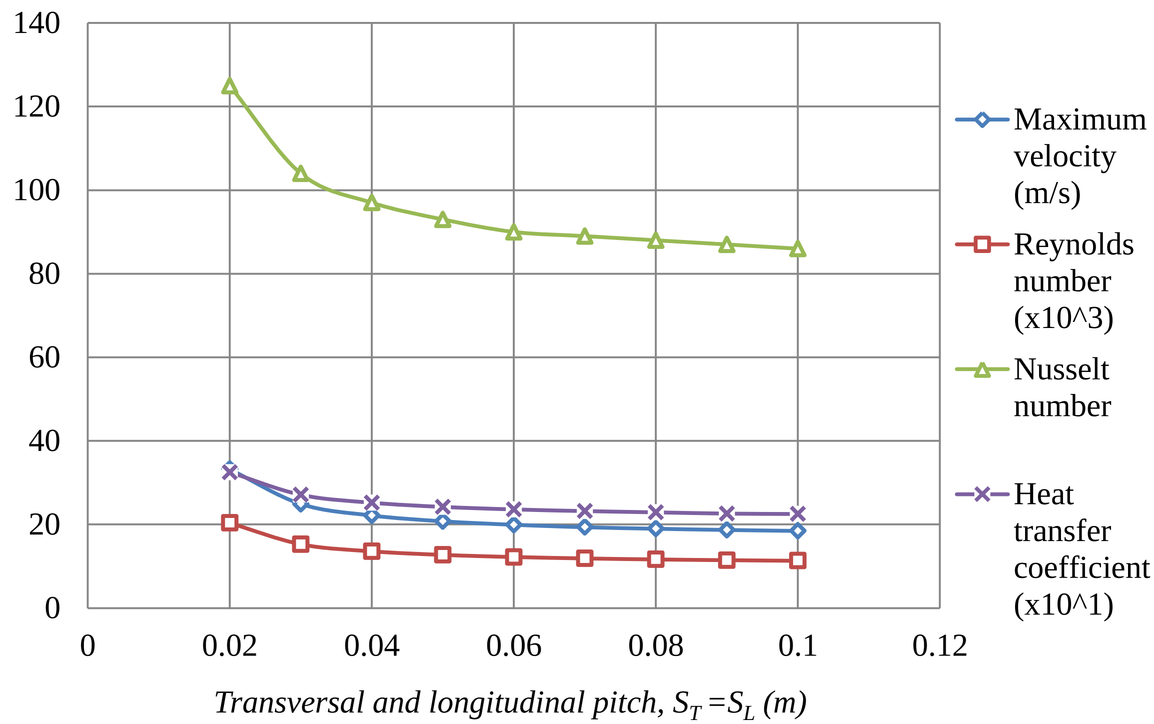

Figure 42: Effect of longitudinal and transversal pitch in other parameters (case of coffee dryer)

Table 16: Effect of drying time in other parameters (case of coffee dryer)

Drying time (hr)	Inlet velocity (m/s)	Heat transfer rate (kW)	Mass flow rate of hot source (kg/s)	hot fluid velocity (m/s)	Pump power requirements (kW)
6	16.60	33.74	1.15	14.8	6.11
12	5.52	16.90	0.58	7.5	0.82
24	1.84	8.44	0.29	3.7	0.10

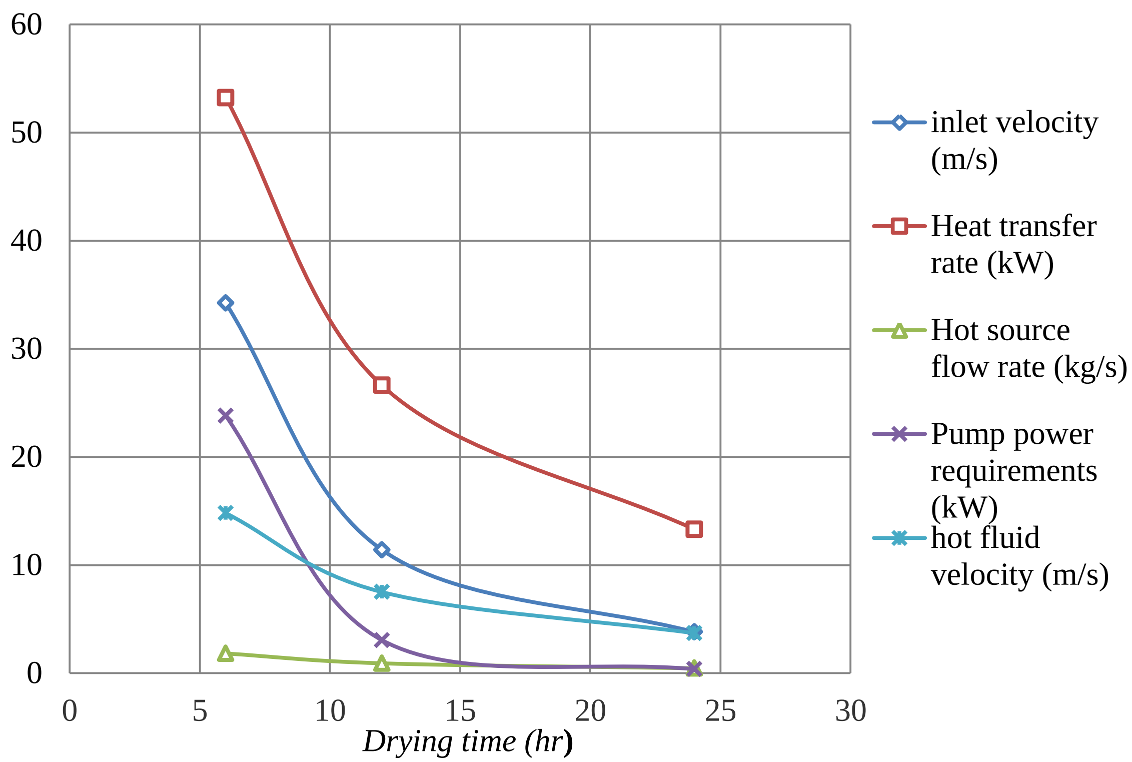

Figure 43: Effect of drying time in other parameters (coffee case)

4.1.4. Beans drying system

Summary of maize properties

Heat capacity (kJ/kg^{o}C)	Initial humidity (%)	Final humidity (%)	Latent heat of moisture (kJ/kg)
C_{PP} = 3.99	H_{r1} = 90.27	H_{r2} = 20	h_{fg} =2357.7

Table 17: Calculations summary of required parameters (case of beans dryer)

Time (hr)	Heat required (kW)	Heat transfer coefficients ($W/m^2.k$)	Nusselt number	Reynolds number
6	49.7395773	346.306983	136.971996	23545
12	24.8697886	173.153492	68.4859981	7835
24	12.4348943	86.5767458	34.2429991	2607

Time (hr)	Maximum air velocity V_{max} (m/s)	Optimum Air velocity V (m/s)	Mass flow rate of air m_a (kg/s)	Volumetric flow rate of air $\tilde{V}$ (m^3/s)
6	38.41	30.73	2.42	30.87
12	12.78	10.23	1.21	10.27
24	4.25	3.40	0.61	3.42

Table 18: Effect of longitudinal and transversal pitch in other parameters (case of beans dryer)

(SD = SL) in (m)	Maximum velocity (m/s)	Reynolds number	Nusselt number	Heat transfer coefficient
0.02	61.50	37672	184	480
0.03	46.10	28254	154	400
0.04	40.10	25114	143	372
0.05	**38.41**	**23545**	**137**	**357**
0.06	36.88	22603	133	348
0.07	35.85	21975	131	342
0.08	35.12	21527	129	337
0.09	34.57	21190	128	334
0.1	34.14	20928	127	331

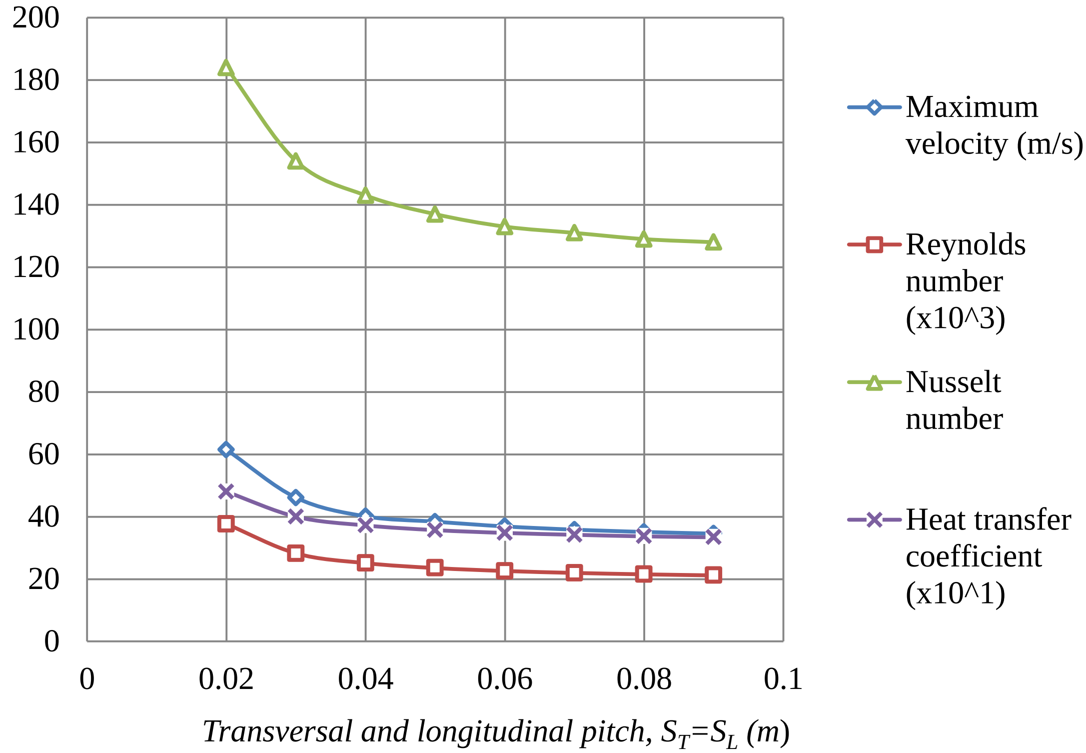

Figure 44: Effect of longitudinal and transversal pitch in other parameters (beans case)

Similar to previous cases of tomatoes and coffee, drying time effect on other parameters of the dryer for beans is explained in Table 19 and graphically in Figure 45.

Table 19: Effect of drying time in other parameters (case of beans dryer)

Drying time (hr)	Inlet velocity (m/s)	Heat transfer rate (kW)	Mass flow rate of hot source (kg/s)	hot fluid velocity (m/s)	Pump power requirements (kW)
6	30.73	49.74	1.70	22	19.9
12	10.22	24.87	0.85	10.9	2.55
24	3.40	12.44	0.42	5.4	0.31

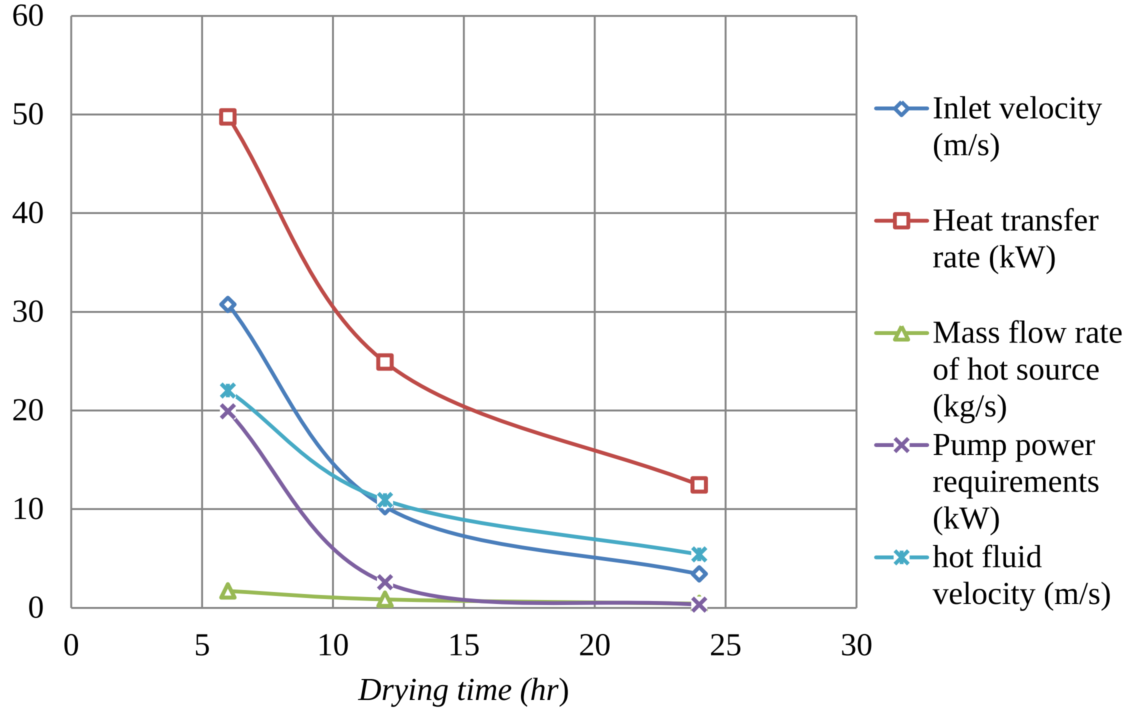

Figure 45: Effect of drying time in other parameters (case of beans dryer)

4.1.5. Maize drying system

Maize is an all-important crop which provides an avenue for making various types of foods. Every part of the maize plant has economic value: the grain, leaves, stalk, tassel, and cob can all be used to produce a large variety of food and non-food products.

According to Bola et al., (2013), initial moisture content of the matured maize (*average specific heat capacity of 1.8 kJ/kg.^{o}C*) to be dried is 35% and the final desired moisture content for the maize to preserve without damage is 13%.

Summary of maize properties

Heat capacity (kJ/kg^{o}C)	Possible drying temperature range (^{o}C)	Initial water content when matured (%)	Required humidity for better durability (%)	Latent heat of moisture at mean temperature (kJ/kg)
$\mathbf{C_{pp}}$= 1.8	45-50	H_{r_1}= 35	H_{r_2}= 13	h_{fg}=2357.7

Table 20: Calculation summary of other parameters (case of maize dryer)

Time (hr)	Heat required (kW)	Heat transfer coefficients (W/m^2.k)	Nusselt number	Reynolds number
6	14.61	101.74	40.24	3369
12	7.31	50.87	20.121	1121
24	3.65	25.43	10.10	373

Time (hr)	Maximum air velocity V_{max} (m/s)	Optimum Air velocity V (m/s)	Mass flow rate of air m_a (kg/s)	Volumetric flow rate of air $\tilde{V}$ (m^3/s)
6	5.45	4.40	0.71	4.42
12	1.83	1.46	0.36	1.47
24	0.61	0.48	0.20	0.50

Table 21: Effect of longitudinal and transversal pitch in other parameters (case of maize dryer)

(S_D = S_L) in (m)	Maximum velocity (m/s)	Reynolds number	Nusselt number	Heat transfer coefficient
0.02	8.80	5390	54.11	141
0.03	6.60	4043	45.14	117
0.04	5.90	3593	41.91	109
0.05	**5.50**	**3369**	**40.24**	**105**
0.06	5.30	3234	39.22	102
0.07	5.13	3144	38.53	100
0.08	5.03	3080	38.03	99
0.09	4.95	3032	37.66	98
0.1	4.89	2994	37.36	97

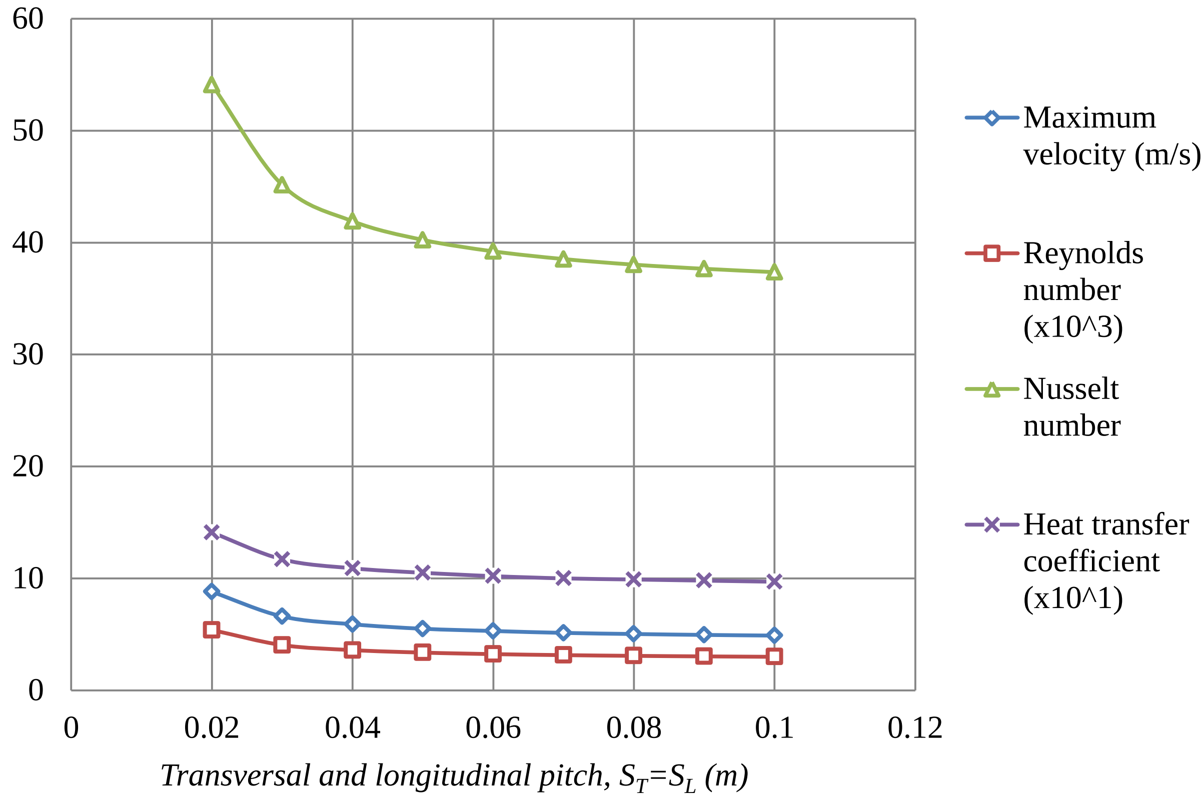

Figure 46: Effect of longitudinal and transversal pitch in other parameters (case of maize dryer)

Similar to previous cases of tomatoes, coffee and beans drying time effect on other parameters of the dryer for maize is explained in Table 22 and graphically in Figure 47.

Table 22: Effect of drying time in other parameters (case of maize dryer)

Drying time (hr)	Inlet velocity (m/s)	Heat transfer rate (kW)	Mass flow rate of hot source (kg/s)	hot fluid velocity (m/s)	Pump power requirements (kW)
6	4.40	14.61	0.5	6.44	0.53
12	1.46	7.31	0.25	3.22	0.07
24	0.49	3.65	0.12	1.55	0.01

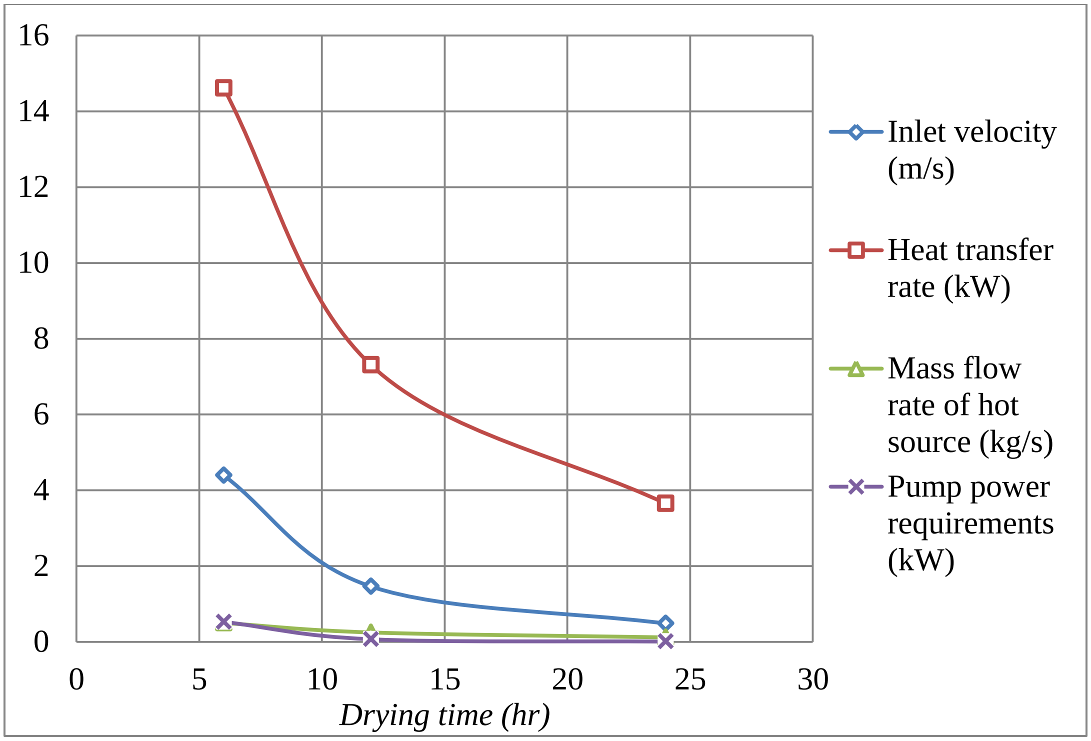

Figure 47: Effect of drying time in other parameters (case of maize dryer)

More generally, Figure 40, Figure 42, Figure 44, and Figure 46 show effects of longitudinal and transversal pitches on maximum velocity, Reynolds & Nusselt number, and heat transfer coefficient for in-line arrangement of tube bank heat exchanger of tomatoes, coffee, beans, and maize dryer, respectively. Thus, the Reynolds number, Nusselt number, and then heat-transfer coefficients increase mainly with decreasing the pitches. **Note that**: these results are consistent with that has been found in the study of (Khan, 2006) and (Gupta, 2014).

4.1.6. Pressure drop and pumping power

Geothermal mass flow rate, m_{hot} through the heat exchanger of tube bank is calculated based on heat transfer rate needed for different crops. For example, the heat transfers Q from the values calculated so far are 53.22 kW for tomatoes, 33.74 kW for coffee, 49.73 kW for beans, and 14.61 kW for maize to accomplish drying purpose at 6 hrs. Dynamic viscosity of water (at 54 ^{o}C), μ = 5.122 x10^{-3} Pa.s.

Logarithmic mean temperature difference is taken to be ΔT_{ln}= 7^{o}C and specific heat of the geothermal water is approximated to C_P = 4.186 kJ/kg °C. Therefore, mass flow rate of the water is calculated and tabulated in Table 23, from $\dot{m} = Q/C_P\Delta T_{lm}$.

Table 23: Mass flow rates of hot water required at different drying times

	Mass flow rate of hot water (kg/s)		
Items	@ t = 6 hrs	@ t = 12 hrs	@ t = 24 hrs
1. Tomatoes	1.82	0.91	0.45
2. Coffee	1.15	0.58	0.29
3. Beans	1.70	0.85	0.42
4. Maize	0.5	0.25	0.12

Darcy-Weisbach friction coefficient λ**,** from *Colebrooke* equation (29) can be calculated for surface roughness value of the tube k = 0.0015 x10^{-3} m and Reynolds number of R_E= 45,242. Thus, friction coefficient at 6 hrs drying time in the case of tomatoes will become: λ = 0.0446.

In similar manner, calculated values of Reynolds number, Darcy-Weisbach friction, and the hot fluid velocity in the case of tomatoes, coffee, beans, and maize at different drying time are tabulated in Table 21. Note that in Table 21, numbers 1, 2, 3, and 4 stands for tomatoes, coffee, beans, and maize, respectively.

Table 24: Reynolds number, friction coefficients, and fluid velocity at different drying time

	@ t = 6 hrs			@ t =12 hrs			@ t =24 hrs		
	R_E	λ	V_f (m/s)	R_E	λ	V_f (m/s)	R_E	λ	V_f (m/s)
1	45242	0.0446	*23.45*	22621	0.0456	*11.7*	11186	0.0474	*5.8*
2	28586	0.0452	*14.8*	14417	0.0466	*7.5*	7457.5	0.0491	*3.7*
3	42259	0.0447	*22*	21129	0.0457	*10.9*	10440	0.0477	*5.4*
4	12429	0.0471	*6.44*	6214	0.0501	*3.22*	2983	0.0557	*1.55*

Now, major pressure loss, ΔP_{maj} of hot fluid flowing due to friction, inside the tube bank will be calculated by rearranging equation (28). In addition, pressure drop due to curved structures will be calculated from equation (30).

ΔP_{maj}= 4.8 x10^6 Head, ΔP_{min}= 359 Head, and ΔP_{dry}= 4.8 x10^6 Head

Finally, hydraulic power needed and then maximum electrical power consumption for this drying system will be:

$P_{m,dry}$= 23.8kW

Similarly, hydraulic power requirement in order to supply hot source for the drying systems to accomplish at different time are calculated and values are tabulate below.

Table 25: Hydraulic power requirement at different drying time

Product type	@ *t* =6 hrs		@ *t* =12 hrs		@ *t* =24 hrs	
	Head Loss x10^6m	Power req (kW)	Head Loss x10^6m	Power req (kW)	Head Loss x10^6m	Power req (kW)
Tomatoes	4.8	23.8	1.23	3.05	0.3	0.37
Coffee	1.95	6.11	0.52	0.82	0.13	0.10
Beans	4.3	19.9	1.1	2.55	0.27	0.31
Maize	0.386	0.53	0.1	0.07	0.03	0.01

Therefore, electrical motor with maximum rated power of 23.8 kW can be selected in order to supply hot water from source to the drying compartment where heat energy is transferred to forced air across the tube bank.

Once, an electric motor with maximum power is selected, the flow rate of hot source will be at constant value of 1.82 kg/s against the pressure developed in the tube bank. To operate the system for different type of crops and at different drying time, it is possible by only adjusting air velocity V.

The results show that mass of moisture to be removed from different types of crops are different due to variations in thermal as well as physical properties of crops. Thus, 470.95 kg, 303.4 kg, 439.2 kg, and 126.44 kg of moistures are to be removed from each of 500 kg of tomatoes, coffee, beans, and maize respectively in order to obtain their suitable storage humidity.

It is also seen that mass flow rates of forced air across the tube banks vary with the drying time. The fast we need the crops to dry, the great will be mass flow rates of forced air and therefore, high consumptions of power. For example, if given amount of tomatoes are to be dry at 6, 12, and 24 hrs, thus 1.82, 0.91, and 0.45 kg/s flow of hot spring are required respectively (as shown in Table 23).

4.2. Mathematical analysis of VARS

4.2.1. The refrigeration capacity

For mass of water, m = 66,000 kg with initial approximate value of 37.5 ^{o}C to cool in to recommended value of 16 ^{o}C, cooling load of the system using equation (38) will be $\dot{Q}_{tot} = 103.12$ kW.

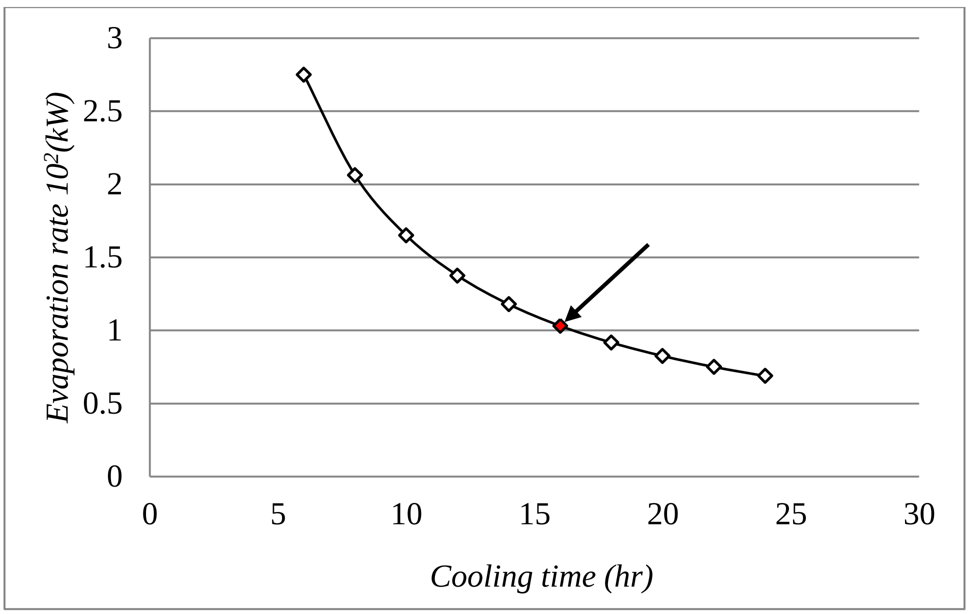

Figure 48: Variation of evaporation rate with cooling time

From the graph of Figure 48, it can be seen that evaporation rate (or) cooling capacity of the system increases with decreasing cooling time. This means that the fast we need to cool given volume of water in to final recommended temperature, the great will be rate of removal of heat in the evaporator for corresponding period of time. The point on this graph indicated with filled-arrow shows the operating point of the system to be designed. The system is able to cool 66,000 liters of the water at 16 hrs.

4.2.2. Enthalpies (from enthalpy-concentrations diagram)

Enthalpy values of the refrigerant evaluated at different states from enthalpy-concentration chart (Appendix A-9) are, h_1= 1425.2 kJ/kg, h_2 = 310 kJ/kg, $h_3 = h_2$ = 310 kJ/kg, h_4 = 1325 kJ/kg, $h_5 = h_6$ = 98.9 kJ/kg, and $h_7 = h_8$ = -60 kJ/kg, temperature at the outlet of condenser ($t_{out\ cond}$ =21 ^{o}C). A positive value indicates the products have greater enthalpy, or that it is an endothermic reaction (heat is required) a negative value indicates the reactants have greater enthalpy, or that it is an exothermic reaction (heat is produced).

4.2.3. Mass flow rate

Substituting known values in equations (39-41), the mass flow rates will be $\dot{m}_r$ = 0.102 kg/s, $\dot{m}_w$ = 1.224 kg/s, and $\dot{m}_s$ = 1.33 kg/s. The relations between mass flow rates and desired cooling time are plotted in Figure 44.

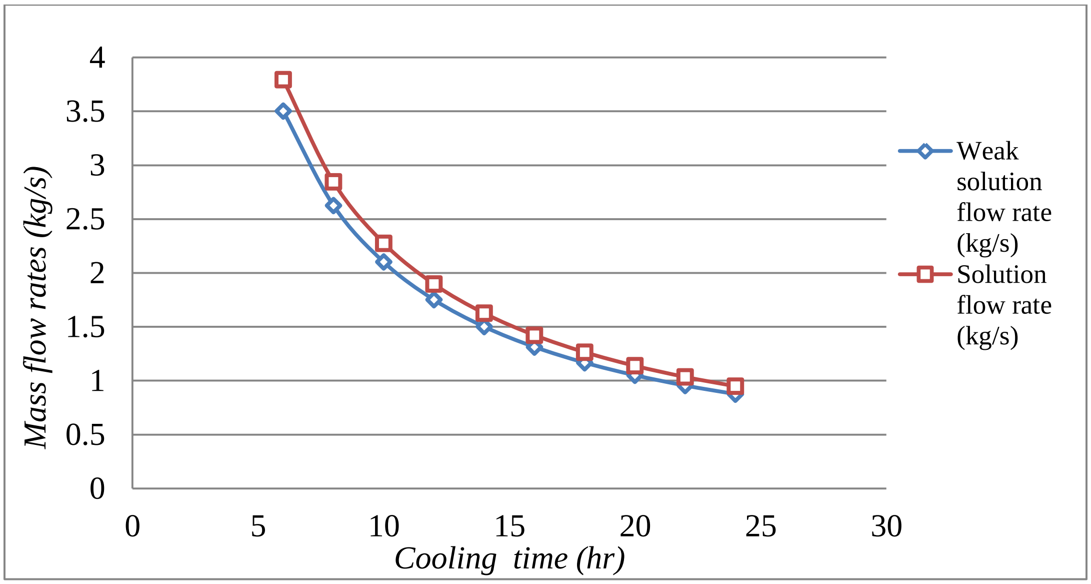

Figure 49: Weak and strong solution flow rates variation with required freezing time

Based on the results of mass flow rates shown in Figure 50, flow rates of both strong and weak solutions increase if cooling effect is to be performed during short period of time. This seems resulting in consuming more pumping power. But, it will be for short period of time.

4.2.4. Condenser with its finned surfaces

Heat rejected by condenser as given by equation (42) is Q_C = 113.8 kW and Surface area of condenser tubes equation (44 a) is A_c = 1.51 m^2.

Face areas and effective diameter for the heat exchangers from the given volumetric flows are calculated (using equations 29) as FA = 1 m^2 and D_E = 1.13 m.

Then refrigerant-side Reynolds number, Prandtl number, and heat transfer coefficient of the flow using equation (46) will be: $\mathrm{R_E}$ = 1526, $\mathrm{P_r}$ = 1.346, and $\mathrm{h_i}$ = 225.7 W/m^2.^{o}C

Then air-side Reynolds number, Prandtl number, and heat transfer coefficient of the flow using equation (48) will be: R_E = 422,806, P_r= 0.71378, and h_o = 12.06 w/m^2.^{o}C

Overall heat transfer coefficient U_t, based on the total fin-side surface area equation (53 a) and assuming fin efficiency of η_f = 80%, finned surface area equation (52) will be: U_t = 4.47 w/m^2.^{o}C and A_t= 1850 m^2.

4.2.5. Capillary tube

Selected diameter of capillary tube for the cooling capacity of 103.12 kW is 3 mm. Saturated liquid ammonia from condenser exit enters the tube at 30 ^{o}C and flow through it until its temperature drops to 6 ^{o}C. The assumed intermediate sections have the temperatures of 25, 20, 15, 10, and 6^{o}C. All the calculations are completed by utilizing principles and equations applied for capillary tube and the results are tabulated from Table 26 through Table 29.

The mass flow rate, $\dot{\mathrm{m}}_\mathrm{r}$ = 0.102 kg/s, cross section, A = 7.1 x10^{-6} m^2, and mass constant, G = 14.4 x10^3 kg/m^{2}s.

Table 26: Calculations done for isenthalpic flow but with Δh= -Δ(KE)

Section	t *(^{o}C)*	P *(bar)*	*x*	10^3(*v*) m^3/kg	u=G*v* (m/s)	Δh (kJ/kg)
c	30	11.7	0	1.68	24.2	0
1	25	10.04	0.021	4.28	61.61	1.60
2	20	8.60	0.040	7.63	109.86	4.14
3	15	7.29	0.060	11.92	171.72	8.71
4	10	6.20	0.078	17.48	251.78	16.95
5	6	5.16	0.092	23.84	343.25	27.21

Results of table 26 are calculated by equation (55) for quality, equation (56) for specific volume, equation (60) for velocity, and equation (61) for change in enthalpies through all sections.

Table 27: Final iterations for enthalpy, specific volume, and enthalpy change

Section	(h) iterated (kJ/kg)	x	$10^3(v)$ iterated (m^3/kg)	(u) iterated (m/s)	(Δh) iterated (kJ/kg)
c	342.08	0	1.68	24.2	0
1	317.92	0.004	2.16	31.1	0.19
2	293.96	0.008	2.80	40.4	0.33
3	270.195	0.010	3.45	49.6	0.41
4	246.62	0.012	4.03	57.9	0.44
5	227.89	0.012	4.53	65.3	0.45

Table 28: Viscosities, Friction factor, and Reynolds number (equations 62, 63, and 64)

Section	x	μ_f	μ_g	μ	f	R_E
c	0	0.134	0.01031	0.134	0.01342936	322388
1	0.004	0.139	0.01012	0.13848448	0.01354033	311948
2	0.008	0.145	0.00994	0.14391952	0.01367127	300167
3	0.010	0.151	0.00976	0.1495876	0.01380394	288793
4	0.012	0.158	0.00958	0.15621896	0.01395444	276534
5	0.012	0.164	0.00943	0.16214516	0.01408494	266427

Table 29: Total, acceleration, & friction pressure drop, total length required (equations 52-54)

Section	Δp (bar)	Δp_A (bar)	Δp_F (bar)	Mean friction factor (f_{mean})	Mean velocity u_{mean}, (m/s)	Incremental in Length (ΔL)
c-1	1.66	0.093	1.56	0.0060	27.65	1.74
1-2	1.44	0.132	1.30	0.0130	35.75	1.12
2-3	1.31	0.132	1.17	0.0140	45	0.79
3-4	1.09	0.121	0.96	0.0130	53.75	0.54
4-5	1.04	0.106	0.93	0.0138	61.6	0.45
		Total length of capillary required				4.65 m

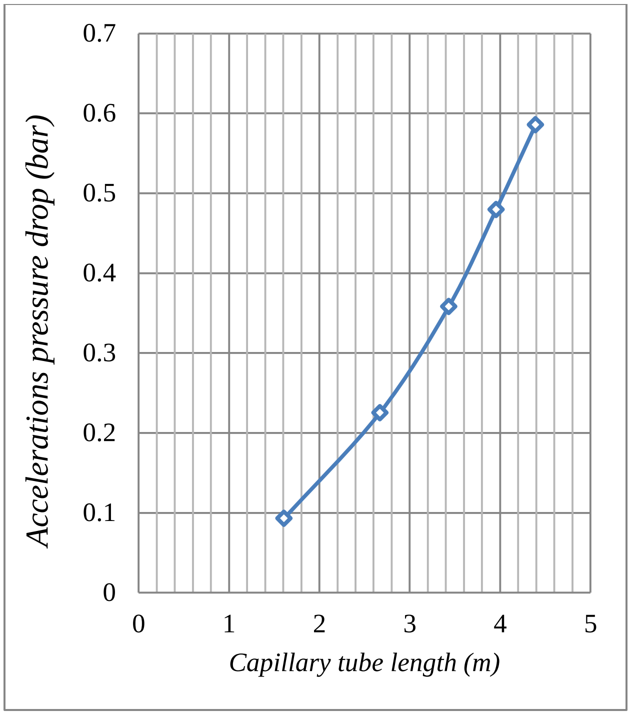

(a)

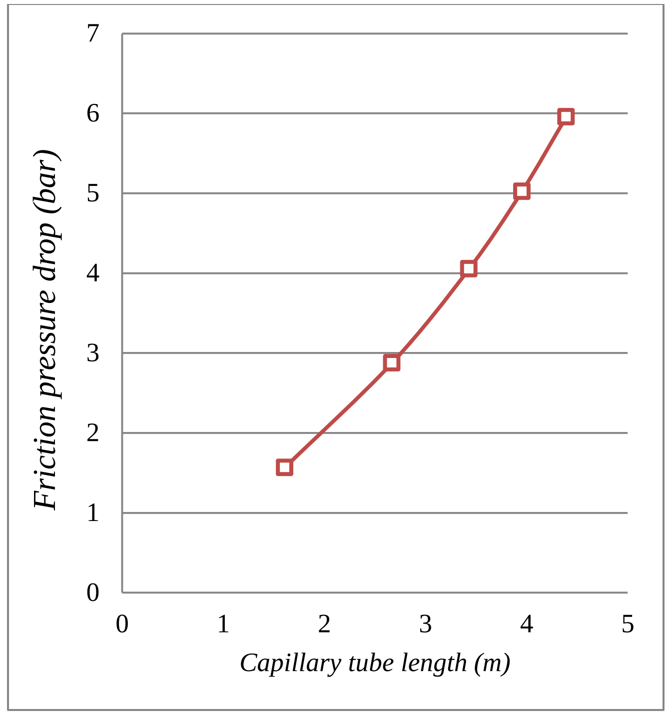

(b)

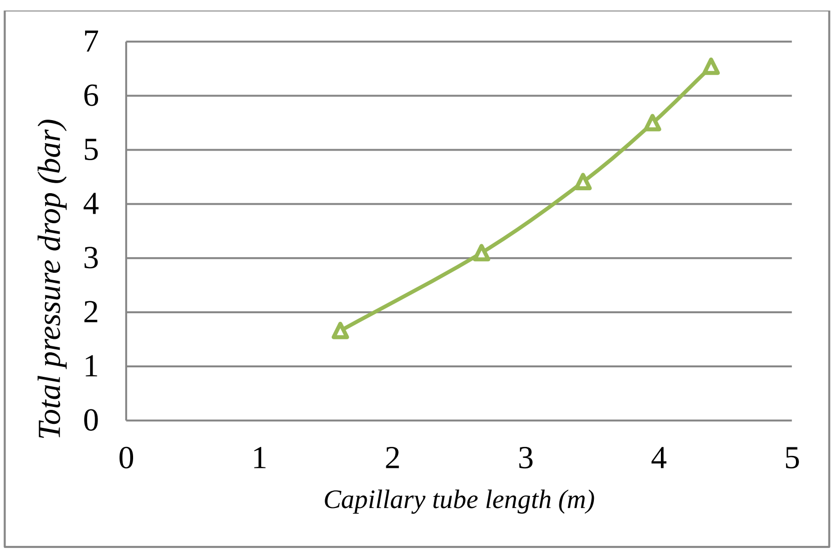

(c)

Figure 50: Pressure drop increment versus capillary tube length (a) Acceleration pressure drop (b) Friction pressure drop, and (c) Total pressure drop.

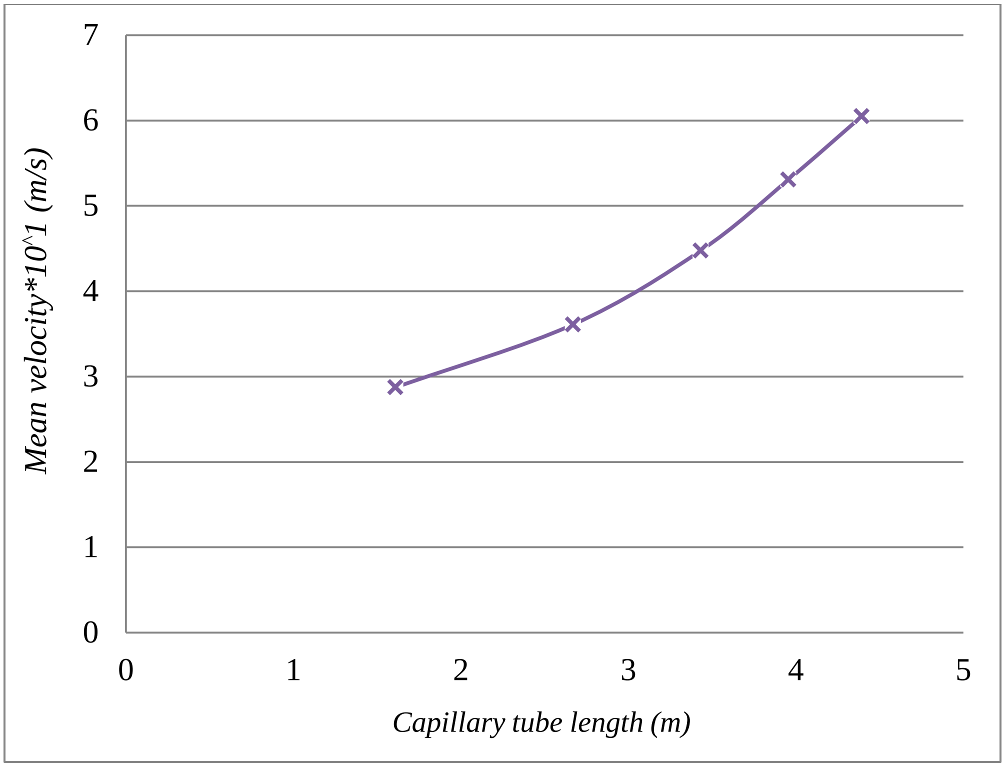

Figure 51: Mean velocity versus capillary tube length

Final iterations values of enthalpy, specific volume, velocity, and adiabatic enthalpy losses (Table 26) have been used to calculate viscosities, friction factor, Reynolds number, Total, acceleration, & friction pressure drop, and total length required by using equations 54-68. The results of these calculations are listed in Table 27-29 and plotted in graphs of Figure 50 and 51.

Pressure drop increments with increasing total length of capillary tube indicate that as a length of capillary tube increases total pressure of refrigerant will decreases. Thus, in order to obtain pressure drop from 10 bar of condenser pressure to 2 bar of evaporator pressure over 4.6 m capillary tube of given diameter has to be used.

4.2.6. Evaporator

Hence, the evaporators are assumed as air-cooled heat exchanger for water cooling applications (overall heat transfer coefficient, U is then within range of 600-750 W/m^2.^{o}C). Therefore, heat transfer area A_E for 103.12 kW capacity of the chiller is calculated by equation (70).

$$A_E = 12.22 \text{ m}^2$$

Furthermore, selecting evaporator copper tube of diameter D_{ev} =1.5cm for the developing cooling system, from equation (70 a) total tube length L required is calculated to be $L = 237.7\ m$.

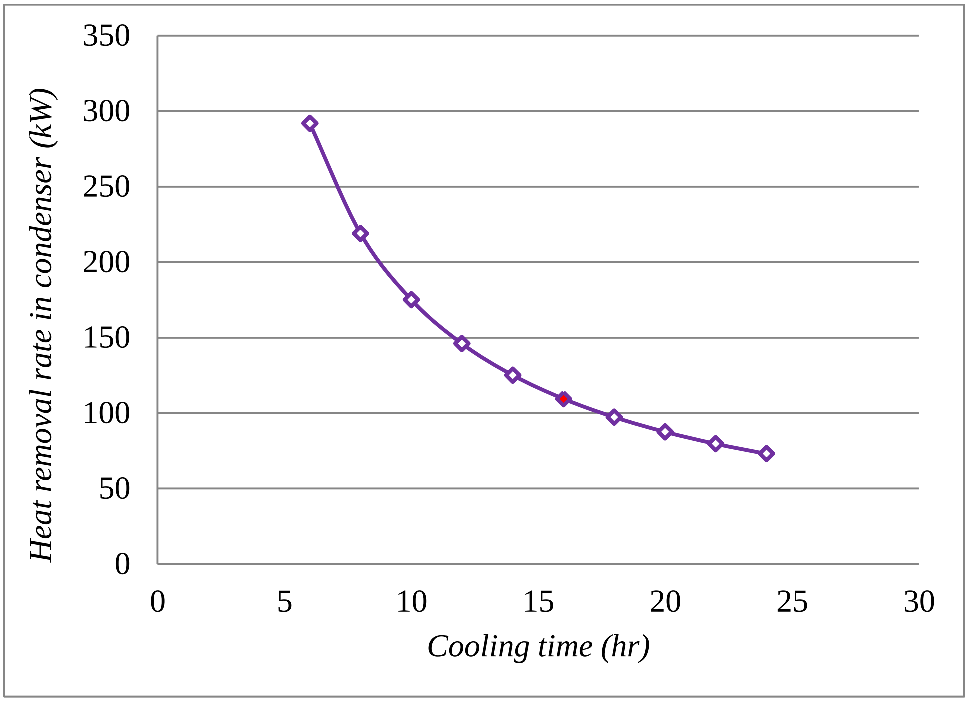

Figure 52: *Heat removal rate in condenser versus* required cooling time

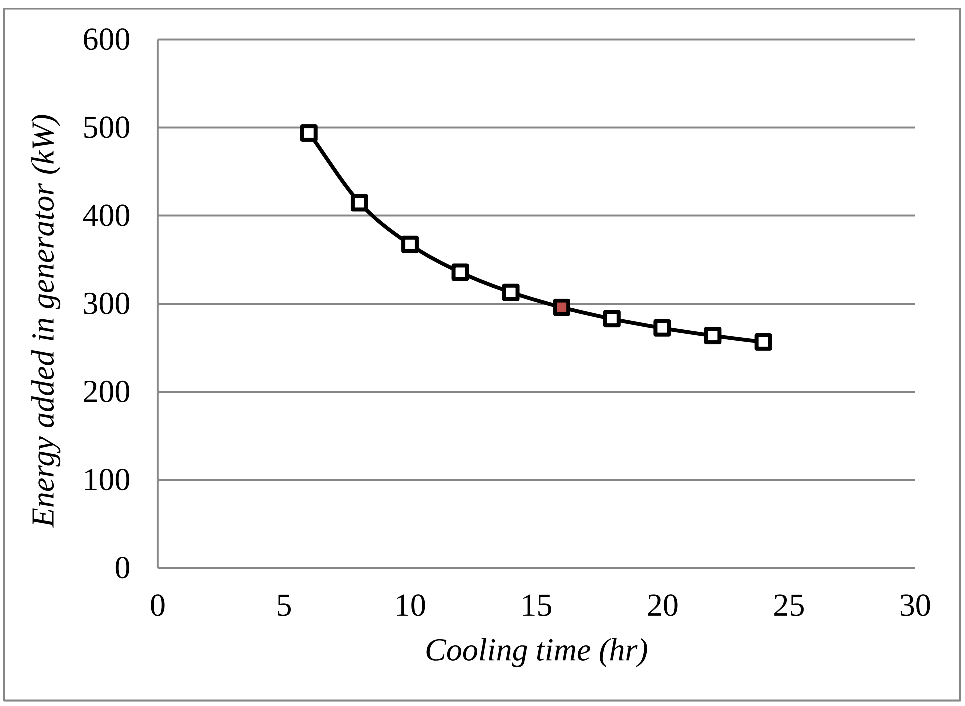

Figure 53: *Energy added in generator versus* required cooling time

4.2.7. Generator

Energy to be added from hot source Q_G is calculated from equation (72) is Q_G= 295.96 kW. Therefore, 295.96 kW of thermal energy have to be collected in heat exchanger of generator at 2.28 kg/s flow rate of hot water with *54°C* in order to meet refrigeration capacity of 103.12 kW in 16 hrs.

For the values of 2.28 kg/s and C_P = 4.31 kJ/kg°C for geothermal hot spring change in temperature of the source after heat exchanged in the generator, is Δt = 35 °C and Δt_m = 12 °C. Applying overall heat transfer coefficient of U = 550 W/m^2.°C, surface area of tube heat exchanger of generator and its length will be A_G= 0.05 m^2 and *L*= 1.65 m, respectively. Therefore, copper tube of *1 cm* diameter with length of about *1.67 m* can be used in the generator to heat-up the aqua-ammonia solution.

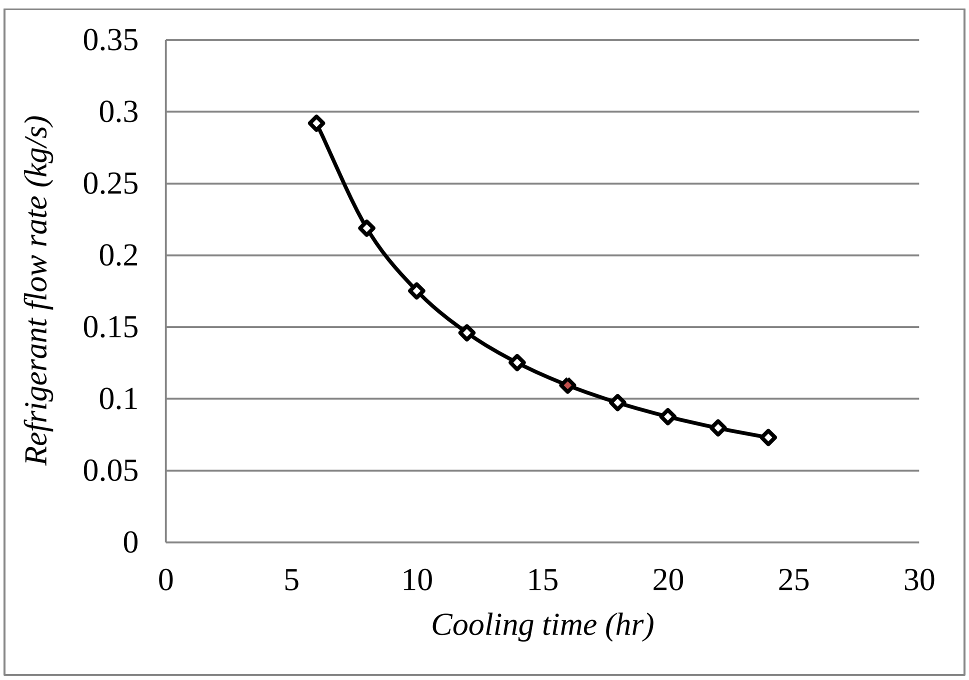

Figure 54: Refrigerant flow rates versus cooling time

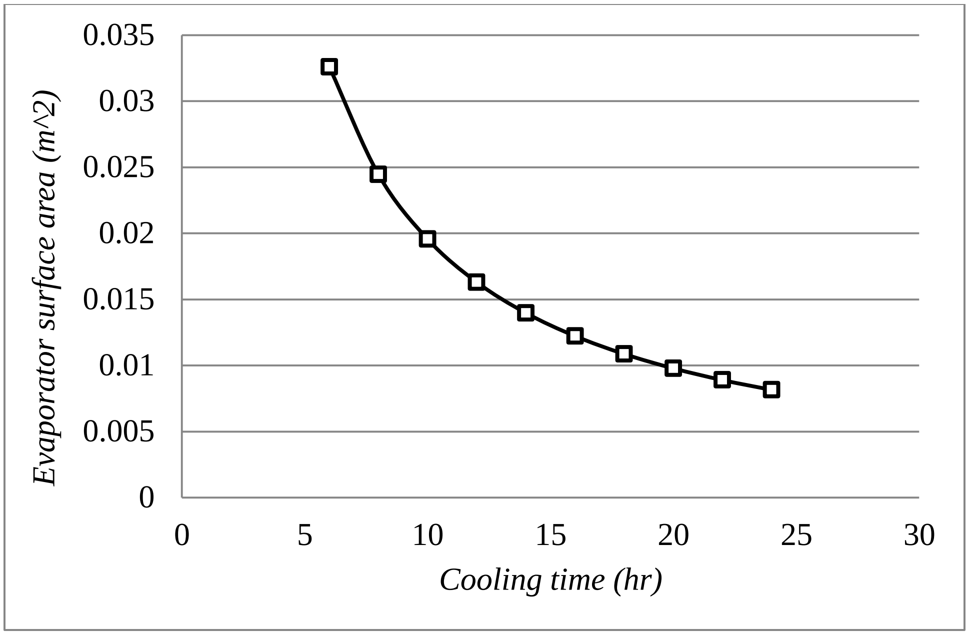

Figure 55: Evaporator surface area versus cooling time

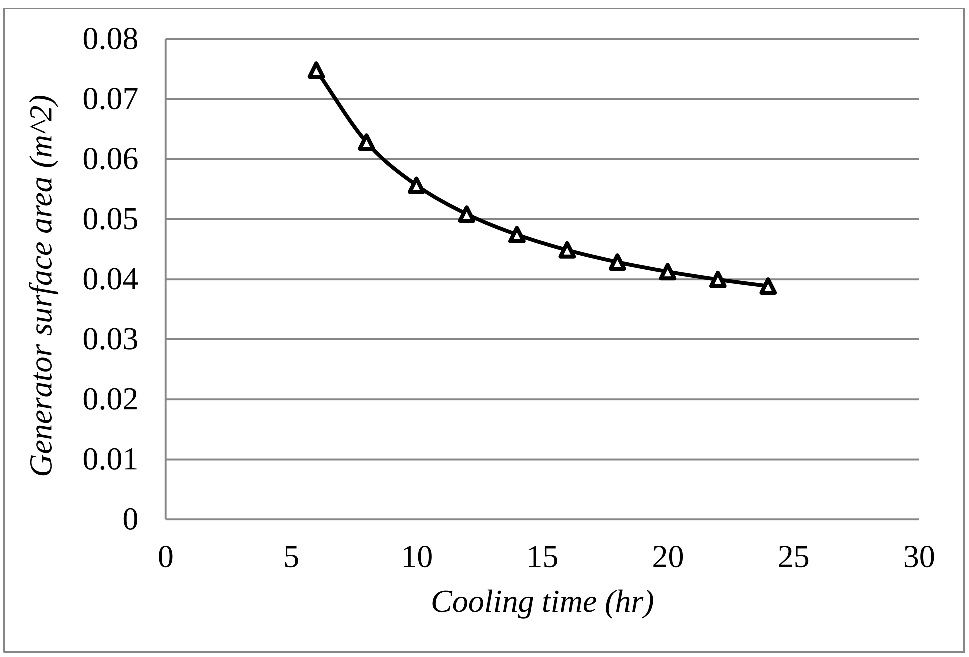

Figure 56: Generator surface area versus cooling time

4.2.8. Absorber

Heat of absorption rejected from the solution in the absorber is calculated from equation (76) and then surface area of absorber is from equation (76 a) Q_A = 336 kW.

4.2.9. Pressure relief valve

Pressure relief valve of poppet type is designed to maintain pressure difference between generator and absorber and therefore its parameters are given in Table 30.

Table 30: Dimensions of poppet valve

No.	Parameters	Values
1.	Poppet seat diameter	d = 2 cm
2.	vertex angle	$\alpha = 60^o$
3.	Maximum distance spring has to be deflected	x = 0.004 m
4.	poppet area subjected to the pressure	d_P= 0.0165m
5.	Area of conical poppet subjected to the pressure force	$A_P = 2.14 \text{ x}10^{-4}\ m^2$
6.	Pressure force	F_P=128.4 N
7.	Spring stiffness	k_{rv} = 32 kN/m

Now, the spring material to overcome against the difference in generator and evaporator pressure in the valve should have the dimensions listed in Table 31.

Table 31: Dimensions of spring used in poppet valve

No.	Parameters	Values
1.	Diameter of spring wire	d = 2 mm
2.	Mean coil diameter	D = 1cm
3.	Number of turns	n = 6
4.	Spring stiffness	k = 32 kN/m
5.	Modulus of rigidity	G = 95x109 Pa
6.	Outer diameter of coil	D+d = 1.2 cm

4.2.10. Pump

A. Solution pump

For known parameters given in Table 32; hydraulic, shaft and electrical power are calculated as follows (equations 84-89). Therefore, volumetric flow rates $\dot{V}_s$= 5.8 m^3/h, hydraulic power P_h= 0.85 kW, shaft power P_S= 0.95 kW, and electrical power P_{el} = 0.97 kW.

Table 32: Known parameters for solution pump design

No.	Parameters	Values
1.	strong solution flow rate	$\dot{m}_s$= 1.417 kg/s
2.	density of the solution	ρ = 880 kg/m^3
3.	pressure difference	ΔP = (10.7- 4.7) bar = 6 bar = 61.2 meters Head
4.	acceleration due to gravity	g = 9.81 m/s^2
5.	pump efficiency	η_p= 90%
6.	electrical efficiency	η_p= 98%

B. Hot spring pump

For given and known parameters summarized in Table 33, values of power requirement to pump hot water is calculated by using equations 90-95.

Table 33: Known parameters for hot source pump design

No.	Parameters	Values
1.	mass flow rate of hot water source	m= 2.28 kg/s
2.	diameter of coiled tube of generator	d= 1cm
3.	total length of tube	L= 1.65 m
4.	coil diameter	D_{coil}= 10 cm
5.	density of water	ρ = 988 kg/m^3
6.	length of one turn of coil	πd = 0.314 m
7.	total number of turn of coil	1.6/0.314 = 5
8.	Volumetric flow rate	0.0023 m^3/s
9.	Cross-section of tube	A= 7.85 x10^{-}5 m^2
10.	Velocity of flow	V= 29.04 m/s
11.	Viscosity (at 54^{o}C)	μ = 5.122 x10^{-3} Pa.s
12.	Reynolds number	R_E= 56, 016
13.	surface roughness (copper material)	k= 0.0015 x10^{-3} m
14.	friction coefficient	λ = 0.0209
15.	and relative roughness	k/D_h= 0.00015
16.	correction coefficient	λ_C= 0.0240
17.	head loss	ΔH_h= 1.6 x10^6

Finally, mechanical and electrical power required are $P_{m,h}$= 9.9 kW and $P_{el,h}$= 10.53 kW. Total power consumptions of system $P_{total} = P_{el,h} + P_{el,s}$= 10.53+0.9 =11.432 kW.

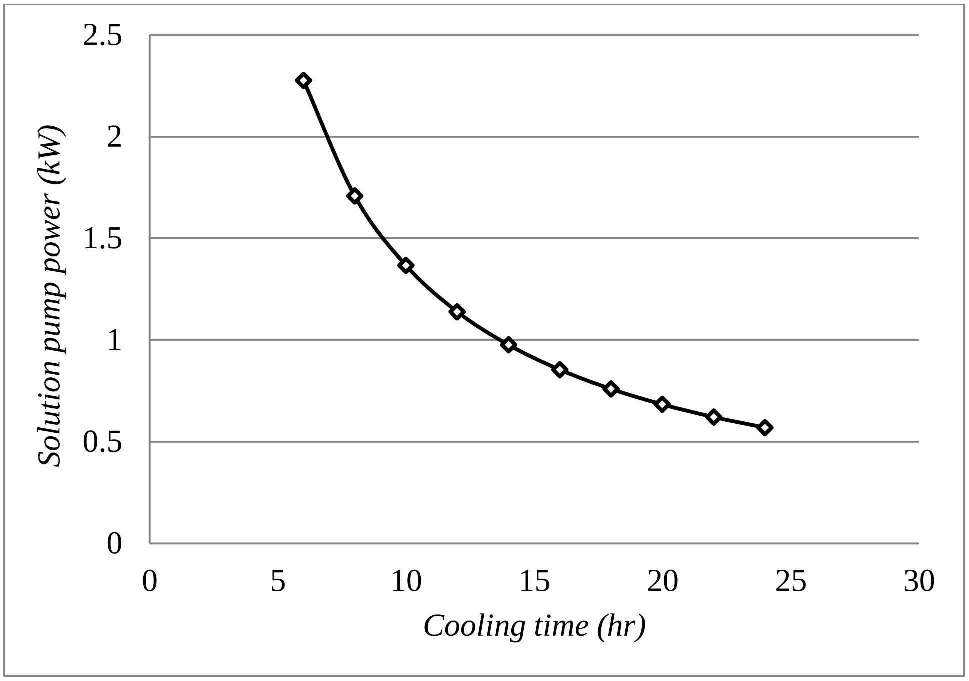

Figure 57: Solution pumping power versus cooling time

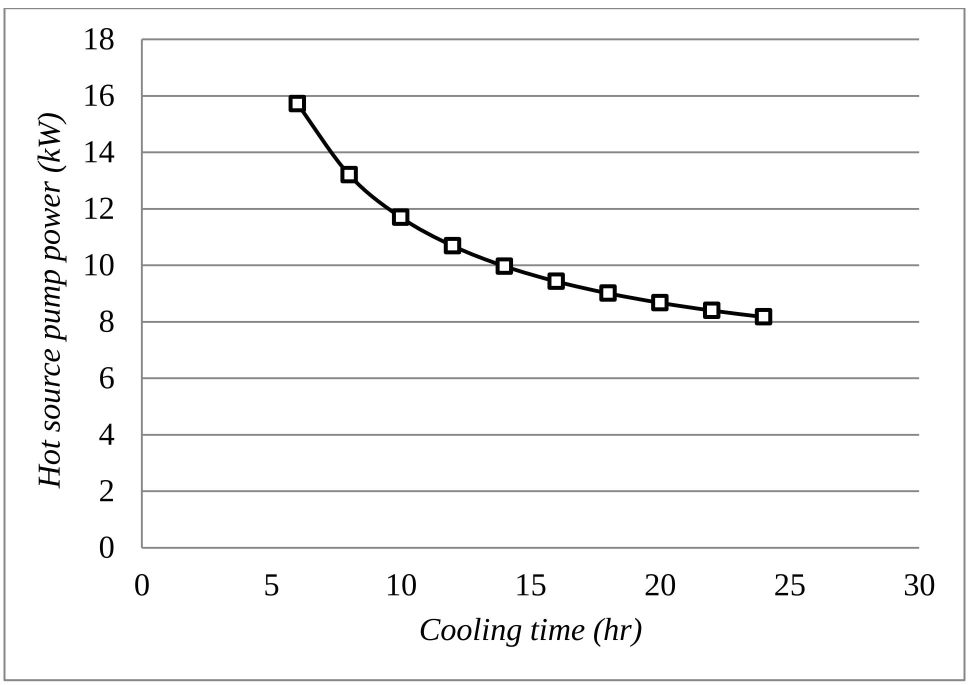

Figure 58: Hot source pumping power versus cooling time

4.3. COP

Coefficient of performance of the VARS analyzed is:

$$COP_{Absorption} = 0.30$$

Plot of Figure 59 clearly shows at constant generator temperature and pressure of 50 ^{o}C and 10 bars, respectively, increase in coefficient of performance of the system with increasing evaporator temperature. This is due to enthalpy of ammonia refrigerant at state (4); h_4 is increasing with evaporator temperature.

Table 34: COP versus evaporator temperature

Evaporator temperature (^{o}C)	h_4 (kJ/kg)	Evaporation rate (kW)	Heat transfer rate in the generator (kW)	COP
6	1325	103.53	346.224	0.309026
10	1350.4	106.1208	346.224	0.316509
15	1360	107.1	346.224	0.319337
20	1368.2	107.9364	346.224	0.321753

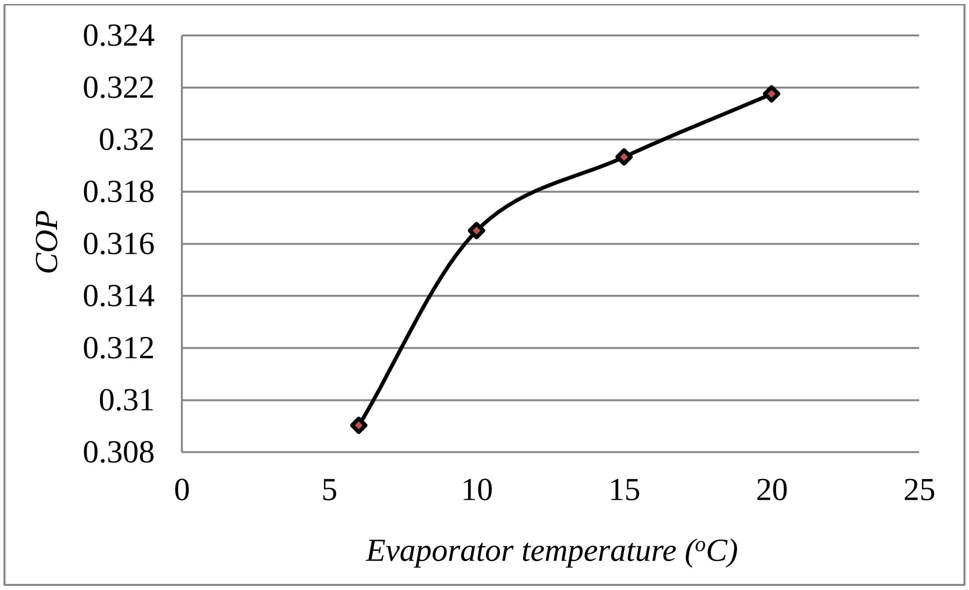

Figure 59: COP versus evaporator temperature

In other hand, at constant evaporator temperature and pressure of 6°C and 2 bar, respectively, coefficient of performance of the system is decreasing with increasing generator temperature as show in Table 35 and Figure 60.

Table 35: COP versus Generator temperature

Generator temperature (°C)	h_1(kJ/kg)	Evaporation rate (kW)	Heat transfer rate in the generator (kW)	COP
50	1425.2	103.53	346.22	0.300
60	1475.8	103.53	351.38	0.294
70	1650	103.53	369.15	0.280
80	1725	103.53	376.80	0.274
90	1848.5	103.53	389.40	0.265

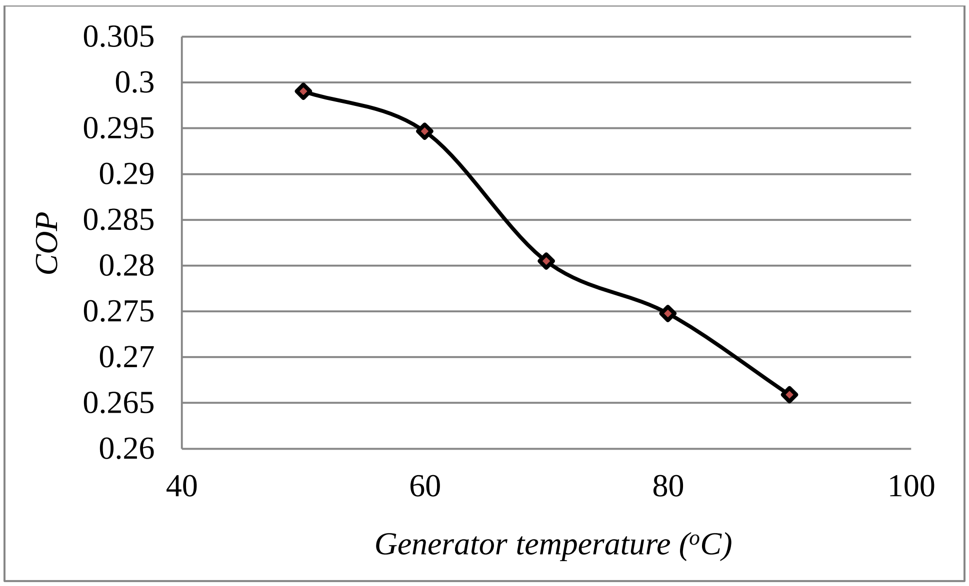

Figure 60: COP versus Generator temperature

Note that relations between (COP versus evaporator temperature) and (COP versus generator temperature are similar with the results that has been found by (Anand et al., 2016), (Maheshwari et al., 2011) and (Srikanth et al., 2010).

4.4. Vapor compression system analysis

Seeking other alternatives, thermodynamic and mathematical analyses of an existing refrigeration system for the load of the same effect (*cooling 66,000 liters of water per day*) are done.

Vapor compression system is assumed to operate ideally under similar pressures and temperatures. The refrigerant to be used is R-134a and its thermodynamic states at different points are evaluated using *Thermo physical property table* (Appendix A-11) as follows.

State 1. Saturated vapor

Enthalpy, $h_1 = h_g = 254.8$ kJ/kg , $h_f = 197.66$ kJ/kg

Entropy, $s_1 = s_g = 0.9120$ kJ/kg.^{o}C

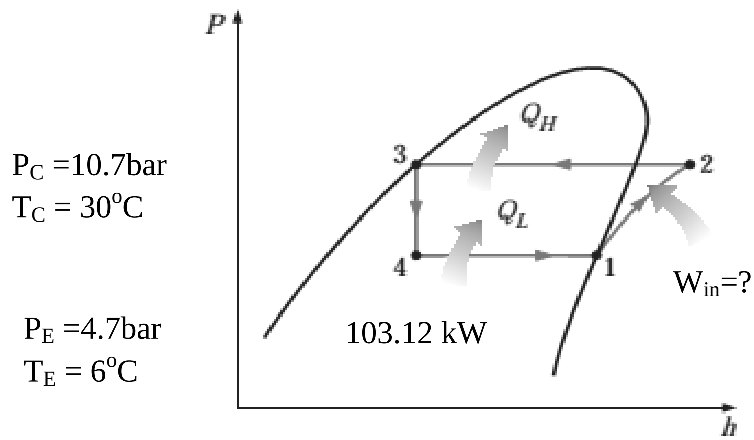

Figure 61: P-h diagram for mathematical analysis of VCR system

State 2. Superheated vapor (after isentropic compression in the compressor)

Entropy, $s_2 = s_1 = 0.9120$ kJ/kg.^{o}C and $P_C = 1.07$ MPa

Enthalpy, $h_2 = 268.68$ kJ/kg

State 3. Saturated liquid at condenser pressure and temperature

Enthalpy, $h_3 = 231.62$ kJ/kg

State 4. Saturated liquid at evaporator pressure and temperature (after isenthalpic expansion in the capillary tube)

Enthalpy, $h_4 = h_3$ = 231.62 kJ/kg

The rate of heat removal from the refrigerated space and the power input to the compressor are written (below) from their definitions of energy conservations. Therefore, mass flow rate of refrigerant and the work input to the compressor (*Assuming efficiency of motor to be 94%*) is calculated as $\dot{m}_r$ = 4.445 kg/s and $\dot{W}_{in}$= 62.2 kW.

- Total power consumptions of system $P_{el,comp} = 62.2/0.94$ = 66.2 kW

CHAPTER-FIVE

COST ANALYSES

5.1. Capital and running costs of refrigeration systems

5.1.1. Investment (construction and installation) cost

Generally, it is clear that direct use of geothermal projects require a relatively large initial capital investment however, with small annual operating costs thereafter. The average investment cost distribution in the case of absorption cooling system based on the current price of pumps, fans, storage tanks, tubes and other type of auxiliary equipment will approximately be calculated in this chapter.

Prices of components of vapor absorption refrigeration system based on current market prices are discussed for each component. Bear in mind that the total investment cost of the system will be cumulative of installation cost and price of each component.

Condenser and its accessories

From the results for the design analysis of condenser so far, it will be composed of tube of copper material, fans, fins and accumulator. Copper tube of diameter 2 cm having totaled required length of 33 m in current market will cost over 3300 ETB. In addition, cost of condenser fans four in number is over 6000 ETB (2000 per single fan). Accumulator, to be constructed in between condenser tube and capillary tube will cost about 500 ETB.

Fins made of light plates of aluminum materials with thickness about 0.1524 mm (based on standard of seven fins per one millimeter width of tubes) will be 3267 in numbers. Based on current price of similar materials in the market, over 3000 ETB will be required for fins. A total cost for condenser and its accessories is equals to 12,800 ETB.

Capillary and Evaporator tubes

Similarly, capillary tube made of copper material with the diameter of 3 mm and totaled length about 4.65 m is required. Currently, capillary tube of 15 m length is available in the market costing 1500 ETB. In addition, evaporator tube of 237.7 m in length will cost over 23,700 ETB. A total cost for these components is equals to 24,200 ETB.

Generator and Absorber

Generator can be constructed as hollow cylinder closed from both sides with diameter and height equals to 12 cm and 15 cm, respectively. It will be made of nickel material of one millimeter thickness. Coiled tube of 1.65 m length inserted in to this hollow cylinder will together form the generator through which hot source will circulate to exchange heat with aqua-ammonia solution. Based on current price of similar equipment and materials in the market, these will costs about 500 ETB.

Absorber can be constructed in the form of cube hollow inside by using sheet metal of steel material. The volume of absorber is taken as $20x20x20 \ cm^3$ and it will costs about 1000 ETB. A total cost for these components is equals to 1,500 ETB.

Pressure relief valve and Pumps

Based on the analysis made so far, pressure relief valve can be constructed using small spring of stiffness $k = 32$ kN/m and coil diameter of 1.2 cm. In addition, poppet to be clipped together with spring and which, as a result of its motion with spring deflections, controls the pressure drop between generator and evaporator is made of very small solid steel material. The pressure relief valve will cost about 250 ETB.

Prices of pumps depend on the power it will apply on working fluids. Two pumps of different powers are required for the absorption refrigeration system analyzed in this thesis. These are the one with 1.0 kW costs 2900 ETB and the other about 11 kW costs 12,500 ETB. A total cost for these components is equals to 15,650 ETB.

Aqua-ammonia solution

1.0 liter of ammonia and 2.0 liters of pure water can be used to form aqua-ammonia solutions circulating in two circuits of the system. Based on the current price in the market, these solutions will costs about 1000 ETB.

Total Costs of VARS

Based on existing price of equipment, materials and (or) components to be purchased from the markets as discussed so far, total cost of equipment, materials and (or) components equals to 55,150 ETB. Assuming installation cost for the system equals to 15,000 ETB and contingency 2,757.5 ETB, total of investment and installations costs of the system will be **72,907.5** ETB.

Based on existing price of equipment, materials and (or) components to be purchased from the markets, investment cost of VAR system was calculated as **72,907.5** ETB and with less than one year payback period (*in few months after system installed and operations started*).

Running cost

Once the system installed, this is Operating cost that are to be expended to the operation of system. This is the cost of electric power used by system just to maintain existence supply of cooling water every day.

Solution and hot water pumps are components that consume electric power. The amount of power they require and annual costs based on existing electric tariff of 0.57 ETB per kWh are summarized in the Table 36.

Table 36: Running cost of vapor absorption refrigeration system

Running cost Summary (VARS)	
Inputs	
Watts (11.432kW)	11,432.00
Average usage per day (in hours)	18.00
Number of days used	365.00
Cost per KWH	0.57
Output	
Kilowatt hours (kWh)	75,108.24
Cost (ETB)	**42,961.91**

5.1.2. Capital and running costs of VCRS

Existing vapor compression refrigeration systems are available in the market with different capacity and costs. If this system is used for cooling requirements of 66,000 liters of drinking water to cool from 37.8^{o}C to 16^{o}C, and if refrigerator of maximum volume of 687 liter (over 22,940 ETB per piece) is used, about 96 pieces are needed with costing purchase from current market is over 2,202,240 ETB. Furthermore, based on existing electric tariff in Ethiopia, electrical consumptions to run the system continuously in every year is given in Table 37.

Table 37: Running cost of vapor compression refrigeration system

Running cost calculation (VCRS)	
Inputs	
Watts (66.2 kW)	66,200.00
Average usage per day (in hours)	18.00
Number of days used	365.00
Cost per KWH	0.57
Output	
Kilowatt hours (kWh)	434,934.00
Cost (ETB)	248,782.25

5.1.3. Payback period of VARS

Use of vapor absorption refrigeration system instead of vapor compression refrigeration system will save (248,782.25-42,961.91) = 205,820.34 ETB each year. Therefore, payback period, which is the length of time required for investment to recover its initial outlay in terms of profits or savings will be calculated as:

$$\text{Payback period} = \frac{\text{Initial investment or Original cost of asset}}{\text{Cash inflow}} = \frac{72{,}907.5}{205{,}820.34}$$

$\text{Payback period} = 0.354$ year. (Less than a year)

CHAPTER-SIX

CONCLUSIONS AND RECOMMENDATIONS

6.1. Conclusions

As stated in the introduction, the research was conducted on geothermal energy, as one of renewable energies that Ethiopia is enriched with, investigating for thermal applications such as drying and vapor absorption refrigeration systems. This analysis was done for "Wallame/Chombe" geothermal sources near DU, is one of sources found in the country.

Based on the results found, this source can be used for drying different types of crops at required periods of time. Thus, the quality reducing problems related with the spoilage of crops/grains such as tomatoes, beans, coffee, and maize could be overcome. Even though different types of crops needs different drying time under similar operating conditions, drying can be accomplished for different types of crops at similar period of time by varying system operating conditions.

In addition, the evidence from this study suggests "Wallame/Chombe" geothermal source is feasible to be utilizing in refrigeration absorption system that can meet water freezing requirements of DU. As it can be seen from the results discussed above, 346.2 kW of thermal energy collected from the source can overcome refrigeration capacity of 103.12 kW at the expenses of 11.432 kW of electrical power.

It was found that 11.432 kW of electrical power to be consumed in order to meet refrigerating capacity of the plant daily. In addition, comparison that was done; if the same refrigeration effect to be obtained by using VCRS that consumes 66.2 kW while compressing R-134a, shows that large amount of electrical power will be used unwisely. Thus, based on cost analysis, running cost of 82.73% of money that would be consumed if VCRS (R-134a) running at 66.2 kW of electrical power is used instead for the same capacity, will be saved annually.

This study clearly has limited to the place where only geothermal sources are available. Despite of this, with a number limitations need to be considered, it is believed that this study could provide the basis in our country towards enhancing our knowledge to shift from expensive high grade energy consumptions to easily available thermal energy such as geothermal source in the field of thermal systems (such as refrigeration).

6.2. Recommendations

Measurements of the data for geothermal sources under investigation as well as drinking water temperature of Dilla University were held for short period of time due to both financial and materials problems. Data collected for long duration is preferred for better investigations.

The capital cost of the system is high, therefore it was not able to implement and take an experimental data of the system. But, if the fund is available experimental data should be compared with the mathematical results for better design of the system.

I recommend the concerning bodies to emerge into the development of low price geothermal energy and it is better if mini-scale drying system is constructed around these areas so that farmers suffering from perishable agricultural products could overcome these problems.

As far as, use of vapor absorption refrigeration system instead of vapor compression refrigeration system saves money and energy. So, Dilla University has to launch small-scale project on at least 1.5 kW capacity absorption refrigeration systems that can provide cooling of drinking water for the staff members.

6.3. Further study

As long as geothermal sources of Gede'o and Guji considered, their reservoir capacity and other interrelated parameters are not measured and known well. Therefore, by investigating such parameters, further study area will be seeking for the possibility of the sources for air conditioning and mini-scale power generations.

However, the pump analysis is considered, this study has only investigated numerical values of hydraulic, shaft, and electrical power required to the pump. It is appreciated if its further design is done on pump mechanisms (piston diameter, length of connecting rod and crankshaft, etc.) to deliver better volumetric flow of solution through the circuit.

It is known that lower thermal conductive material or combinations of materials have been in use for both minimum heat losses by providing resistances for heat flow and protection of people burning themselves by touching heated surfaces. Next stage of this study, therefore, should consider thermal insulations for components of drying and VAR systems related with heat interactions such as: drying chamber, evaporator, hot fluid tubes, and generator.

REFERENCES

1. A.Boles, Y. A. (2006). Thermodynamics*:* An engineering approach (Fifth edition). New York, United States: McGraw-Hill.

2. A.Y. Arku, N. A. (2012). Specific heat of selected legumes and cereal grains grown in north eastern Nigeria. *Arid zone journal of engineering, technology and environment*, pp105-114.

3. Abdollah Hosseinlou, S. K. (2013). The effect of water temperature and voluntary drinking on the post rehydration sweating. *International journal of clinical and experimental medicine, 6*, pp 683–687.

4. Abdulmalik I. O, A. M. (2014). Appropriate technology for tomato powder production. *International journal of engineering inventions*, pp 29-34.

5. Aman Shukla, A. M. (2015). C.O.P derivation and thermodynamic calculation of ammonia-water vapor absorption refrigeration system. *International journal of mechanical engineering and technology,* pp 72-81.

6. Ambecha O. Gemechis, P. C. (2013). Tomato production in Ethiopia: constraints and opportunities. Addis Ababa, Ethiopia.

7. Arora, C. P. (2006). Refrigeration and air conditioning. New Delhi, India: Tata McGraw-Hill.

8. Ashish K Pandey, P. K. (2014). Hydrodynamic characteristics of single phase fluid flow inside a helically coiled tube of small diameter. *International journal of emerging technologies and engineering (IJETE)*, pp 2348 –8050.

9. ASHRAE Handbook—Refrigeration, (. (2006). Thermal properties of foods. ASHRAE.

10. Bureau, O. C. (2015). The southern tourist route. *Oromia culture and tourism bureau* .

11. Cao, Y. (2010). The specific heat of wheat. *10th international working conference on stored product protection* (pp. 243-249). Beijing, P. R. China: Julius-Kühn-Archiv.

12. Carlos José Pimenta, C. L. (2018). Challengs in coffee quality: cultural, chemical and microbiological aspects. pp 337-349.

13. Çengel. (2008). Introduction to thermodynamics and heat transfer (2nd Edition). New York, United States: McGraw-Hill.

14. Cengel, Y. A. (n.d.). Heat transfer, a practical approach.

15. Christy V Vazhappilly, T. T. (2013). Modeling and experimental analysis of generator in vapour absorption refrigeration system. *Int. journal of engineering research and applications*, pp 63-67.

16. Ethiopia, M. o. (2015). Global geothermal alliance stakeholders meeting. Nairobi.

17. Fashina Adepoju Bola., A. F. (2013). Design parameters for a small- scale batch in-bin maize dryer. *Journal of agricultural Sciences*.

18. Firmansyah, J. H. (2018). Thermal design of 5 kg capacity coffee bean dryer simulator using geothermal energy. *Journal of earth and environmental science*.

19. Ganesh, S. a. (2017). Development of thermo-physical properties of aqua ammonia for Kalina cycle system. *International journal of materials and product technology*, pp 113-140.

20. Hammock, G. L. (2011). *Cro*ss-flow, staggered-tube heat exchanger analysis for high enthalpy flows. University of Tennessee, Knoxville. *Tennessee research and creative exchange*.

21. Jerko M. LABUS, J. C. (2012). Review on absorption technology with emphasis on small capacity absorption machines.

22. K.R. Ullah, R. S. (2013). A review of solar thermal refrigeration and cooling methods. *Renewable and sustainable energy reviews*, pp 499–513.

23. Kamnang, J. K. (2008). Development of a simple intermittent absorption solar refrigeration system. *International journal of low carbon technologies*, pp 127-138.

24. Kanshie, D. T. (2002). Five Thousand Years of Sustainability? A case study on Gedeo land use. Wageningen, Neatherlands.

25. Kebede, M. T. (2010). Geological survey of ethiopia. Bali, Indonesia.

26. Kiril Popovski, S. P. (2001). Geothermal Energy Direct Application in Industry in Europe. Oradea, Romania.

27. M. Galal Rabie, P. (2009). Fluid power engineering. Modern academy for engineering and technology Cairo, Egypt.

28. M. Ishak, T. A. (2013). Experimental investigation on heat transfer and pressure drop characteristics of air flow over a staggered flat tube bank in crossflow. *International journal of automotive and mechanical engineering (IJAME), volume 7*.

29. M.Cimbala, Y. A. (2006). Fluid mechanics: fundamentals and applications. 1221 Avenue of the Americas, New York: McGraw-Hill, a business unit of The McGraw-Hill companies, Inc.

30. Maheshwari, S. R. (2011). Analysis of Ammonia –Water (NH3-H2O) VaporAbsorption Refrigeration System based on First Law of Thermodynamics. *International journal of scientific & engineering research, volume 2*, 1-7.

31. Minh Van Nguyen, S. A. (2015). uses of geothermal energy in food and agriculture opportunities for developing countries. Rome: Food and agriculture organization of the united nations.

32. Muluneh Bekele, K. F. (2016). Challenges and opportunities of marketing fruit andvegetables at logia, northeastern Ethiopia. The case of onion,tomato and banana. *Journal of marketing and consumer research*, pp 51-58.

33. Muthyalu, M. a. (2014). The major problems and prospects of tomato marketing: an empirical analysis. *International journal of management research and business strategy*, pp 82-93.

34. NASA. (2019). Watching the ozone hole before and after the montreal protocol.

35. Novrisal Prasetya, D. E. (2017). Smart geo-energy village development by using cascade direct use of geothermal energy in Bonjol, West Sumatera. *Journal of earth and environmental science*. IOP publishing Ltd.

36. Parulian Siagian, E. Y. (2017). A field survey on coffee beans drying methods of Indonesian small holder farmers. *1st Nommensen international conference on technology and engineering* . Indonesia: IOP publishing Ltd.

37. Pongsid Srikhirin, S. A. (2001). A review of absorption refrigeration technologies. *Renewable and sustainable energy reviews*, pp 334-372.

38. Raziye Ince, E. G. (2008). Thermal propertis of some oily seeds. *Journal of agricultural machinery science*, pp 399-405.

39. S. Anand, A. G. (2016). Use of process steam in vapor absorption refrigeration system for cooling and heating applications: An exergy analysis.

40. S.N.Gupta, M. G. (2014). Effect of tube bank configuration and geometry on heat transfer coefficient for the flow of Newtonian and power law non-Newtonian fluids flowing across tube banks. *International journal of science, engineering and technology research*, 1166-1172.

41. Sandeep, P. C. (2008). Heat transfer coefficient in helical heat exchangers under turbulent flow conditions. *International journal of food engineering*.

42. Sikorska-Bączek, R. (2015). The use of geothermal energy in absorption refrigeration circuits. *International journal of environment engineering*, 119-125.

43. Solomon, K. a. (2016). Country update on geothermal exploration and development in ethiopia. *Sixth African rift geothermal conference, geological survey of ethiopia.* Addis Ababa, Ethiopia.

44. Suchita Patel, J. P. (2015). Say yes to warm for remove harm: amazing wonders of two stages of water! *European journal of pharmaceutical and medical research,* pp 444-460.

45. Theodore L. Bergman, A. S. (2011, 2007, 2002). Introduction to Heat Transfer. United States of America: John Wiley & Sons, Inc.

46. V Hristov, N. S. (2019). Utilization of low enthalpy geothermal energy in Bulgaria. *2nd international geothermal conference.* Sofia, Bulgaria: IOP publishing.

47. V.Srikanth, B. N. (2012). Thermodynamic analysis of vapour absorption refrigeration system using solar energy. *International journal of latest trends in engineering and technology,* pp 17-26.

48. Van Nguyen, M. A. (2015). Uses of geothermal in food and agriculture – Opportunities for developing countries . Rome.

49. W Afuar, B. S. (2016). Design of tomato drying system by utilizing brine geothermal. *Journal of earth and environmental science.*

50. W.A. Khan, J. C. (2006). Convection heat transfer from tube banks in crossflow: Analytical approach. *International journal of heat and mass transfer*, 4831–4838.

51. Wu, H. T. (2018). Farmers' Value Assessment of Sociocultural and Ecological Ecosystem Services in Agricultural Landscapes. *Journal of sustainability*, 1-18.

(APPENDIX-A) PROPERTY TABLES AND CHARTS

A-1: Properties of air at atmospheric pressure

Temp. T, °C	Density ρ, kg/m^3	Specific Heat c_p, J/kg · K	Thermal Conductivity k, W/m · K	Thermal Diffusivity α, m^2/s	Dynamic Viscosity μ, kg/m · s	Kinematic Viscosity ν, m^2/s	Prandtl Number Pr
−150	2.866	983	0.01171	4.158×10^{-6}	8.636×10^{-6}	3.013×10^{-6}	0.7246
−100	2.038	966	0.01582	8.036×10^{-6}	1.189×10^{-6}	5.837×10^{-6}	0.7263
−50	1.582	999	0.01979	1.252×10^{-5}	1.474×10^{-5}	9.319×10^{-6}	0.7440
−40	1.514	1002	0.02057	1.356×10^{-5}	1.527×10^{-5}	1.008×10^{-5}	0.7436
−30	1.451	1004	0.02134	1.465×10^{-5}	1.579×10^{-5}	1.087×10^{-5}	0.7425
−20	1.394	1005	0.02211	1.578×10^{-5}	1.630×10^{-5}	1.169×10^{-5}	0.7408
−10	1.341	1006	0.02288	1.696×10^{-5}	1.680×10^{-5}	1.252×10^{-5}	0.7387
0	1.292	1006	0.02364	1.818×10^{-5}	1.729×10^{-5}	1.338×10^{-5}	0.7362
5	1.269	1006	0.02401	1.880×10^{-5}	1.754×10^{-5}	1.382×10^{-5}	0.7350
10	1.246	1006	0.02439	1.944×10^{-5}	1.778×10^{-5}	1.426×10^{-5}	0.7336
15	1.225	1007	0.02476	2.009×10^{-5}	1.802×10^{-5}	1.470×10^{-5}	0.7323
20	1.204	1007	0.02514	2.074×10^{-5}	1.825×10^{-5}	1.516×10^{-5}	0.7309
25	1.184	1007	0.02551	2.141×10^{-5}	1.849×10^{-5}	1.562×10^{-5}	0.7296
30	1.164	1007	0.02588	2.208×10^{-5}	1.872×10^{-5}	1.608×10^{-5}	0.7282
35	1.145	1007	0.02625	2.277×10^{-5}	1.895×10^{-5}	1.655×10^{-5}	0.7268
40	1.127	1007	0.02662	2.346×10^{-5}	1.918×10^{-5}	1.702×10^{-5}	0.7255
45	1.109	1007	0.02699	2.416×10^{-5}	1.941×10^{-5}	1.750×10^{-5}	0.7241
50	1.092	1007	0.02735	2.487×10^{-5}	1.963×10^{-5}	1.798×10^{-5}	0.7228
60	1.059	1007	0.02808	2.632×10^{-5}	2.008×10^{-5}	1.896×10^{-5}	0.7202
70	1.028	1007	0.02881	2.780×10^{-5}	2.052×10^{-5}	1.995×10^{-5}	0.7177
80	0.9994	1008	0.02953	2.931×10^{-5}	2.096×10^{-5}	2.097×10^{-5}	0.7154
90	0.9718	1008	0.03024	3.086×10^{-5}	2.139×10^{-5}	2.201×10^{-5}	0.7132
100	0.9458	1009	0.03095	3.243×10^{-5}	2.181×10^{-5}	2.306×10^{-5}	0.7111
120	0.8977	1011	0.03235	3.565×10^{-5}	2.264×10^{-5}	2.522×10^{-5}	0.7073
140	0.8542	1013	0.03374	3.898×10^{-5}	2.345×10^{-5}	2.745×10^{-5}	0.7041
160	0.8148	1016	0.03511	4.241×10^{-5}	2.420×10^{-5}	2.975×10^{-5}	0.7014
180	0.7788	1019	0.03646	4.593×10^{-5}	2.504×10^{-5}	3.212×10^{-5}	0.6992
200	0.7459	1023	0.03779	4.954×10^{-5}	2.577×10^{-5}	3.455×10^{-5}	0.6974
250	0.6746	1033	0.04104	5.890×10^{-5}	2.760×10^{-5}	4.091×10^{-5}	0.6946
300	0.6158	1044	0.04418	6.871×10^{-5}	2.934×10^{-5}	4.765×10^{-5}	0.6935
350	0.5664	1056	0.04721	7.892×10^{-5}	3.101×10^{-5}	5.475×10^{-5}	0.6937
400	0.5243	1069	0.05015	8.951×10^{-5}	3.261×10^{-5}	6.219×10^{-5}	0.6948
450	0.4880	1081	0.05298	1.004×10^{-4}	3.415×10^{-5}	6.997×10^{-5}	0.6965
500	0.4565	1093	0.05572	1.117×10^{-4}	3.563×10^{-5}	7.806×10^{-5}	0.6986
600	0.4042	1115	0.06093	1.352×10^{-4}	3.846×10^{-5}	9.515×10^{-5}	0.7037
700	0.3627	1135	0.06581	1.598×10^{-4}	4.111×10^{-5}	1.133×10^{-4}	0.7092
800	0.3289	1153	0.07037	1.855×10^{-4}	4.362×10^{-5}	1.326×10^{-4}	0.7149
900	0.3008	1169	0.07465	2.122×10^{-4}	4.600×10^{-5}	1.529×10^{-4}	0.7206
1000	0.2772	1184	0.07868	2.398×10^{-4}	4.826×10^{-5}	1.741×10^{-4}	0.7260
1500	0.1990	1234	0.09599	3.908×10^{-4}	5.817×10^{-5}	2.922×10^{-4}	0.7478
2000	0.1553	1264	0.11113	5.664×10^{-4}	6.630×10^{-5}	4.270×10^{-4}	0.7539

A-2: Saturated water-temperature table

		Specific volume, m^3/kg		Internal energy, kJ/kg			Enthalpy, kJ/kg			Entropy, kJ/kg · K		
Temp., T °C	Sat. press., P_{sat} kPa	Sat. liquid, v_f	Sat. vapor, v_g	Sat. liquid, u_f	Evap., u_{fg}	Sat. vapor, u_g	Sat. liquid, h_f	Evap., h_{fg}	Sat. vapor, h_g	Sat. liquid, s_f	Evap., s_{fg}	Sat. vapor, s_g
0.01	0.6117	0.001000	206.00	0.000	2374.9	2374.9	0.001	2500.9	2500.9	0.0000	9.1556	9.1556
5	0.8725	0.001000	147.03	21.019	2360.8	2381.8	21.020	2489.1	2510.1	0.0763	8.9487	9.0249
10	1.2281	0.001000	106.32	42.020	2346.6	2388.7	42.022	2477.2	2519.2	0.1511	8.7488	8.8999
15	1.7057	0.001001	77.885	62.980	2332.5	2395.5	62.982	2465.4	2528.3	0.2245	8.5559	8.7803
20	2.3392	0.001002	57.762	83.913	2318.4	2402.3	83.915	2453.5	2537.4	0.2965	8.3696	8.6661
25	3.1698	0.001003	43.340	104.83	2304.3	2409.1	104.83	2441.7	2546.5	0.3672	8.1895	8.5567
30	4.2469	0.001004	32.879	125.73	2290.2	2415.9	125.74	2429.8	2555.6	0.4368	8.0152	8.4520
35	5.6291	0.001006	25.205	146.63	2276.0	2422.7	146.64	2417.9	2564.6	0.5051	7.8466	8.3517
40	7.3851	0.001008	19.515	167.53	2261.9	2429.4	167.53	2406.0	2573.5	0.5724	7.6832	8.2556
45	9.5953	0.001010	15.251	188.43	2247.7	2436.1	188.44	2394.0	2582.4	0.6386	7.5247	8.1633
50	12.352	0.001012	12.026	209.33	2233.4	2442.7	209.34	2382.0	2591.3	0.7038	7.3710	8.0748
55	15.763	0.001015	9.5639	230.24	2219.1	2449.3	230.26	2369.8	2600.1	0.7680	7.2218	7.9898
60	19.947	0.001017	7.6670	251.16	2204.7	2455.9	251.18	2357.7	2608.8	0.8313	7.0769	7.9082
65	25.043	0.001020	6.1935	272.09	2190.3	2462.4	272.12	2345.4	2617.5	0.8937	6.9360	7.8296
70	31.202	0.001023	5.0396	293.04	2175.8	2468.9	293.07	2333.0	2626.1	0.9551	6.7989	7.7540
75	38.597	0.001026	4.1291	313.99	2161.3	2475.3	314.03	2320.6	2634.6	1.0158	6.6655	7.6812
80	47.416	0.001029	3.4053	334.97	2146.6	2481.6	335.02	2308.0	2643.0	1.0756	6.5355	7.6111
85	57.868	0.001032	2.8261	355.96	2131.9	2487.8	356.02	2295.3	2651.4	1.1346	6.4089	7.5435
90	70.183	0.001036	2.3593	376.97	2117.0	2494.0	377.04	2282.5	2659.6	1.1929	6.2853	7.4782
95	84.609	0.001040	1.9808	398.00	2102.0	2500.1	398.09	2269.6	2667.6	1.2504	6.1647	7.4151
100	101.42	0.001043	1.6720	419.06	2087.0	2506.0	419.17	2256.4	2675.6	1.3072	6.0470	7.3542
105	120.90	0.001047	1.4186	440.15	2071.8	2511.9	440.28	2243.1	2683.4	1.3634	5.9319	7.2952
110	143.38	0.001052	1.2094	461.27	2056.4	2517.7	461.42	2229.7	2691.1	1.4188	5.8193	7.2382
115	169.18	0.001056	1.0360	482.42	2040.9	2523.3	482.59	2216.0	2698.6	1.4737	5.7092	7.1829
120	198.67	0.001060	0.89133	503.60	2025.3	2528.9	503.81	2202.1	2706.0	1.5279	5.6013	7.1292
125	232.23	0.001065	0.77012	524.83	2009.5	2534.3	525.07	2188.1	2713.1	1.5816	5.4956	7.0771
130	270.28	0.001070	0.66808	546.10	1993.4	2539.5	546.38	2173.7	2720.1	1.6346	5.3919	7.0265
135	313.22	0.001075	0.58179	567.41	1977.3	2544.7	567.75	2159.1	2726.9	1.6872	5.2901	6.9773
140	361.53	0.001080	0.50850	588.77	1960.9	2549.6	589.16	2144.3	2733.5	1.7392	5.1901	6.9294
145	415.68	0.001085	0.44600	610.19	1944.2	2554.4	610.64	2129.2	2739.8	1.7908	5.0919	6.8827
150	476.16	0.001091	0.39248	631.66	1927.4	2559.1	632.18	2113.8	2745.9	1.8418	4.9953	6.8371
155	543.49	0.001096	0.34648	653.19	1910.3	2563.5	653.79	2098.0	2751.8	1.8924	4.9002	6.7927
160	618.23	0.001102	0.30680	674.79	1893.0	2567.8	675.47	2082.0	2757.5	1.9426	4.8066	6.7492
165	700.93	0.001108	0.27244	696.46	1875.4	2571.9	697.24	2065.6	2762.8	1.9923	4.7143	6.7067
170	792.18	0.001114	0.24260	718.20	1857.5	2575.7	719.08	2048.8	2767.9	2.0417	4.6233	6.6650
175	892.60	0.001121	0.21659	740.02	1839.4	2579.4	741.02	2031.7	2772.7	2.0906	4.5335	6.6242
180	1002.8	0.001127	0.19384	761.92	1820.9	2582.8	763.05	2014.2	2777.2	2.1392	4.4448	6.5841
185	1123.5	0.001134	0.17390	783.91	1802.1	2586.0	785.19	1996.2	2781.4	2.1875	4.3572	6.5447
190	1255.2	0.001141	0.15636	806.00	1783.0	2589.0	807.43	1977.9	2785.3	2.2355	4.2705	6.5059
195	1398.8	0.001149	0.14089	828.18	1763.6	2591.7	829.78	1959.0	2788.8	2.2831	4.1847	6.4678
200	1554.9	0.001157	0.12721	850.46	1743.7	2594.2	852.26	1939.8	2792.0	2.3305	4.0997	6.4302

A-3: Psychometric chart

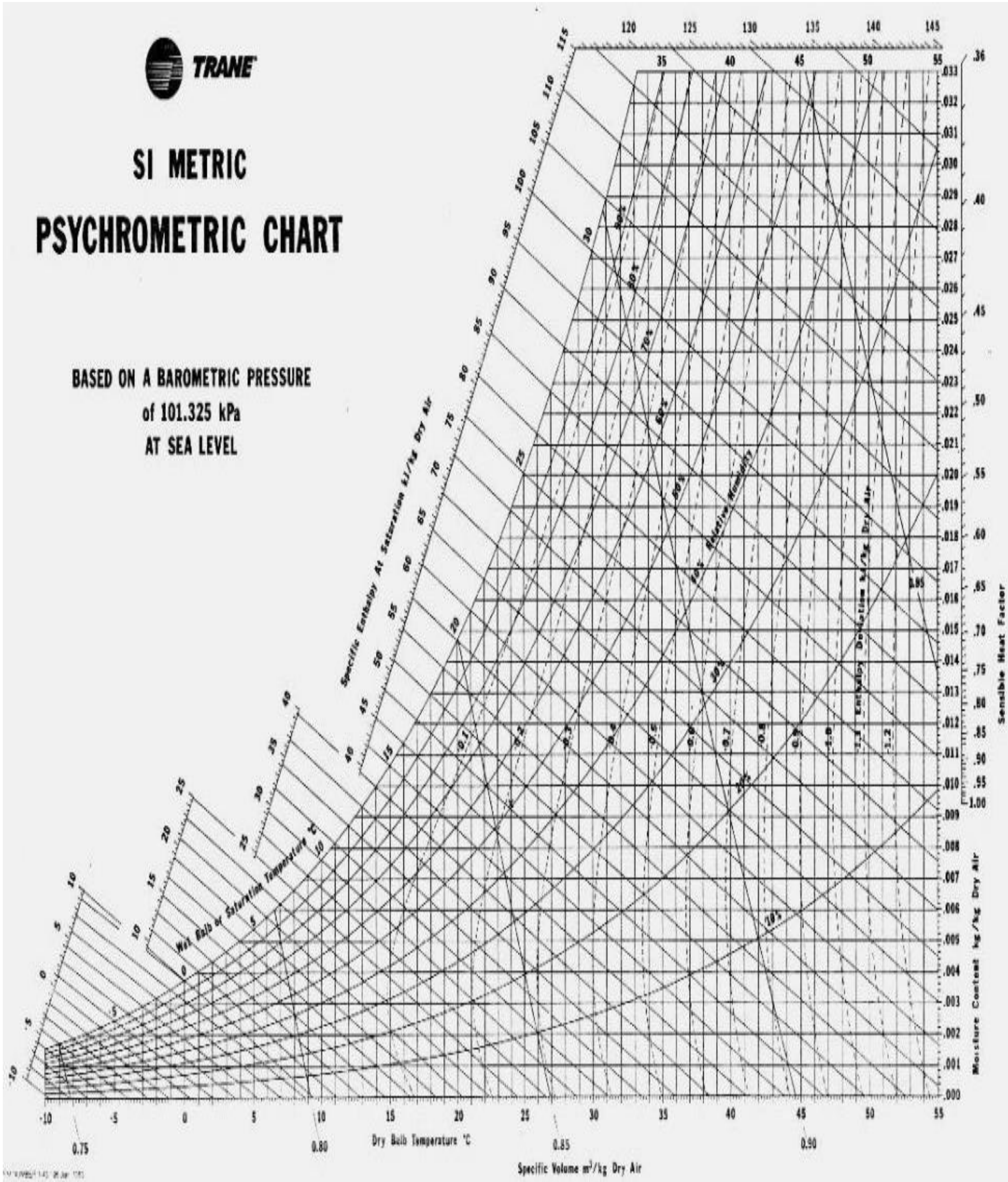

A-4: The friction factor f and the correction factor x for tube banks

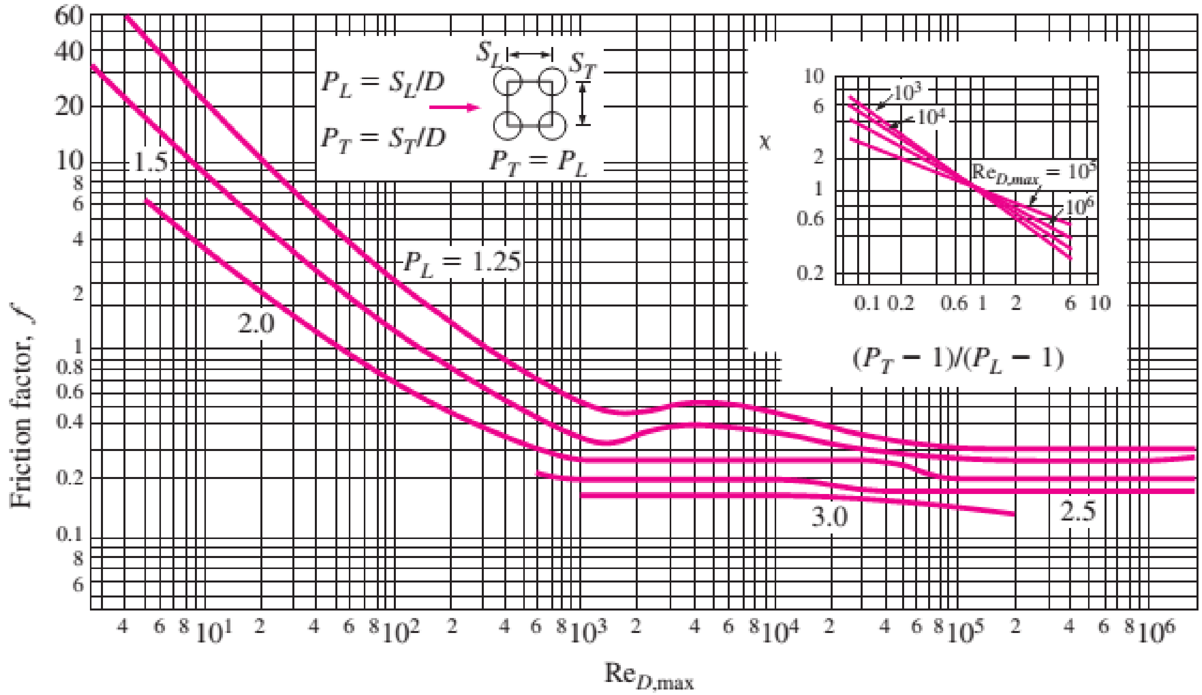

(*a*) In-line arrangement

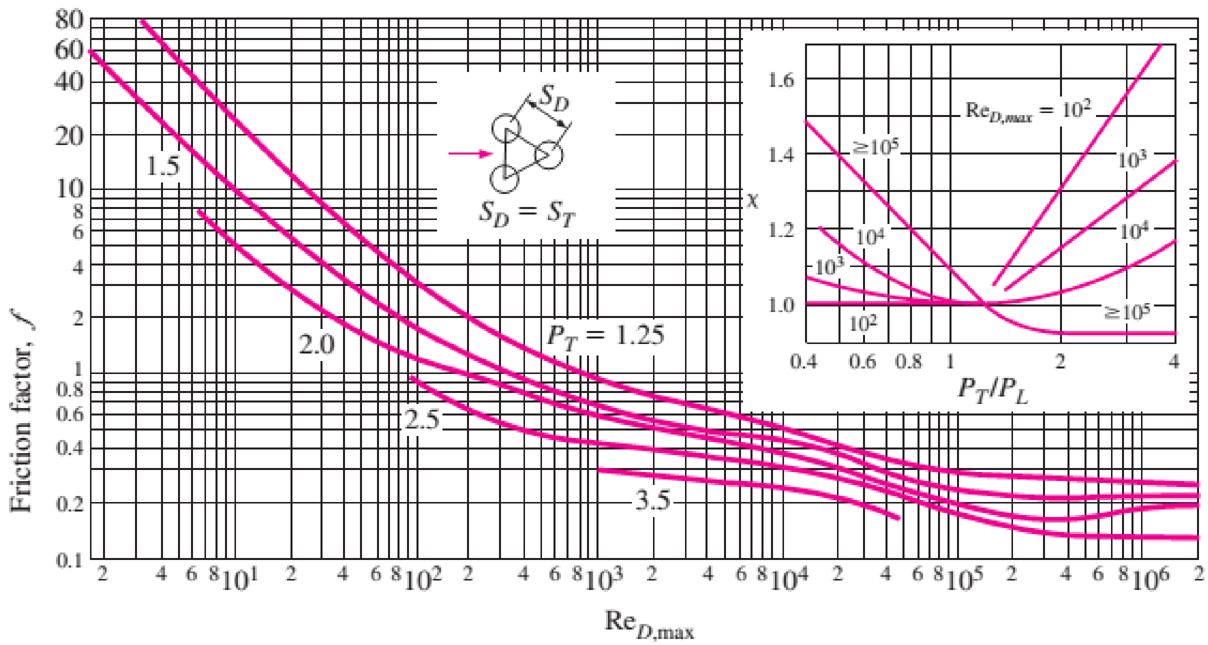

(*b*) Staggered arrangement

A-5: Representative values of the overall heat transfer coefficient

No.	Type of heat exchanger	U, $W/m^2.^oC$
1.	Water-to-water	850-1700
2.	Water-to-oil	100-350
3.	Water-to-gasoline or kerosene	300-1000
4.	Feed water heaters	1000-8500
5.	Steam-to-light fuel oil	200-400
6.	Steam-to-heavy fuel oil	50-200
7.	Steam condenser	1000-6000
8.	Freon condenser (water cooled)	300-1000
9.	Ammonia condensers (water cooled)	800-1400
10.	Alcohol condenser (water cooled)	250-700
11.	Gas-to-gas	10-40
12.	Water-to-air in finned tubes (water in tubes)	30-60[†] 400-850[‡]
13.	Steam-to-air in finned tubes (steam in tubes)	30-300[†] 400-4000[‡]

[†]Based on air-side surface area. [‡]Based on water- or steam-side surface area.

A-6: Derivation of formula for maximum velocity of the flow through tube banks

The maximum velocity is determined from the conservation of mass requirement for steady incompressible flow. For in-line tubes arrangement, conservation of mass equation can be written as (see figure 3.2)

$$\rho V A_1 = \rho V_{max} A_T$$

$$V S_T = V_{max}(S_T - D)$$

$$V_{max} = \frac{S_T}{S_T - D} V$$

For staggered tubes arrangement, the fluid approaching through area A_1 (see figure 3.3) passes through area A_T and then through area $2A_D$ as it wraps around the pipe in the next row.

If, $2A_D > A_T$, #. $V_{max} = \frac{S_T}{S_T - D} V$

If, $2A_D < A_T$ or, $2(S_D - D) < (S_T - D)$, conservation of mass equation can be written as

$\rho V A_1 = \rho V_{max}(2A_D)$ or $V S_T = 2V_{max}(S_D - D)$ #. $V_{max} = \frac{S_T}{2(S_T - D)} V$

A-7: Moody diagram (*https://www.engineeringtoolbox.com/moody-diagram-d_618.html*)

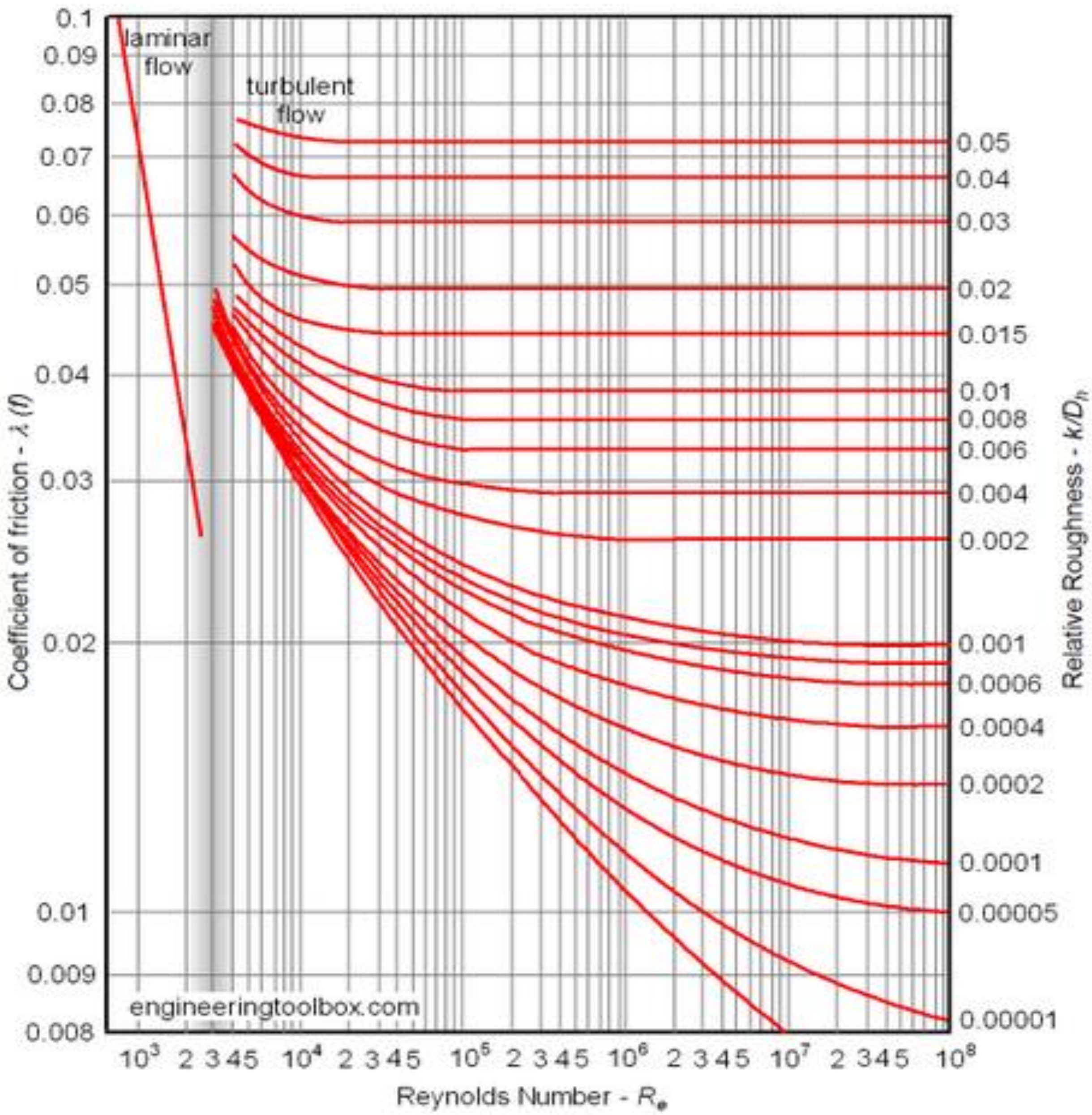

A-8: Absolute roughness for some common materials

Surfaces	**Absolute Roughness - *k*** (10^{-3} m)
Copper, Lead, Brass, Aluminum (new)	0.001 - 0.002
PVC and Plastic Pipes	0.0015 - 0.007
Epoxy, Vinyl Ester and Isophthalic pipe	0.005
Stainless steel, bead blasted	0.001 - 0.006
Stainless steel, turned	0.0004 - 0.006
Stainless steel, electropolished	0.0001 - 0.0008
Steel commercial pipe	0.045 - 0.09
Stretched steel	0.015
Weld steel	0.045
Galvanized steel	0.15
Rusted steel (corrosion)	0.15 - 4
New cast iron	0.25 - 0.8
Worn cast iron	0.8 - 1.5
Rusty cast iron	1.5 - 2.5
Sheet or asphalted cast iron	0.01 - 0.015
Smoothed cement	0.3
Ordinary concrete	0.3 - 1
Coarse concrete	0.3 - 5
Well planed wood	0.18 - 0.9
Ordinary wood	5

A-9: Ammonia-Water solution concentrations-enthalpy chart (Ganesh, 2017)

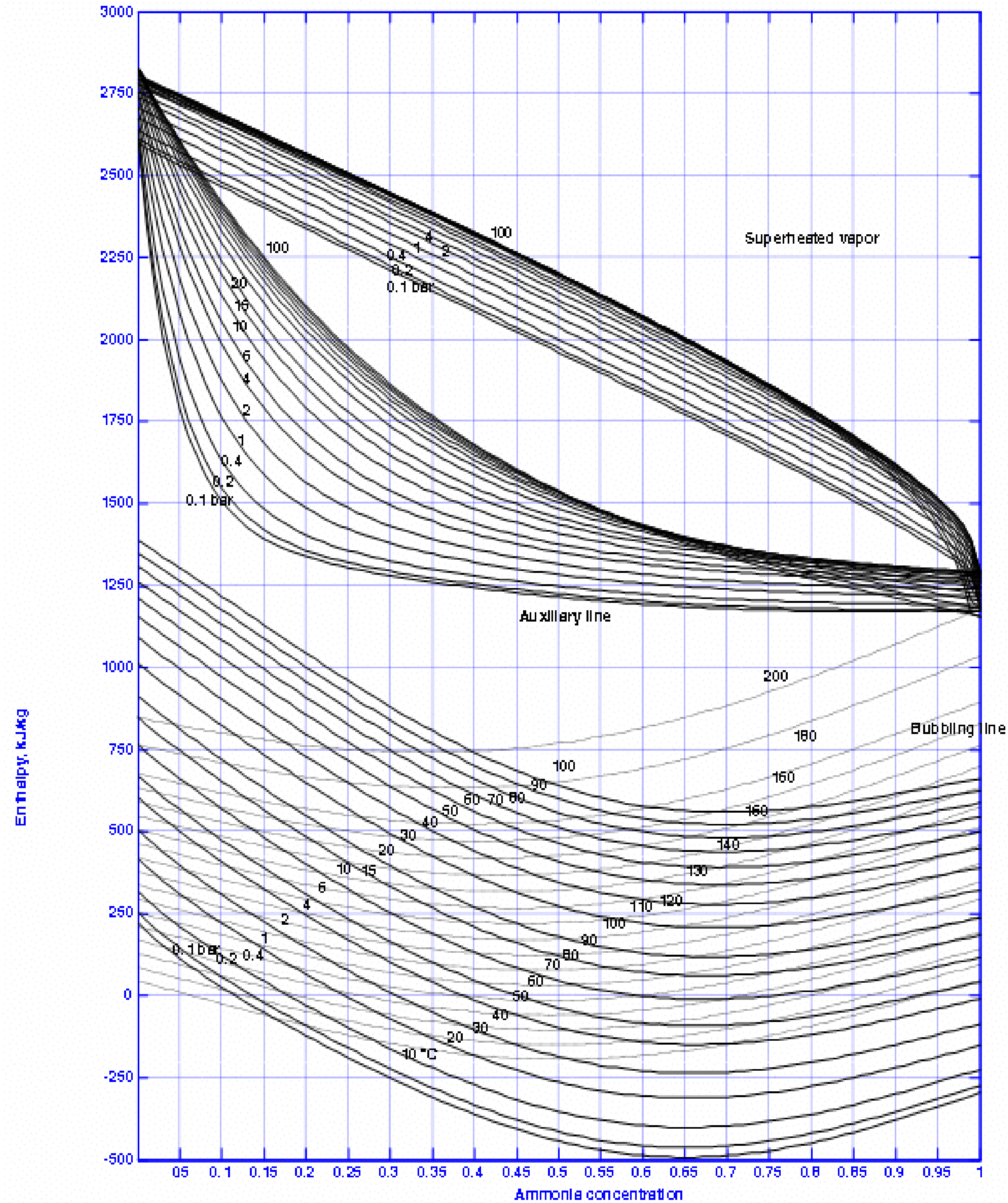

A-10: Thermo physical properties of saturated ammonia refrigerant (Çengel, 2008)

Temp. T, °C	Saturation Pressure P, kPa	Density ρ, kg/m^3 Liquid	Vapor	Enthalpy of Vaporization h_{fg}, kJ/kg	Specific Heat c_p, J/kg·K Liquid	Vapor	Thermal Conductivity k, W/m·K Liquid	Vapor	Dynamic Viscosity μ, kg/m·s Liquid	Vapor	Prandtl Number Pr Liquid	Vapor	Volume Expansion Coefficient β, 1/K Liquid	Surface Tension N/m
−40	71.66	690.2	0.6435	1389	4414	2242	—	0.01792	2.926×10^{-4}	7.957×10^{-6}	—	0.9955	0.00176	0.03565
−30	119.4	677.8	1.037	1360	4465	2322	—	0.01898	2.630×10^{-4}	8.311×10^{-6}	—	1.017	0.00185	0.03341
−25	151.5	671.5	1.296	1345	4489	2369	0.5968	0.01957	2.492×10^{-4}	8.490×10^{-6}	1.875	1.028	0.00190	0.03229
−20	190.1	665.1	1.603	1329	4514	2420	0.5853	0.02015	2.361×10^{-4}	8.669×10^{-6}	1.821	1.041	0.00194	0.03118
−15	236.2	658.6	1.966	1313	4538	2476	0.5737	0.02075	2.236×10^{-4}	8.851×10^{-6}	1.769	1.056	0.00199	0.03007
−10	290.8	652.1	2.391	1297	4564	2536	0.5621	0.02138	2.117×10^{-4}	9.034×10^{-6}	1.718	1.072	0.00205	0.02896
−5	354.9	645.4	2.886	1280	4589	2601	0.5505	0.02203	2.003×10^{-4}	9.218×10^{-6}	1.670	1.089	0.00210	0.02786
0	429.6	638.6	3.458	1262	4617	2672	0.5390	0.02270	1.896×10^{-4}	9.405×10^{-6}	1.624	1.107	0.00216	0.02676
5	516	631.7	4.116	1244	4645	2749	0.5274	0.02341	1.794×10^{-4}	9.593×10^{-6}	1.580	1.126	0.00223	0.02566
10	615.3	624.6	4.870	1226	4676	2831	0.5158	0.02415	1.697×10^{-4}	9.784×10^{-6}	1.539	1.147	0.00230	0.02457
15	728.8	617.5	5.729	1206	4709	2920	0.5042	0.02492	1.606×10^{-4}	9.978×10^{-6}	1.500	1.169	0.00237	0.02348
20	857.8	610.2	6.705	1186	4745	3016	0.4927	0.02573	1.519×10^{-4}	1.017×10^{-5}	1.463	1.193	0.00245	0.02240
25	1003	602.8	7.809	1166	4784	3120	0.4811	0.02658	1.438×10^{-4}	1.037×10^{-5}	1.430	1.218	0.00254	0.02132
30	1167	595.2	9.055	1144	4828	3232	0.4695	0.02748	1.361×10^{-4}	1.057×10^{-5}	1.399	1.244	0.00264	0.02024
35	1351	587.4	10.46	1122	4877	3354	0.4579	0.02843	1.288×10^{-4}	1.078×10^{-5}	1.372	1.272	0.00275	0.01917
40	1555	579.4	12.03	1099	4932	3486	0.4464	0.02943	1.219×10^{-4}	1.099×10^{-5}	1.347	1.303	0.00287	0.01810
45	1782	571.3	13.8	1075	4993	3631	0.4348	0.03049	1.155×10^{-4}	1.121×10^{-5}	1.327	1.335	0.00301	0.01704
50	2033	562.9	15.78	1051	5063	3790	0.4232	0.03162	1.094×10^{-4}	1.143×10^{-5}	1.310	1.371	0.00316	0.01598
55	2310	554.2	18.00	1025	5143	3967	0.4116	0.03283	1.037×10^{-4}	1.166×10^{-5}	1.297	1.409	0.00334	0.01493
60	2614	545.2	20.48	997.4	5234	4163	0.4001	0.03412	9.846×10^{-5}	1.189×10^{-5}	1.288	1.452	0.00354	0.01389
65	2948	536.0	23.26	968.9	5340	4384	0.3885	0.03550	9.347×10^{-5}	1.213×10^{-5}	1.285	1.499	0.00377	0.01285
70	3312	526.3	26.39	939.0	5463	4634	0.3769	0.03700	8.879×10^{-5}	1.238×10^{-5}	1.287	1.551	0.00404	0.01181
75	3709	516.2	29.90	907.5	5608	4923	0.3653	0.03862	8.440×10^{-5}	1.264×10^{-5}	1.296	1.612	0.00436	0.01079
80	4141	505.7	33.87	874.1	5780	5260	0.3538	0.04038	8.030×10^{-5}	1.292×10^{-5}	1.312	1.683	0.00474	0.00977
85	4609	494.5	38.36	838.6	5988	5659	0.3422	0.04232	7.646×10^{-5}	1.322×10^{-5}	1.338	1.768	0.00521	0.00876
90	5116	482.8	43.48	800.6	6242	6142	0.3306	0.04447	7.284×10^{-5}	1.354×10^{-5}	1.375	1.871	0.00579	0.00776
95	5665	470.2	49.35	759.8	6561	6740	0.3190	0.04687	6.946×10^{-5}	1.389×10^{-5}	1.429	1.999	0.00652	0.00677
100	6257	456.6	56.15	715.5	6972	7503	0.3075	0.04958	6.628×10^{-5}	1.429×10^{-5}	1.503	2.163	0.00749	0.00579

A-11: Thermo physical properties of saturated refrigerant (R-134)

		Specific Volume m³/kg		Internal Energy kJ/kg		Enthalpy kJ/kg			Entropy kJ/kg · K		
Temp. °C	Press. bar	Sat. Liquid $v_f \times 10^3$	Sat. Vapor v_g	Sat. Liquid u_f	Sat. Vapor u_g	Sat. Liquid h_f	Evap. h_{fg}	Sat. Vapor h_g	Sat. Liquid s_f	Sat. Vapor s_g	Temp. °C
−40	0.5164	0.7055	0.3569	−0.04	204.45	0.00	222.88	222.88	0.0000	0.9560	−40
−36	0.6332	0.7113	0.2947	4.68	206.73	4.73	220.67	225.40	0.0201	0.9506	−36
−32	0.7704	0.7172	0.2451	9.47	209.01	9.52	218.37	227.90	0.0401	0.9456	−32
−28	0.9305	0.7233	0.2052	14.31	211.29	14.37	216.01	230.38	0.0600	0.9411	−28
−26	1.0199	0.7265	0.1882	16.75	212.43	16.82	214.80	231.62	0.0699	0.9390	−26
−24	1.1160	0.7296	0.1728	19.21	213.57	19.29	213.57	232.85	0.0798	0.9370	−24
−22	1.2192	0.7328	0.1590	21.68	214.70	21.77	212.32	234.08	0.0897	0.9351	−22
−20	1.3299	0.7361	0.1464	24.17	215.84	24.26	211.05	235.31	0.0996	0.9332	−20
−18	1.4483	0.7395	0.1350	26.67	216.97	26.77	209.76	236.53	0.1094	0.9315	−18
−16	1.5748	0.7428	0.1247	29.18	218.10	29.30	208.45	237.74	0.1192	0.9298	−16
−12	1.8540	0.7498	0.1068	34.25	220.36	34.39	205.77	240.15	0.1388	0.9267	−12
−8	2.1704	0.7569	0.0919	39.38	222.60	39.54	203.00	242.54	0.1583	0.9239	−8
−4	2.5274	0.7644	0.0794	44.56	224.84	44.75	200.15	244.90	0.1777	0.9213	−4
0	2.9282	0.7721	0.0689	49.79	227.06	50.02	197.21	247.23	0.1970	0.9190	0
4	3.3765	0.7801	0.0600	55.08	229.27	55.35	194.19	249.53	0.2162	0.9169	4
8	3.8756	0.7884	0.0525	60.43	231.46	60.73	191.07	251.80	0.2354	0.9150	8
12	4.4294	0.7971	0.0460	65.83	233.63	66.18	187.85	254.03	0.2545	0.9132	12
16	5.0416	0.8062	0.0405	71.29	235.78	71.69	184.52	256.22	0.2735	0.9116	16
20	5.7160	0.8157	0.0358	76.80	237.91	77.26	181.09	258.36	0.2924	0.9102	20
24	6.4566	0.8257	0.0317	82.37	240.01	82.90	177.55	260.45	0.3113	0.9089	24
26	6.8530	0.8309	0.0298	85.18	241.05	85.75	175.73	261.48	0.3208	0.9082	26
28	7.2675	0.8362	0.0281	88.00	242.08	88.61	173.89	262.50	0.3302	0.9076	28
30	7.7006	0.8417	0.0265	90.84	243.10	91.49	172.00	263.50	0.3396	0.9070	30
32	8.1528	0.8473	0.0250	93.70	244.12	94.39	170.09	264.48	0.3490	0.9064	32
34	8.6247	0.8530	0.0236	96.58	245.12	97.31	168.14	265.45	0.3584	0.9058	34
36	9.1168	0.8590	0.0223	99.47	246.11	100.25	166.15	266.40	0.3678	0.9053	36
38	9.6298	0.8651	0.0210	102.38	247.09	103.21	164.12	267.33	0.3772	0.9047	38
40	10.164	0.8714	0.0199	105.30	248.06	106.19	162.05	268.24	0.3866	0.9041	40
42	10.720	0.8780	0.0188	108.25	249.02	109.19	159.94	269.14	0.3960	0.9035	42
44	11.299	0.8847	0.0177	111.22	249.96	112.22	157.79	270.01	0.4054	0.9030	44
48	12.526	0.8989	0.0159	117.22	251.79	118.35	153.33	271.68	0.4243	0.9017	48
52	13.851	0.9142	0.0142	123.31	253.55	124.58	148.66	273.24	0.4432	0.9004	52
56	15.278	0.9308	0.0127	129.51	255.23	130.93	143.75	274.68	0.4622	0.8990	56
60	16.813	0.9488	0.0114	135.82	256.81	137.42	138.57	275.99	0.4814	0.8973	60
70	21.162	1.0027	0.0086	152.22	260.15	154.34	124.08	278.43	0.5302	0.8918	70
80	26.324	1.0766	0.0064	169.88	262.14	172.71	106.41	279.12	0.5814	0.8827	80
90	32.435	1.1949	0.0046	189.82	261.34	193.69	82.63	276.32	0.6380	0.8655	90
100	39.742	1.5443	0.0027	218.60	248.49	224.74	34.40	259.13	0.7196	0.8117	100

A-12: Thermo physical properties of super-heated refrigerant (R-134)

T °C	v m³/kg	u kJ/kg	h kJ/kg	s kJ/kg · K	v m³/kg	u kJ/kg	h kJ/kg	s kJ/kg · K
	p = 8.0 bar = 0.80 MPa (T_{sat} = 31.33°C)				p = 9.0 bar = 0.90 MPa (T_{sat} = 35.53°C)			
Sat.	0.02547	243.78	264.15	0.9066	0.02255	245.88	266.18	0.9054
40	0.02691	252.13	273.66	0.9374	0.02325	250.32	271.25	0.9217
50	0.02846	261.62	284.39	0.9711	0.02472	260.09	282.34	0.9566
60	0.02992	271.04	294.98	1.0034	0.02609	269.72	293.21	0.9897
70	0.03131	280.45	305.50	1.0345	0.02738	279.30	303.94	1.0214
80	0.03264	289.89	316.00	1.0647	0.02861	288.87	314.62	1.0521
90	0.03393	299.37	326.52	1.0940	0.02980	298.46	325.28	1.0819
100	0.03519	308.93	337.08	1.1227	0.03095	308.11	335.96	1.1109
110	0.03642	318.57	347.71	1.1508	0.03207	317.82	346.68	1.1392
120	0.03762	328.31	358.40	1.1784	0.03316	327.62	357.47	1.1670
130	0.03881	338.14	369.19	1.2055	0.03423	337.52	368.33	1.1943
140	0.03997	348.09	380.07	1.2321	0.03529	347.51	379.27	1.2211
150	0.04113	358.15	391.05	1.2584	0.03633	357.61	390.31	1.2475
160	0.04227	368.32	402.14	1.2843	0.03736	367.82	401.44	1.2735
170	0.04340	378.61	413.33	1.3098	0.03838	378.14	412.68	1.2992
180	0.04452	389.02	424.63	1.3351	0.03939	388.57	424.02	1.3245

T °C	v m³/kg	u kJ/kg	h kJ/kg	s kJ/kg · K	v m³/kg	u kJ/kg	h kJ/kg	s kJ/kg · K
	p = 10.0 bar = 1.00 MPa (T_{sat} = 39.39°C)				p = 12.0 bar = 1.20 MPa (T_{sat} = 46.32°C)			
Sat.	0.02020	247.77	267.97	0.9043	0.01663	251.03	270.99	0.9023
40	0.02029	248.39	268.68	0.9066				
50	0.02171	258.48	280.19	0.9428	0.01712	254.98	275.52	0.9164
60	0.02301	268.35	291.36	0.9768	0.01835	265.42	287.44	0.9527
70	0.02423	278.11	302.34	1.0093	0.01947	275.59	298.96	0.9868
80	0.02538	287.82	313.20	1.0405	0.02051	285.62	310.24	1.0192
90	0.02649	297.53	324.01	1.0707	0.02150	295.59	321.39	1.0503
100	0.02755	307.27	334.82	1.1000	0.02244	305.54	332.47	1.0804
110	0.02858	317.06	345.65	1.1286	0.02335	315.50	343.52	1.1096
120	0.02959	326.93	356.52	1.1567	0.02423	325.51	354.58	1.1381
130	0.03058	336.88	367.46	1.1841	0.02508	335.58	365.68	1.1660
140	0.03154	346.92	378.46	1.2111	0.02592	345.73	376.83	1.1933
150	0.03250	357.06	389.56	1.2376	0.02674	355.95	388.04	1.2201
160	0.03344	367.31	400.74	1.2638	0.02754	366.27	399.33	1.2465
170	0.03436	377.66	412.02	1.2895	0.02834	376.69	410.70	1.2724
180	0.03528	388.12	423.40	1.3149	0.02912	387.21	422.16	1.2980

T °C	v m³/kg	u kJ/kg	h kJ/kg	s kJ/kg · K	v m³/kg	u kJ/kg	h kJ/kg	s kJ/kg · K
	p = 14.0 bar = 1.40 MPa (T_{sat} = 52.43°C)				p = 16.0 bar = 1.60 MPa (T_{sat} = 57.92°C)			
Sat.	0.01405	253.74	273.40	0.9003	0.01208	256.00	275.33	0.8982
60	0.01495	262.17	283.10	0.9297	0.01233	258.48	278.20	0.9069
70	0.01603	272.87	295.31	0.9658	0.01340	269.89	291.33	0.9457
80	0.01701	283.29	307.10	0.9997	0.01435	280.78	303.74	0.9813
90	0.01792	293.55	318.63	1.0319	0.01521	291.39	315.72	1.0148
100	0.01878	303.73	330.02	1.0628	0.01601	301.84	327.46	1.0467
110	0.01960	313.88	341.32	1.0927	0.01677	312.20	339.04	1.0773
120	0.02039	324.05	352.59	1.1218	0.01750	322.53	350.53	1.1069
130	0.02115	334.25	363.86	1.1501	0.01820	332.87	361.99	1.1357
140	0.02189	344.50	375.15	1.1777	0.01887	343.24	373.44	1.1638
150	0.02262	354.82	386.49	1.2048	0.01953	353.66	384.91	1.1912
160	0.02333	365.22	397.89	1.2315	0.02017	364.15	396.43	1.2181
170	0.02403	375.71	409.36	1.2576	0.02080	374.71	407.99	1.2445
180	0.02472	386.29	420.90	1.2834	0.02142	385.35	419.62	1.2704
190	0.02541	396.96	432.53	1.3088	0.02203	396.08	431.33	1.2960
200	0.02608	407.73	444.24	1.3338	0.02263	406.90	443.11	1.3212

A-13: Viscosity of water as a function of temperature

Temperature	Pressure	Dynamic viscosity			Kinematic viscosity
[°C]	[MPa]	[Pa s], [N s/m2]	[cP], [mPa s]	[lbf s/ft^2 *10^{-5}]	[m^2/s*10^{-6}], [cSt])
0.01	0.000612	0.0017914	1.79140	3.7414	1.7918
10	0.0012	0.0013060	1.30600	2.7276	1.3065
20	0.0023	0.0010016	1.00160	2.0919	1.0035
25	0.0032	0.0008900	0.89004	1.8589	0.8927
30	0.0042	0.0007972	0.79722	1.6650	0.8007
40	0.0074	0.0006527	0.65272	1.3632	0.6579
50	0.0124	0.0005465	0.54650	1.1414	0.5531
60	0.0199	0.0004660	0.46602	0.9733	0.4740
70	0.0312	0.0004035	0.40353	0.8428	0.4127
80	0.0474	0.0003540	0.35404	0.7394	0.3643
90	0.0702	0.0003142	0.31417	0.6562	0.3255
100	0.101	0.0002816	0.28158	0.5881	0.2938
110	0.143	0.0002546	0.25461	0.5318	0.2677
120	0.199	0.0002320	0.23203	0.4846	0.2460
140	0.362	0.0001966	0.19664	0.4107	0.2123
160	0.618	0.0001704	0.17043	0.3559	0.1878
180	1.00	0.0001504	0.15038	0.3141	0.1695
200	1.55	0.0001346	0.13458	0.2811	0.1556
220	2.32	0.0001218	0.12177	0.2543	0.1449
240	3.35	0.0001111	0.11106	0.2320	0.1365
260	4.69	0.0001018	0.10181	0.2126	0.1299
280	6.42	0.0000936	0.09355	0.1954	0.1247
300	8.59	0.0000859	0.08586	0.1793	0.1206
320	11.3	0.0000783	0.07831	0.1636	0.1174
340	14.6	0.0000703	0.07033	0.1469	0.1152
360	18.7	0.0000603	0.06031	0.1260	0.1143

A-14: Local loss coefficients used in minor head loss calculations

Loss Coefficients for Pipe Components $\left(h_L = K_L \dfrac{V^2}{2g}\right)$

Component	K_L
a. Elbows	
Regular 90°, flanged	0.3
Regular 90°, threaded	1.5
Long radius 90°, flanged	0.2
Long radius 90°, threaded	0.7
Long radius 45°, flanged	0.2
Regular 45°, threaded	0.4
b. 180° return bends	
180° return bend, flanged	0.2
180° return bend, threaded	1.5
c. Tees	
Line flow, flanged	0.2
Line flow, threaded	0.9
Branch flow, flanged	1.0
Branch flow, threaded	2.0
d. Union, threaded	0.08
***e. Valves**	
Globe, fully open	10
Angle, fully open	2
Gate, fully open	0.15
Gate, $\frac{1}{4}$ closed	0.26
Gate, $\frac{1}{2}$ closed	2.1
Gate, $\frac{3}{4}$ closed	17
Swing check, forward flow	2
Swing check, backward flow	∞
Ball valve, fully open	0.05
Ball valve, $\frac{1}{3}$ closed	5.5
Ball valve, $\frac{2}{3}$ closed	210

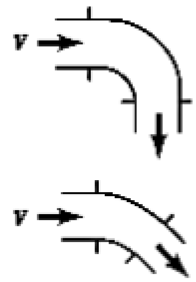

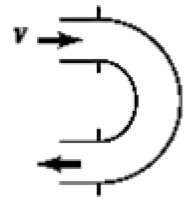

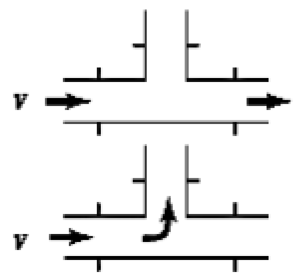

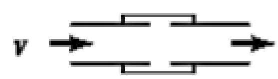

(APPENDIX-B) METEOROLOGICAL AND COLLECTED DATA

B-1: Average monthly temperature (2004-2018)

በብሔራዊ ሚቲዎሮሎጂ ኤጀንሲ
NATIONAL METEOROLOGICAL AGENCY
የደ/ብ/ብ/ሕ/ክልል የሚቲዎሮሎጂ አገልግሎት ማዕከል
SNNPR Meteorological Service Center

Station Name: Dilla **Element:** Monthly average Maximum Temp. in °C

Year	Jan	Feb	Mar	Apr	May	Jun	Jul	Aug	Sep	Oct	Nov	Dec	Jan
2004	30.2	29.9	31.2	27.0	28.0	26.1	26.2	26.8	26.7	27.4	28.2	29.2	30.2
2005	30.8	32.8	31.1	30.1	26.0	26.2	25.5	26.5	26.5	26.5	28.0	29.9	30.8
2006	31.2	30.8	29.6	27.4	27.6	27.3	25.4	26.0	26.7	27.2	27.3	28.1	31.2
2007	29.5	31.0	30.4	28.3	28.3	27.1	26.2	25.8	25.5	27.1	28.2	29.1	29.5
2008	30.7	30.9	31.7	28.5	26.1	25.9	24.6	25.2	26.3	26.3	27.3	29.2	30.7
2009	29.6	30.9	32.3	28.1	NA	27.3	26.9	27.6	27.1	27.4	29.5	29.0	29.6
2010	29.2	29.5	28.5	27.9	26.8	26.4	25.1	25.6	25.9	27.5	29.5	29.9	29.2
2011	31.0	31.9	32.0	31.7	27.0	26.0	25.9	25.5	25.5	27.3	26.5	28.1	31.0
2012	30.7	31.9	32.4	28.3	27.5	26.6	NA	26.0	25.4	27.3	NA	29.1	30.7
2013	30.6	32.4	30.2	27.6	NA	25.6	24.7	25.0	26.2	26.1	27.2	NA	30.6
2014	30.2	30.3	30.7	28.6	27.0	26.7	26.0	25.8	26.2	26.3	27.7	28.6	30.2
2015	30.4	31.9	32.0	28.8	27.5	26.6	26.7	28.0	27.5	27.6	NA	NA	30.4
2016	30.5	31.9	31.8	28.4	27.2	26.2	25.5	NA	26.5	27.0	28.2	29.1	30.5
2017	30.8	31.2	32.2	30.1	27.1	27.3	25.3	25.4	24.8	26.6	27.3	29.3	30.8
2018	30.3	30.3	27.7	26.0	26.6	25.0	24.9	NA	26.5	27.0	27.6	29.1	30.3

Station Name: Dilla **Element:** Monthly average Minimum Temp. in °C

Year	Jan	Feb	Mar	Apr	May	Jun	Jul	Aug	Sep	Oct	Nov	Dec	Jan
2004	11.3	11.3	11.3	14.4	12.9	13.1	13.6	14.5	13.3	12.3	12.7	11.6	11.3
2005	10.1	10.5	13.8	14.1	14.9	13.8	13.7	14.3	14.0	13.6	11.4	7.2	10.1
2006	9.9	12.3	13.3	14.1	13.6	13.9	14.9	14.1	14.0	14.8	13.2	12.7	9.9
2007	12.3	12.3	12.1	14.0	14.3	15.2	14.8	14.4	14.7	12.2	11.8	8.1	12.3
2008	9.3	9.9	11.1	13.7	14.1	13.9	15.1	14.4	14.4	13.8	11.5	9.2	9.3
2009	10.2	11.2	12.4	14.3	NA	13.2	13.6	13.8	14.2	14.1	11.3	17.5	10.2
2010	11.3	14.8	14.4	15.0	15.7	14.7	15.1	15.4	14.7	13.9	11.1	9.6	11.3
2011	10.0	9.7	12.9	13.8	15.4	15.2	14.7	14.8	14.7	13.0	13.8	9.9	10.0
2012	8.2	8.3	10.8	14.2	13.9	14.5	NA	14.7	14.4	13.3	NA	11.1	8.2
2013	10.4	10.6	15.4	14.9	NA	14.9	15.1	14.6	14.1	14.0	12.9	NA	10.4
2014	10.6	12.9	13.0	13.1	14.3	13.6	14.5	13.9	13.6	14.2	12.6	9.9	10.6
2015	8.1	9.9	12.3	13.5	14.4	14.5	14.0	13.1	13.1	13.7	NA	NA	8.1
2016	13.3	11.6	13.5	16.1	15.0	14.0	15.7	NA	13.8	14.1	12.1	9.3	13.3
2017	5.8	11.1	13.0	13.7	14.9	14.0	15.4	14.8	14.7	15.2	11.8	7.2	5.8
2018	9.2	12.5	13.7	14.8	14.6	14.5	14.4	14.4	13.4	13.5	13.0	11.8	9.2

●Note:------------NA……..Data is not Available

19/Aug/2019

☎ 046 – 220 74 75, 046 220 67 96 Fax: 046 – 220 67 97 P.O.Box 161, Hawassa

e-mail: debubmet@yahoo.com Web-site: www.ethiomet.gov.et

B-2: Average monthly relative humidity (2004-2018) and wind speed (2006-2018)

በብሔራዊ ሚቲዎሮሎጂ ኤጀንሲ

NATIONAL METEOROLOGICAL AGENCY

የደ/ብ/ብ/ሕ/ክልል የሚቲዎሮሎጂ አገልግሎት ማዕከል

SNNPR Meteorological Service Center

Station Name: Dilla **Element:** Monthly average Relative Humidity in %

Year	Jan	Feb	Mar	Apr	May	Jun	Jul	Aug	Sep	Oct	Nov	Dec	Jan
2004	65	66	52	72	70	73	71	70	72	68	67	64	68
2005	55	45	57	63	80	76	77	74	76	79	68	59	67
2006	58	56	65	73	75	76	77	77	74	78	72	70	71
2007	60	57	NA	NA	NA	74	NA	NA	81	77	NA	63	NA
2008	53	49	26	52	63	63	68	66	64	61	53	40	55
2009	37	34	31	52	NA	56	52	50	54	57	42	73	NA
2010	42	48	53	59	NA	63	63	NA	NA	NA	NA	NA	NA
2011	NA	32	32	37	60	65	65	66	64	57	60	47	NA
2012	29	26	25	48	60	58	NA	62	61	56	NA	45	NA
2013	37	32	42	53	NA	72	74	72	71	71	NA	57	NA
2014	NA	56	70	60	68	66	69	69	70	73	65	62	NA
2015	NA	NA	NA	NA	NA	NA	NA	NA	NA	NA	NA	NA	NA
2016	NA	NA	53	69	69	71	72	NA	NA	NA	NA	NA	NA
2017	NA	NA	NA	40	70	67	73	72	74	72	60	42	NA
2018	31	34	48	60	62	65	64	64	60	63	59	51	55

Station Name: Dilla **Element:** Monthly average wind speed in m/s

Year	Jan	Feb	Mar	Apr	May	Jun	Jul	Aug	Sep	Oct	Nov	Dec	Jan
2006	0.65	0.80	0.59	0.60	0.58	0.36	0.32	0.37	0.37	0.37	0.36	0.35	0.65
2007	0.50	0.59	0.57	0.46	0.47	0.45	0.41	0.33	0.41	0.49	0.51	0.50	0.50
2008	0.59	0.78	0.86	0.61	0.46	0.44	0.33	0.36	0.37	0.34	0.37	0.46	0.59
2009	0.53	0.63	0.78	0.52	NA	0.39	0.39	0.50	0.43	0.40	0.48	0.17	0.53
2010	0.49	0.49	0.49	0.42	0.33	0.32	0.28	0.28	0.31	0.42	0.42	0.46	0.49
2011	0.57	0.66	0.67	0.65	0.41	0.34	0.30	0.29	0.30	0.33	0.27	0.33	0.57
2012	0.44	0.53	0.65	0.48	NA	0.30	NA	0.29	0.30	0.35	NA	0.38	0.44
2013	0.43	0.70	0.60	0.41	NA	0.28	0.25	0.31	0.31	0.29	NA	0.35	0.43
2014	NA	0.52	0.60	0.43	0.34	0.28	0.27	0.28	0.29	0.25	0.31	0.35	NA
2015	NA	NA	NA	NA	NA	0.26	0.25	0.36	0.33	0.31	NA	NA	NA
2016	0.96	3.66	0.65	0.39	0.33	1.21	0.31	NA	NA	NA	NA	NA	0.96
2017	0.47	0.61	0.68	0.60	0.37	0.38	0.33	0.34	0.28	0.36	1.48	0.41	0.47
2018	0.45	0.64	0.38	0.36	0.36	0.32	0.32	0.42	0.38	0.35	0.31	0.35	0.45

●Note:------------NA……..Data is not Available

19/Aug/2019

☎ 046 – 220 74 75, 046 220 67 96 Fax: 046 – 220 67 97 P.O.Box 161 Hawassa

e-mail: debubmet@yahoo.com Web-site: www.ethiomet.gov.et

National Meteorology Agency S/N/N/P/R/Meteorological Service Center

B-3: Drinking water temperature and daily consumptions rate

DATA COLLECTED FOR DRINKING WATER TEMPERATURE AND DAILY CONSUMPTIONS RATE, [*Dilla University, Odayaa'a campus (Gede'o, Dilla, Ethiopia)*]

Drinking water temperature,(°C)
(Taken from a tap)

	Date	Representative Hour	Measured value (°C)
1.	Hamle 12/2011 E.C (July 19/2019)	9:00-9:16 AM	38
		9:34 AM	37.5
		9:47 AM	36.4
		9:55 AM	36
		10:00 AM	36.5
2.	Hamle 13/2011 E.C (July 20/2019)	10:00-10:09 AM	36.8
		10:25 AM	37.4
		10:35AM	38
		10:46 AM	37
		11:00 AM	38
3.	Hamle 14/2011 E.C (July 21/2019)	3:00-3:25 AM	38.5
		3:30 AM	37.5
		3:40 AM	38
		3:50 AM	37.6
		4:00 AM	37
4.	Hamle 15/2011 E.C (July 22/2019)	12:00-12:20 AM	38
		12:28 AM	37.8
		12:38 AM	38
		12:48 AM	37.9
		01:00 AM	37.5
5.	Hamle 16/2011 E.C (July 23/2019)	11:00-11:10 AM	36.9
		11:20 AM	37
		11:30 AM	37.5
		11:45 AM	38
		12:00 AM	38
6.	Hamle 17/2011 E.C (july 24/2019)	01:00-3:22 AM	39
		01:35	38
		01:42	38.5
		01:53	37.6
		02:00	37.6
7.	Hamle 18/2011 E.C (july 25/2019)	02:00-3:15 AM	38
		02:25	37
		02:35	36
		02:45	36.5
		03:00	37.5
	Average value		**37.5**

Drinking water daily consumptions

		Average No. (in Thousands)	Average consumptions (Liters)
1.	Students	31	62,000 Liters
2.	Staffs	3	6,000 Liters
Total			68,000

Collected by Yonas Tetemke.

Approved by Fikru Tadele.

Dean, School of Mechanical & Automotive Engineering

B-4: Average hot water temperature value (Barsiso/Chombe, Gedeo)

MEASURED DATA FOR AVERAGE TEMPERATURE VALUE OF GEOTHERMAL WATER ("*BARSISO/CHOMBE" HOT SPRING*) [*SNNPR, GEDEO, ODAYA'A*]

Hourly measured values (Hamle 04/2011 July 12, 2019)

No.	Representative Hours	Measured values(°C)
1.	4:35 PM	56.7
2.	5:36 PM	55.8
3.	6:35 AM	56.2
4.	7:34 AM	56.8
5.	8:37 AM	56
6.	9:33 AM	55
7.	10:35 AM	56
8.	11:36 AM	55.9
9.	12:38 AM	54.8
10.	13:33 AM	55
11.	14:32 AM	56.7
12.	15:36 AM	56
13.	16:37 AM	55.6
14.	17:34 AM	56.6
15.	18:35 PM	56.2
16.	19:38 PM	56.9
17.	20:37 PM	57
18.	21:35 PM	56.9
19.	22:33 PM	56.8
20.	23:32 PM	57.4
21.	24:36 PM	58
22.	1:35 PM	57.9
23.	2:35 PM	57
Average value		56.4

Daily measured values (Three weeks)

No.	Days (three weeks)	Representative Hours	Measured values
1.	Sene 19/2011 June 27/2019	10:20 AM	56.8
2.	Sene 20/2011 June 28/2019	8:50 AM	55.2
3.	Sene 21/2011 June 29/2019	5:05 AM	56.7
4.	Sene 22/2011 June 30/2019	7:30 AM	56
5.	Sene 23/2011 July 01/2019	8:00 AM	54.7
6.	Sene 24/2011 July 02/2019	9:30 AM	54.5
7.	Sene 25/2011 July 03/2019	12:40 AM	55
8.	Sene 26/2011 July 04/2019	01:00 AM	54.8
9.	Sene 27/2011 July 05/2019	02:02 AM	56.7
10.	Sene 28/2011 July 06/2019	02:10 AM	56.8
11.	Sene 29/2011 July 07/2019	03:00 AM	55.9
12.	Sene 30/2011 July 08/2019	04:34 AM	55.6
13.	Hamle 01/2011 July 09/2019	05:00 AM	56
14.	Hamle 02/2011 July 10/2019	8:00 AM	55
15.	Hamle 03/2011 July 11/2019	9:00 AM	55.2
16.	Hamle 04/2011 July 12/2019	10:20 AM	56.3
17.	Hamle 05/2011 July 13/2019	10:25 AM	56
18.	Hamle 06/2011 July 14/2019	11:00 AM	56.2
19.	Hamle 07/2011 July 15/2019	11:15 AM	56
20.	Hamle 08/2011 July 16/2019	11:22 AM	55.4
21.	Hamle 09/2011 July 17/2019	10:30 AM	56.7
Average value			55.78

Collected by: Yonas Tetemke.

Approved by: Tariku Figa.(Gedeo zone water, mineral, and energy sector expert)

Tel: +251-910-907-025

B-5: Average hot water temperature value (Wallame, Guji)

MEASURED DATA FOR AVERAGE TEMPERATURE VALUE OF GEOTHERMAL WATER ("WALAME" *HOT SPRING*) [*OROMIA REGION, WEST GUJJI, ODOMIQE*]

Hourly measured values (Nehase 09/2011 August 15, 2019)

No.	Representative Hours	Measured values(°C)
1.	4:00PM	90
2.	5:00 PM	89.2
3.	6:00 AM	88
4.	7:00 AM	88.5
5.	8:00 AM	87.7
6.	9:00 AM	89
7.	10:00 AM	88
8.	11:00 AM	87.8
9.	12:00 AM	87.9
10.	13:00 AM	88.3
11.	14:00 AM	88
12.	15:00 AM	88.6
13.	16:00 AM	87.6
14.	17:00 AM	87.6
15.	18:00 PM	87.4
16.	19:00 PM	87.9
17.	20:00 PM	87
18.	21:00 PM	88
19.	22:00 PM	88.1
20.	23:00 PM	89
21.	24:00 PM	89.1
22.	1:00 PM	88.5
23.	2:00 PM	88
24.	3:00 PM	88.8
Average value		88.25

Collected by: *Yonas Tetemke.*

Approved by: *Tariku Figa.*(Gedeo zone water, mineral, and energy sector expert)

Tel: +251-910-907-025

Wode'a Bullin Giddixxa Karranaa Enete Akaakkaaba BIGIGIAG/Mootumma'n Gedeo'n Zoone'n

End of the paper!